The diverse roles of inhibition in identified neural circuits

Inauguraldissertation

zur

Erlangung der Würde eines Doktors der Philosophie

vorgelegt der

Philosophisch-Naturwissenschaftlichen Fakultät

der Universität Basel

von

Tim James Viney

aus Grossbritannien

Basel, 2010

creative commons

Attribution-Noncommercial-No Derivative Works 2.5 Switzerland

---

You are free:

to Share — to copy, distribute and transmit the work

Under the following conditions:

Attribution. You must attribute the work in the manner specified by the author or licensor (but not in any way that suggests that they endorse you or your use of the work).

Noncommercial. You may not use this work for commercial purposes.

No Derivative Works. You may not alter, transform, or build upon this work.

- For any reuse or distribution, you must make clear to others the license terms of this work. The best way to do this is with a link to this web page.
- Any of the above conditions can be waived if you get permission from the copyright holder.
- Nothing in this license impairs or restricts the author's moral rights.

Your fair dealing and other rights are in no way affected by the above.

This is a human-readable summary of the Legal Code (the full license) available in German:
http://creativecommons.org/licenses/by-nc-nd/2.5/ch/legalcode.de

Disclaimer:
The Commons Deed is not a license. It is simply a handy reference for understanding the Legal Code (the full license) — it is a human-readable expression of some of its key terms. Think of it as the user-friendly interface to the Legal Code beneath. This Deed itself has no legal value, and its contents do not appear in the actual license. Creative Commons is not a law firm and does not provide legal services. Distributing of, displaying of, or linking to this Commons Deed does not create an attorney-client relationship.

Quelle: http://creativecommons.org/licenses/by-nc-nd/2.5/ch/deed.en Datum: 3.4.2009

Genehmigt von der Philosophisch-Naturwissenschaftlichen Fakultät auf Antrag von

Prof. Dr. Silvia Arber (Fakultätsverantwortlicher)

Dr. Botond Roska (Dissertationsleiter)

Prof. Dr. Reto Weiler (Korreferent)

Basel, den 22. Juni 2010

Prof. Dr. Eberhard Parlow (Dekan)

Table of Contents

Abstract

Inhibitory interneurons represent a diverse population of cell types in the central nervous system, whose general role is to suppress activity of target neurons. The timing of spikes in principal neurons has millisecond precision, and I asked what are the roles of inhibition in shaping the temporal codes that emerge from different parallel local neural circuits. First I investigated the local circuitry of melanopsin-containing ganglion cells in the mouse retina, which are intrinsically photosensitive and responsible for circadian photoentrainment. Using transsynaptic viral tracing, I identified three types of melanopsin-containing ganglion cell, and found that inhibitory (GABAergic) dopaminergic amacrine cells are presynaptic to one of these types. These results provided a direct circuitry link between the medium time scale process of light-dark adaptation, which involves dopamine, and the longer time scale of the circadian rhythm. Next I characterised a subpopulation of genetically-identified neurons in the mouse retina, in order to compare the precise timing of inhibition in different circuits at a high temporal resolution. I identified eight physiologically and morphologically distinct ganglion cell types and found that each circuit could be described by a 'motif' that represented the inhibitory-excitatory interactions that lead to cell-type-specific firing patterns. The cell would fire only when the change in excitation was faster than the change in inhibition. Therefore the role of inhibition is to detect 'irrelevance' in the visual scene, only allowing the ganglion cell to fire at specific time points relating to functions that are both parallel and complementary to the other cell types. Finally, I looked deeper within the neural circuitry of one of the genetically-identified cell types, to study the mechanism of 'fast inhibition' in detecting approaching objects. Through two-photon targeted paired recordings of postsynaptic ganglion cells and presynaptic amacrine cells, I found evidence that the AII amacrine cell - a well-characterised glycinergic inhibitory interneuron known to be involved in night vision circuits - conveys fast inhibitory information to the ganglion cell via an electrical synapse with an excitatory neuron of day vision circuitry only during non-approach motion. Therefore, it appears that the role of inhibition is to dynamically interact with direct excitatory neural pathways during 'irrelevant' stimulation, suppressing or completely blocking activity, resulting in precisely timed spikes that occur in the brief moments when excitation changes faster than inhibition.

Introduction

Neural circuits in the retina

The retina, like all parts of the central nervous system, is composed of neural circuits - networks of connected neurons - that exist to enable the organism to perform specialised functions relevant to its activities in the environment (Wässle 2004, Gollisch and Meister 2010). Neural circuits of the retina are responsible for transducing visible light into meaningful messages that are used by the organism for a range of functions that include detecting single photons of starlight, identifying the correct shape, texture and colour of fruit, stabilising eye movements relative to the head, and entraining the body to the day-light cycle. The mammalian retina is a thin sheet of laminated neural tissue that covers the interior surface of the back of the eye (Fig. Ia). Light entering the eye through the pupil is focussed via the lens onto the retina, where it is detected, processed, and converted into a neural code that is delivered via the optic nerve to 'higher' brain regions for further processing. There are four main advantages for studying neural circuits in the retina. First, we know that the input to the retina is light, and we know that the output is the optic nerve. Second, this information flow is unidirectional, and is a condition of the first point, i.e. we know which direction the information is flowing. This is in contrast to the cortex, where information flow is bidirectional and not sequential. Third, the retina is conveniently situated outside the skull, making it easy to isolate for experiments. It also remains fully intact after isolation and can be kept alive *ex vivo* for many hours. Finally, it is possible to experimentally record from every cell type of the retina (a condition of the third point). The mouse eye, which is used throughout this thesis for retina isolation, has an unusually large lens (Fig. Ib). The mouse retina also does not have a fovea, which is the primary region in human retina for high-acuity colour vision. Besides the lack of a fovea or visual streak, there are some spectral differences in the range of visible light that the mouse can detect; otherwise all findings in this thesis in terms of neural circuitry can be thought of as universal for mammals.

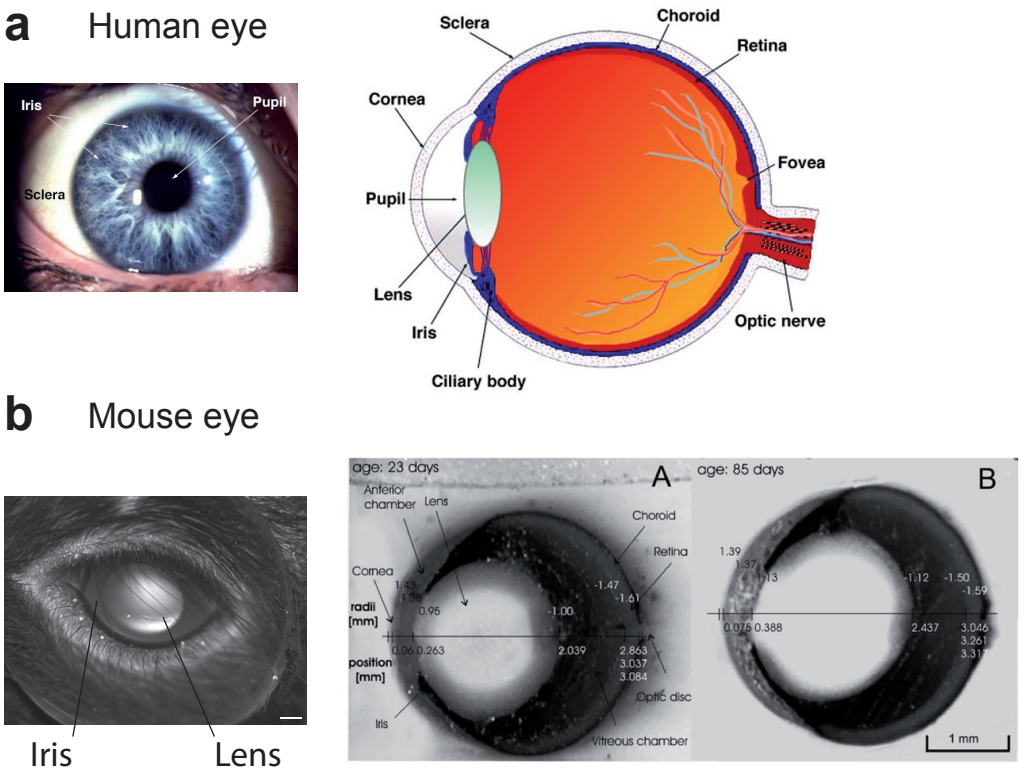

Figure I. The mammalian eye. (a) Left, human eye. Right, schematic of the human eye (from Webvision website). (b) Left, mouse eye with coverslip used to image mouse lens (centre). Sclera is obscured behind eyelids. Scale bar: 500 µm. Right, frozen sections of mouse eye (Schmucker and Schaeffel 2004 Figure 4). Note anterior chamber between cornea and lens: this is the site of injection for viral tracing experiments in Chapter 1. Also note vitreous chamber and choroid near retina: these must be thoroughly removed from the retina in order to target retinal neurons with an electrode (see Materials and Methods).

Figure I

Neural circuits are composed of cell types

How does the retina process light? As with all sensory systems, the stimulus - in this case, light - must first be detected, then processed in a meaningful way before the relevant information is sent to other brain regions. The processing, from detection to transmission, is achieved by different cell types, each having a specialised function but working together as components of neural circuits. Before touching on the cell types, one must bear in mind that the stimulus itself has a structure in both space and time and that parallel channels within the retina are thought to have distinct roles in processing particular features of the stimulus (Roska and Werblin 2001, Wässle 2004). Therefore, if particular features are not present in the stimulus at a given space or time, the channel responsible for that feature or features will not process and transmit information. In other words, the retina acts as a spatiotemporal filter, governed by the limits set by each parallel neural circuit.

A controversy exists as to what actually constitutes a neural cell type (Rowe and Stone 1977, Hughes 1979, Roedick and Brenning 1983). This controversy is not restricted to the retina but is found across all of neuroscience (Ascoli et al. 2008). In my thesis I have been very careful in my definition of cell type, since terms such as 'class', 'type', 'subtype' and 'group' have been used interchangeably in the literature and often lead to confusion when discussing neural circuits. Wherever possible, cell type should be quantified (see Chapter 2). Thus, in the retina, cell types represent the single-cell components of neural circuits, but all the different cell types exist within defined functional classes of neurons (Wässle and Boycott 1991, Masland 2001). There are five neuronal cell classes in the retina, which are localised to different layers (laminae) of the tissue (Fig. II).

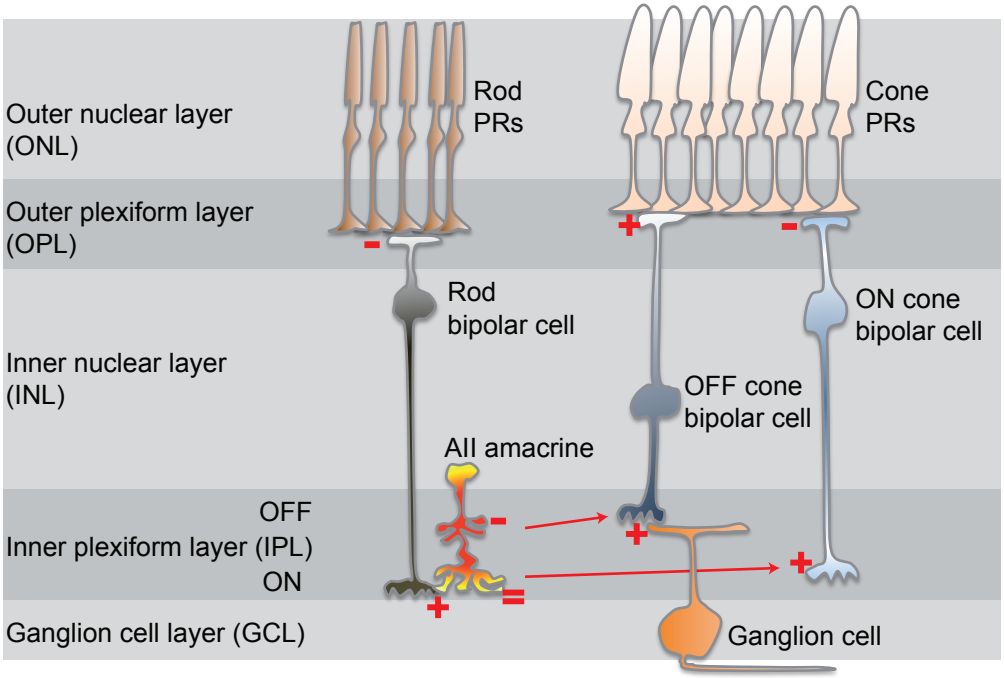

Figure II. The mammalian retina (simplified). Retinal layers are shown as grey boxes. The outer nuclear layer (ONL) contains the photoreceptors (PRs), which catch photons. Rod PRs operate in dim light (night vision pathway) and cone PRs operate in bright light (day vision pathway). The outer plexiform layer (OPL) is where PR terminals, horizontal cell dendrites and axons, and bipolar cell dendrites make synaptic contacts. Horizontal cells are not shown. In the night vision (rod) pathway, rod bipolar cells form sign inverting synapses with the rod PRs due to metabotropic glutamate receptors. In the day vision (cone) pathways, ON and OFF cone bipolar cells form sign inverting and sign conserving synapses with the cone PRs, due to metabotropic and ionotropic glutamate receptors, respectively. The bipolar cell somata are located in the inner nuclear layer (INL), along with the inhibitory amacrine cells. The inner plexiform layer (IPL) is broadly divided into 'OFF' and 'ON' sublayers. In the rod pathway, rod bipolar cell axon terminals synapse with special 'AII' amacrine cell dendrites in the innermost part of the IPL (sign conserving). In the cone pathways, ON and OFF cone bipolar cell axon terminals synapse with ganglion cell dendrites in the 'ON' and 'OFF' parts of the IPL, respectively (also sign-conserving). At night (rod pathway), these same cone bipolar cells receive input from the AII amacrine cell via an electrical (sign-conserving) synapse between the AII dendrites and ON cone bipolar cells, and a glycinergic (sign-inverting) synapse between the AII lobular appendages and OFF cone bipolar cells. These then provide sign-conserving input to the ganglion cells, as in the day (cone pathways). See Figure 3.5 for further details. Amacrine cells, which receive input from bipolar cells and other amacrine cells, provide inhibitory input both to the presynaptic bipolar cells and the postsynaptic ganglion cells. Red minus signs represent a sign-inverting synapse. Red plus signs represent a sign-conserving synapse. An red equals sign represents an electrical synapse. Only one ganglion cell, complete with axon, and only two cone bipolar cells are shown. Widefield GABAergic and narrowfield glycinergic amacrine cells (except the AII amacrine cell), and Müller glial cells are not shown. The soma positions have been drawn at their approximate locations within the nuclear layers, as it appears that somata, as well as processes, are organised in sublayers.

Figure II

The first class of retinal neurons is the photoreceptors, and by definition detect light by catching photons. The photoreceptor cell types represent the input layer of the retina, which is in fact the outermost layer, furthest from the light source. Light has to pass through the entire retina to reach the photoreceptors. The class of photoreceptors can be divided into two groups: the cones, which consist of two or more types in mammals (with different spectral sensitivities), and the rods, consisting of only one type. All types of cone operate in daylight but not dim light; rods operate only in dim light but not in daylight. Therefore, the retina is able to detect light over a wide range of intensities, from starlight to bright sunlight. And since there is only one type of rod, meaning one spectral type, colour vision is not possible at night. An important point about the photoreceptors is that they release their neurotransmitter glutamate in the dark, since they hyperpolarize to increases in light intensity and depolarize to decreases in light intensity.

The second class is the horizontal cells, which given their name, extend laterally across the retina and receive input from and give input to the photoreceptors. This interaction occurs in the outer plexiform layer (OPL, with 'plexiform' also meaning 'synaptic'). The dendrites of horizontal cells contact cones whereas the axon terminals contact rods (Kolb 1974). In the mouse there is only one type whereas in other species there are two. They play a key role in the adaptation, or modulation, of photoreceptor light sensitivity by providing negative feedback and lateral inhibition, mediated through electrical coupling that involves Connexin proteins. They have also been found to be presynaptic to dopaminergic amacrine cells (Chapter 1), a so-called 'interplexiform' cell (spans synaptic layers) that plays a role in light-dark adaptation (Viney et al. 2007, Witkovsky 2004).

The third class is the bipolar cells. These cell types are the principal excitatory neurons of the retina, and receive signals from the photoreceptor terminals in the OPL (Euler and Masland 2000). Their somata are located in the inner nuclear layer (INL) and their axon terminals in the inner plexiform layer (IPL). They are divided into two groups, those that depolarize for increases in light intensity ('light ON') - the ON bipolar cells - and those that depolarize for decreases in light intensity ('light OFF') - the OFF bipolar cells. Rod

photoreceptors, which are sensitive to dim light and therefore represent the first cell type of the 'night vision' pathway, only contact one type of bipolar cell, called the rod bipolar cell (Bloomfield and Dacheux 2001). This is a special ON bipolar cell type. The other bipolar cells, which contact cone photoreceptors (the components of the day vision pathway), are called cone bipolar cells and there are several ON types and OFF types. All ON bipolar cell types express metabotropic glutamate receptors, mGluR6 being the most highly expressed, which causes the bipolar cell to hyperpolarize in response to glutamate release (Nawy and Jahr 1990, Nawy and Jahr 1991). Thus at light ON, the photoreceptor hyperpolarizes and releases less glutamate, which activates the ON bipolar cells. OFF bipolar cells express ionotropic glutamate receptors, so that at light OFF, when the photoreceptor depolarizes and releases more glutamate, the OFF bipolar cells are activated. Therefore ON bipolar cells have sign-inverting synapses and OFF bipolar cells have sign-conserving synapses in their dendrites (see Fig. II). These two groups of bipolar cells separate the visual input into two pathways: ON pathways, transduced through ON bipolar cells, and OFF pathways, transduced through OFF bipolar cells (Bloomfield and Miller 1986). Furthermore, there are the night vision and day vision pathways: rod photoreceptors to rod bipolar cells, and cone photoreceptors to cone bipolar cells, respectively.

The fourth class is the ganglion cells, which are defined by their axons that form the optic nerve and project to the higher brain regions. Ganglion cells are the output neurons of the retina, and their spiking activity represents all the information that is transmitted to the rest of the brain (Berry et al. 1997, Gollisch and Meister 2008). Their somata are located in the ganglion cell layer (GCL, innermost layer of the retina), and receive synaptic input to their dendrites from bipolar cell axon terminals at different levels, or strata, in the IPL. The type of bipolar cell the ganglion cell contacts depends on the vertical position, or stratification, of that ganglion cell. Ganglion cells are often defined morphologically by their dendritic stratification (although Chapter 2 will redefine this description). All ganglion cells characterised so far receive input from cone bipolar cells. ON cone bipolar cells terminate in the inner levels of the IPL, closer to the GCL. OFF cone bipolar cells terminate in the outer

levels of the IPL, closer to the INL. In fact the bipolar cell types are organised by stratification (Ghosh et al. 2004). Furthermore, all ganglion cells express ionotropic glutamate receptors, so upon activation of the cone bipolar cells, glutamate is released leading to a depolarisation of the ganglion cell by an increase in the excitatory conductance. Therefore, ON and OFF bipolar cells have sign-conserving synapses with ganglion cells, so in general, an ON bipolar cell is said to be connected to an ON ganglion cell, and an OFF bipolar cell to an OFF ganglion cell. In a simple version of the retina, activation of the ganglion cell by an ON bipolar cell would cause the ganglion cell to fire action potentials at light ON, and vice versa for OFF ganglion cells. Ganglion cells represent a major part of this thesis, and can be used as readouts of retinal circuitry.

The fifth and final cell class is the amacrine cells. These cell types are generally inhibitory, and are essential for the spatiotemporal processing of all the neural circuits in the retina. Their somata are found in both the INL and GCL and they receive input from bipolar cells and other amacrine cells and provide input to bipolar cells, other amacrine cells and, importantly, ganglion cells. Therefore, amacrine cells provide both presynaptic and postsynaptic inhibition to ganglion cells. My thesis concentrates on the roles of these inhibitory neurons in the context of their dynamic interactions with the excitatory input to ganglion cells during light stimulation. The amacrine cell types represent a very diverse class of cells (MacNeil and Masland 1998). In general, narrowfield amacrine cells are glycinergic whereas widefield cells (mirroring in some respects the horizontal cells of the outer retina) are mostly GABAergic (Haverkamp and Wässle 2000). There is also a population of acetylcholinergic amacrine cells called starburst amacrine cells and dopaminergic amacrine cells but both also release GABA (O'Malley et al. 1992, Gustincich et al. 1997). One particularly interesting amacrine cell is the AII amacrine cell (Pourcho and Goebel 1985). It is used as a conduit or bridge between the rod pathway and the ganglion cells. In the rod pathway (night vision pathway), the rod bipolar cells do not contact ganglion cells. Instead they form ionotropic (sign-conserving) synapses with the AII amacrine cells (Fig. II). AII amacrine cells form electrical (and therefore sign-conserving)

synapses with ON cone bipolar cells via their dendrites found in the innermost level of the IPL. Therefore, signals at 'light ON' during the day reach the same ganglion cell with the same sign during the night. The rod pathway also connects with the OFF cone bipolar cells. Here, the AII amacrine cells have lobular appendages in the outer IPL (closer to the INL) that release glycine, inhibiting OFF bipolar cells (sign-inverting). This ensures that signals at 'light OFF' that would reach ganglion cells in the day also reach ganglion cells in the night, via a sign-inverting synapse (metabotropic, rod bipolar dendrites), a sign-conserving synapse (with the AII), another sign-inverting synapse (inhibiting the OFF bipolar cell), and finally a sign-conserving synapse with the ganglion cell. The rod/AII circuit appears to piggyback the cone pathway by taking advantage of the established cone bipolar cell-ganglion cell connections. The AII amacrine cell, in the context of day vision, is studied in Chapter 3.

Before introducing how inhibition can affect the firing rates of ganglion cells, two other concepts need to be addressed. First is centre-surround antagonism (Kuffler 1953). When a spot of light is presented to the retina, specifically over a single ganglion cell that is being recorded, that spot can cause an increase in the firing rate of the cell. Cells that fire at light ON are ON-firing cells and cells that fire at light OFF are OFF-firing cells. However, an interesting discovery was made when the light was presented in a ring around the centre (known as the surround). Here the cell did not fire at the onset of the light. Instead it fired at the offset. This suggested an antagonism between stimulating the centre of a ganglion cell receptive field, and stimulating in the surrounding area. Therefore, the light-evoked responses of ganglion cells were found to depend on the spatial position of the light. Technically, an 'OFF-firing' cell is an OFF-centre-ON-surround-firing cell and vice versa. These experiments demonstrated that ganglion cells respond not to absolute light levels but to the differences in central and surrounding light. In this thesis I always use full spots for visual stimulation, and not rings. What is the origin of this antagonism? It is clearly some form of feedback inhibition, and could arise from the horizontal cells in the outer retina. However, this is a form of spatial coding, and this thesis concentrates on temporal coding. An example of

temporal coding is direction selectivity (Barlow et al. 1964) and is addressed in Chapter 2.

So far the retina has been described by its vertical connections, meaning the flow of information from photoreceptors to bipolar cells to amacrine cells and ganglion cells. However, there are also lateral connections, involving gap junctions, which are formed by Connexin proteins. Ganglion cells can be coupled to other ganglion cells, as well as to amacrine cells (Völgyi et al. 2009). Amacrine cells can also be coupled to each other, and horizontal cells are known to be extensively coupled and express the Connexin57 protein (Homach et al. 2004). Coupling can be homotypic between ganglion cells (i.e. the same cell type is coupled). Examples of coupled ganglion cells are described in Chapter 2, and Chapter 3 examines a specific gap junction in the IPL that expresses Connexin36 and is involved in mediating a fast form of inhibition. Clearly, coupling is important for visual processing and should be taken into account when studying parallel local neural circuits.

Different forms of inhibition in the rabbit retina

An intriguing question to address in studying neural circuitry is how are the precise firing patterns established? It is known that retinal ganglion cells receive both excitatory input and inhibitory input, yet excitation alone is enough to make the cell fire, or not fire, and bipolar cells themselves seem to divide into sustained and transient subtypes, for both the ON and OFF pathway bipolar cells (Awatramani and Slaughter 2000). The inhibitory-excitatory interactions can be described as 'motifs', and the interaction of inhibition does lead to changes in the firing patterns of the ganglion cells, which are cell-type specific. From many semi-random recordings from rabbit ganglion cells, five motifs were discovered representing five cell types (Fig. III, by Botond Roska, unpublished observations). In the 'delay' motif, inhibition occurs at the same time as excitation, causing a delay in the firing, after light onset. In the 'truncation' motif, inhibition arrives slightly later than excitation, limiting the cell to fire only immediately after light onset. For the 'pause' motif, inhibition prevents the cell from firing continuously by interacting with excitation at light onset. In the 'cancellation' motif, inhibition completely blocks the influence of excitation at light ON, so that the cell only fires at light OFF.

Finally for the 'out of phase motif', inhibition appears to have no influence over the firing rate, since it occurs at light ON and not at light OFF. Here inhibition and excitation do not interact. What is the biological meaning of these motifs? When does inhibition interact with excitation, especially for the 'out of phase' motif? These questions will be addressed in Chapters 2 and 3.

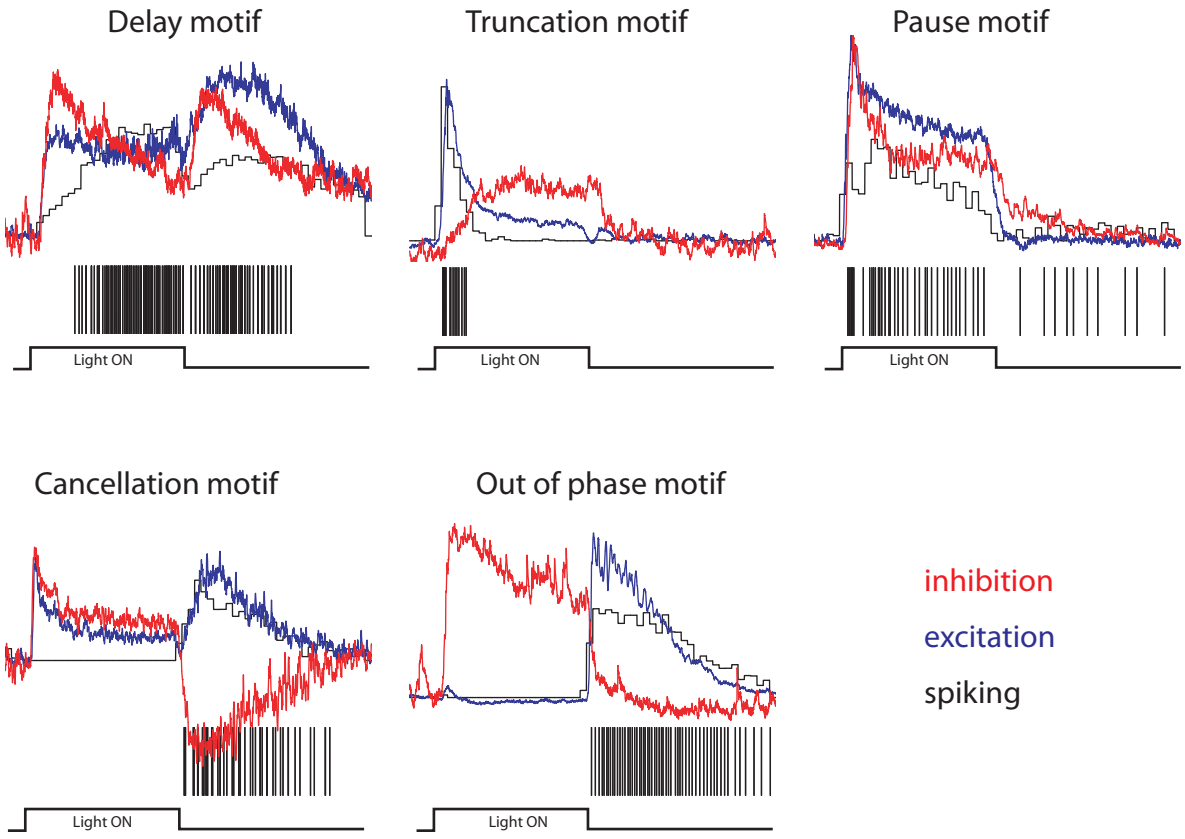

Figure III. Motifs in the rabbit retina for five ganglion cell types. Inhibition (red) and excitation (blue) represent the normalised currents isolated in voltage clamp mode (where excitation is flipped in order to compare with inhibition). Firing rate is shown in time bins and a representative spike train is shown below each motif. Light ON represents a flashed square of light presented to the centre of the ganglion cell for 1 second.

Figure III

Materials and Methods

Animals

Animal experiments were approved by the local Institutional Animal Care and Use Committee at the Friedrich Miescher Institute and the Veterinary Department of the Canton of Basel-Stadt. All experiments were conducted according to the guidelines of the Swiss National Foundation and European Communities Guidelines on the Care and Use of Laboratory Animals (86/609/EEC). For viral tracing experiments (Chapter 1), I used C57/BL6 (wild type) mice. For electrophysiological experiments (Chapters 2 and 3), I mainly used the Parvalbumin-Cre x Thy1-Stop-EYFP mouse line. This "PV mouse line" was generated by crossing knock-in Parvalbumin-Cre mice (Hippenmeyer et al., 2005) with Thy1-Stop-EYFP mice (Buffelli et al., 2003). In Parvalbumin-Cre mice, Cre recombinase is expressed under the control of the parvalbumin locus. In Thy1-Stop-EYFP mice, EYFP is expressed from a Thy1 promoter only in those cells in which the transcriptional STOP sequence flanked by LoxP sites has been removed by Cre recombinase (Metzger and Feil 1999). To establish the PV mouse line, I first back-crossed the heterozygous Thy1-Stop-EYFP mice to make all offspring homozygous. Once this was achieved, no further genotyping of the PV mouse line was necessary. In some experiments (Chapter 3), I recorded from Cx36 knock-out (-/-) mice (Deans et al. 2001). Cx36$^{-/-}$ mice are homozygous knockouts for the electrical synapse protein Connexin36. All mice used were at least 5 weeks old.

Retina preparation

All work was done under normal light levels (‘day vision’). This facilitated preparation and increased the time used for recording. Light-adapted mice were sacrificed by cervical dislocation and decapitated. Both eyes were enucleated using forceps and placed in warm Ringer’s medium (in mM: 110 NaCl, 2.5 KCl, 1 $CaCl_2$, 1.6 $MgCl_2$, 10 D-glucose, 22 $NaHCO_3$, equilibrated with 5% CO_2 and 95% O_2, pH 7.4) under ambient white light. The eye was pierced with a sharp blade at the cornea just above the sclera border to make a small hole; the cornea was cut away, and the lens was removed using

forceps. The retina was carefully exposed by pulling apart the sclera/choroid with forceps. Excess vitreous, pigment epithelium, and suspensory ligaments were carefully pulled away from the ganglion cell layer of the retina without touching the surface of the tissue. Next the retina was transferred to a recording chamber (Open Diamond Bath, Warner Instruments) and mounted with the ganglion cell layer facing up on nitrocellulose filter paper (MF-membrane, Millipore, USA), by stretching the tissue off-centre over a hole in the filter paper that was ~2/3 the diameter of the retina (a 'window'). This ensured a flat preparation, and the stretching facilitated cleaning for patching (see below). If the optic disk region became teared during retina isolation, the retina from the other eye was prepared. If not possible, the mounting procedure was modified to ensure the largest flat area possible was used over the window. The recording chamber preparation was placed on a heated stage under the microscope (see below) with a heated objective and superfused with Ringer's medium at 4-6 ml/min to obtain a temperature of 34.5-36^{0}C. Retinas were stable and light-responsive for at least 10 hours. In some experiments, the orientation of the retina relative to the mouse's eye position was marked. This was achieved by making a small hole with a 33 gauge needle on the temporal region of the eye (in the cornea, near the sclera border) prior to enucleation. Due to the loss of intraocular pressure, the eye in this case was removed with large curved forceps. The retina isolation was the same as above except that a small cut was made into the retina from the site of the hole; this location was recorded when mounting to the filter paper window, as well as which eye the retina came from.

Transsynaptic viral tracing

GFP expressing PRV152 (Smith, Banfield et al. 2000) and RFP expressing PRV614 (kindly provided by B.W. Banfield) (Banfield, Kaufman et al. 2003) Bartha strains were harvested from the PK-15 cell line as previously described (Smith, Banfield et al. 2000). I also used a modified Bartha strain PRV that expresses membrane-targeted green fluorescence protein (memGFP) (Viney et al. 2007). All the PRV work was done in a Biosafety Level 2 laboratory (there is no evidence of PRV being able to infect primates). 6-8 weeks old C57BL/6J mice were injected with 10^3-10^5 plaque forming units

of PRV152 in 1 µl Dulbecco's Modified Eagle Medium (DMEM) into the anterior chamber of the right eye under isoflurane anesthesia (2% in oxygen). The cornea was punctured with a 27-28 gauge needle and PRV152 was injected into the AntC using a 10 µl Hamilton syringe fitted with a 33 gauge needle. For labelling ganglion cells projecting to the Superior colliculus (SC) or to the Lateral geniculate I performed stereotaxic surgery. 10^4 plaque forming units of PRV152 in 100 nl DMEM was injected to either the SC or the Primary visual cortex (V1). Animals were kept in the same laboratory for up to 150 hours after injection. 3-6 days after PRV152 injection into the anterior chamber of the right eye, the left eye was removed and the retina was prepared as described above or fixed in 4% paraformaldehyde in PBS after isolation. For time-lapse imaging experiments of virus-labelled neural circuits, the retina was superfused for one day, and at every hour or half hour a two-photon z-stack of 80 images was acquired with 1 µm spacings (see below for two-photon imaging). At the end of the time-lapse imaging the retina was fixed in 4% paraformaldehyde in PBS and stained with antibodies to visualize the circuit at higher resolution.

Two-photon laser imaging and whole cell recording in the wholemount retina

Two-photon microscopy

To visualize and target fluorescently-labelled neurons in the live wholemount retina without causing bleaching of the photoreceptors, I built a custom two-photon microscope using a modified Nikon Eclipse E600FN microscope and a 5 Watt Millennia Pro pumped Tsunami laser (for experiments in Chapter 1), which was later exchanged with a Spectra-Physics Mai Tai Ti:sapphire laser (for experiments in Chapters 2 and 3). Fluorescence was generated using mode-locked two-photon excitation at 930 nm, attenuated by polarization (beam-splitter), modulated by a Pockels cell (Conoptics model 302), and scanned using mirrors mounted on galvanometers (Cambridge Technologies), which were imaged at the back-aperture of the objective (1.0 numerical apeture (NA) Nikon Fluor 60X water immersion) via the scan lens and tube lens. Energy output at the retina level was 5-20 mW. The fluorescence

emission was detected (~500-600 nm) by a photomultiplier tube (PMT, Hamamatsu model R3896). The retina was illuminated using a Digital Light Processing (DLP) projector (V332 PLUS with lens removed, 75 Hz refresh rate) with an infrared filter before the condenser lens, and detected by a EM-CCD camera (Hamamatsu model C9100). During two-photon excitation, the fluorescence signal detected by the PMT was digitally superimposed onto the infrared image detected by the CCD camera in real time using custom software (Imaginator) written in LabView (National Instruments). A representative composite image was saved and used for identifying the correct cell/area in the fixed tissue *post hoc* (see Fig. 2.1). The light paths and corresponding filter sets of the two-photon microscope are shown in Figure IV.

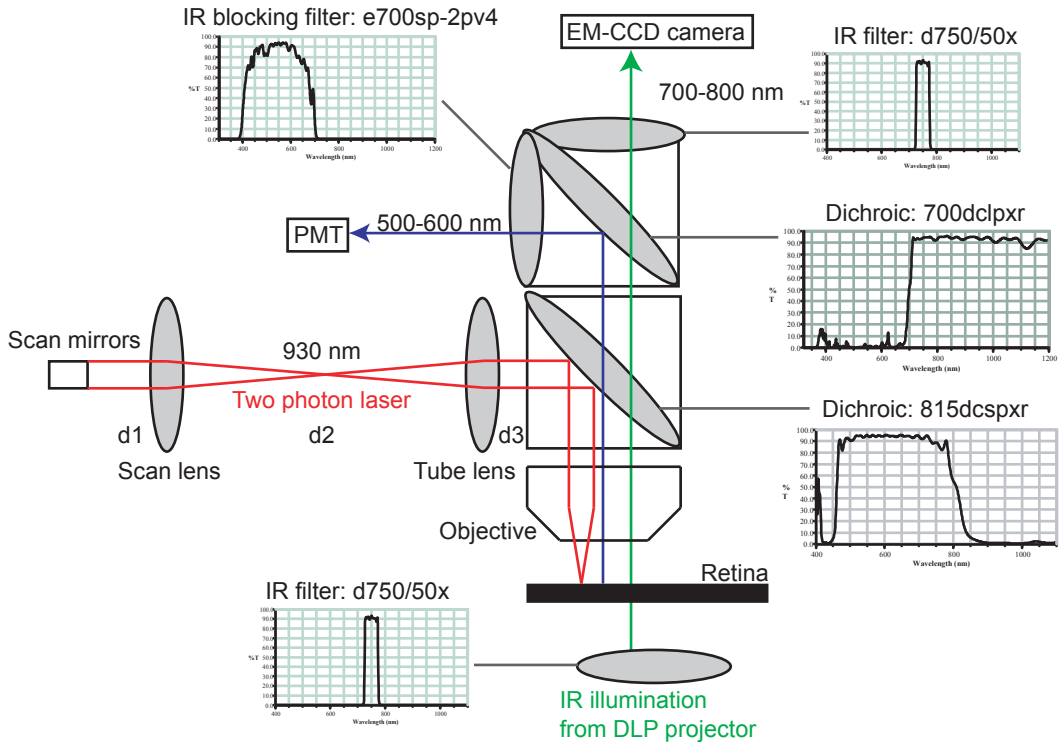

Figure IV. The two-photon microscope. Collimated pulsed laser light is scanned using scan mirrors, aligned with the scan lens and tube lens, reflected with an 815 nm short pass (sp) dichroic mirror, and focussed onto the retina with the objective lens. Emitted fluorescence (from two-photon excitation only at the focal point) passes through the 815sp dichroic mirror and is reflected by a 700 long pass (lp) dichroic mirror and detected by the PMT. The retina is also illuminated from below, through the condenser lens, with infrared light, which is detected by the CCD camera. Graphs show percentage of light transmission (%T) through filters across different wavelengths (nm). d1 = distance between scan mirrors and scan lens (100 mm), d2 = distance between scan lens and tube lens (300 mm), d3 = distance between tube lens and back aperture of objective lens (200 mm). Scan and tube lens focal lengths: fs = 100 and ft = 200 mm, respectively (d2 = fs + ft). To image the galvanometers at the back aperture of the objective, d1 = fs and d3 = ft.

Figure IV

Cleaning the ganglion cell layer

Direct visualization of the patch pipette was used to target all fluorescently-labelled neurons. For all experiments that used the PV retina (Chapters 2 and 3), the YFP-expressing ‘PV cells’ were targeted by acquiring two-photon z-stacks of a chosen area of the PV retina and selecting the PV cell type based on soma size and depth/pattern of primary dendrites. Since light must pass through the entire retina to reach the photoreceptors (see Introduction), the retina from the ganglion cell layer to the photoreceptor layer has a uniform refractive index and low contrast. Curiously, Müller glia, which span the entire retina, act as 'optical guides' and ensheath the neurons, which contributes to the optical clarity of the tissue, hence efficient light propagation (Franze et al. 2007). Consequently, retinal ganglion cell somata are 'hidden' or 'buried' within the ganglion cell layer (Fig. Va). To reveal the cells, the region around the targeted neuron was ‘cleaned’ using a borosilicate glass pipette (BF100-50-10, Sutter Instruments) containing filtered Ringers solution (5-7 MΩ tip). Strong mouth pressure was used along with small rapid lateral movements on the very surface to create a ‘cleaning wave’. This distributed Ringers solution into the tissue to generate higher contrast (by disrupting the Müller glia end feet) (Fig Vb). Large (global) and local cleaning waves were more frequent if the region of interest was very flat. Next, the end feet of Müller glia were removed from the vicinity of the targeted neuron by moving the pipette laterally then briefly vertically (above the tissue) then again laterally. After general cleaning, the neuron was locally cleaned by carefully revealing the cell membrane with the pipette. Once a dimple was visible by touching the membrane with the cleaning pipette, loose cell-attached patch could be performed (Fig. Vb).

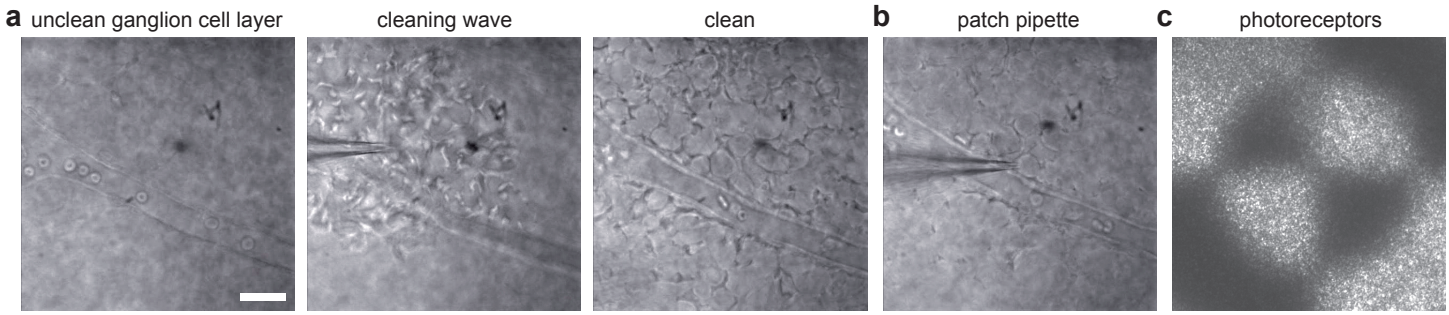

Figure V. Wholemount mouse retina preparation (infrared illumination). (a) Left, 'unclean' translucent ganglion cell layer visualised with the CCD camera. Middle, 'cleaning wave' from pipette solution. Right, 'clean' ganglion cell layer with resolvable somata. Note blood vessel with red blood cells, which move during manipulation of the tissue. (b) A patch pipette on a locally-cleaned ganglion cell. (c) 'Bullseye' image focussed on the photoreceptors. Scale bar for all images: 20 µm.

Figure V

Patch clamp recordings

For whole-cell voltage clamp recordings, the cleaning pipette was replaced with a patch pipette (7-8 MΩ tip with the following filtered intracellular solution in mM: 112.5 $CsMeSO_4$, 1 Mg SO_4, 7.8 x 10-3 $CaCl_2$, 0.5 BAPTA, 10 HEPES, 4 ATP-Na_2, 0.5 GTP-Na_3, 5 lidocaine N-ethyl bromide (QX314-Br), 7.5 neurobiotin chloride (to fill the cell for *post hoc* analysis), adjusted to pH 7.2). In patch electrodes for amacrine cells (Chapter 3), QX314-Br was substituted by 5 CsCl, and BAPTA by 0.1 EGTA; $CsCH_3SO_3$ was adjusted to 113.7 mM. The caesium and QX314 in the intracellular solution were used to improve stability of the voltage clamp, by blocking voltage-gated potassium and sodium currents, respectively. Immediately after giga-seal formation and break-in, capacitative transients were compensated. For current-voltage relations, holding potentials were adjusted by -10 mV to account for the liquid junction potential that forms between the electrode and the patch of cell membrane. Images and movies were presented to the photoreceptor layer of the retina (focussed and centred with the condenser lens and a 'bullseye' image prior to recordings, Fig. Vc) using the DLP projector at a magnification of 3.75 µm per pixel. The infrared filter was exchanged with neutral density filters using a filter wheel (FW102, ThorLabs) and the PMT was switched off or the PMT shutter was closed. The background illumination was grey, so that both positive and negative contrasts could be presented (for example, black and white spots of different sizes), and all experiments were performed in the photopic (daylight, cone-sensitive) range. For presentation of natural scenes, movie frames were taken from a video camera mounted to the head of an exploring cat (Kayser et al. 2003, Betsch et al. 2004). To convert into a format for the mouse, images were scaled given that a one degree visual angle is 31 µm on the mouse retina (Remtulla and Hallett 1985, Yonehara et al. 2009). Images were scaled up by a factor of 6.86/x using bicubic interpolation, where x is the µm per pixel ratio of the DLP projector, and displayed at a frame rate of 75 Hz. All light-evoked activity was measured using a Multiclamp 700A or B amplifier (Axon Instruments) and recorded using custom software (Presentinator) written in LabView. Extracellular (spike) recordings were sampled at 10 kHz with a 4 kHz Bessel filter. Whole cell recordings were downsampled by a factor of 10 and filtered at 1 kHz. Excitatory and inhibitory

currents were isolated by voltage clamping the cell at the equilibrium potential of chloride (-60 mV) and the reversal potential of nonselective monovalent cations (0-20 mV), respectively. In pharmacological experiments, agents were bath-applied at the following concentrations: 10 mM CPP, 10 mM NBQX, 10 mM APB, 10 mM strychnine. All chemicals were obtained from Sigma, with the exception of APB (Calbiochem), ATP (Labforce) and neurobiotin (Vector Laboratories). To visualize the detailed morphology of the cell after recording, Alexa Fluor 488 or Lucifer Yellow was sometimes added to the intracellular solution and two-photon z-stacks were acquired at 930 nm excitation. Due to the high signal intensity from the dye, the dendrites of the recorded cell could be easily resolved from other YFP or GFP positive neurons. Targeted neurons were at least 0.5 mm from the optic disk, where axon bundles were less dense. Neurons in the extreme periphery were not recorded since they were over the filter paper. All data were analyzed offline in Mathematica (Wolfram Research).

Recording from AII amacrine cells in the wholemount retina

The following paragraph describes my strategy for recording from AII amacrine cells in the wholemount retina. First a hole was made in a small cleaned area of the GCL using a pipette filled with extracellular solution (3-6 MΩ) and strong positive mouth pressure. Under infrared illumination, a large step motor mode from the micromanipulator was used to produce robust movements, so that a hole was made by moving the pipette fast through the tissue, mostly laterally (x-dimension), until reaching the INL. The pipette was withdrawn, revealing a 'tunnel'. Next, a patch electrode (filled with Cs-based solution, 7.5 MΩ, positive mouth pressure, see above), was guided through the tunnel to the IPL-INL border. AII amacrine cells have small somata, and represent approximately one third of the somata in the innermost INL (see Chapter 3), giving a 33% probability of patching an AII. Before attempting to patch, the pipette was pushed further into the INL laterally (x-dimension), until an ' INL barrier' was overcome (indicated by the tissue relaxing back and not being stretched anymore by the pipette). This allowed a greater degree of freedom when moving the pipette tip. If the pipette resistance was still 7.5

MΩ, indicating no blockages, the tip was advanced towards a soma. Small lateral movements (y-direction) were carried out to 'locally clean' the cell, making the cell membrane more visible. If there were fluctuations in the pipette resistance upon approaching the membrane with the pipette tip, pressure was released to form a gigaseal, and the standard break-in procedure for whole-cell patch clamp was used. Interestingly, patching with K-based intracellular solutions was not effective. Gigaseal formation was not possible under these conditions; consequently only whole-cell voltage clamp could be used with the Cs-based solution. In the photopic conditions that I used, AII amacrine cells had an inward current at light ON, and a drop in the baseline current at light OFF. Morphological evaluation was also used, by acquiring two-photon z-stacks if Alexa Fluor 488 was included in the pipette solution (see Fig. 3.5).

Paired recordings from ganglion cells and connected amacrine cells

The success of my paired recording strategy was dependent on the order of events. Paired recordings were made between fluorescently-labelled PV-5 ganglion cells in the GCL (see Chapters 2 and 3) and unlabelled amacrine cells in the innermost INL. First, a PV-5 cell was identified from a two-photon z-stack, cleaned, and confirmed by light-evoked spiking activity (fires transiently at light OFF, at all spot sizes, see Chapter 2). Next, the hole in the GCL and tunnel to the INL were made to the side of the PV-5 cell, so that the final position for the amacrine cell pipette would be within the dendritic field of the PV-5 cell, identified from the two-photon z-stack. Two intracellular patch pipettes were positioned near the PV-5 cell: one for the PV-5 cell and another for the amacrine cell. Since the tissue moves when the amacrine cell pipette is advanced, the ganglion cell pipette could only be used once the amacrine cell was patched. Therefore, first the amacrine cell was patched as described above, and held in voltage clamp mode at -60 mV. Then the PV-5 was patched with the other pipette without moving the GCL. To record light-evoked activity from both cells, the infrared filter before the condenser was exchanged with neutral density filters and various light stimuli were presented. Usually the soma of the ganglion cell was positioned in the centre of the screen by carefully moving the stage. To test for a connection between the amacrine cell

and ganglion cell, first the infrared filter was put back, so that the baseline currents of the cells were stable. Switching from bright light to infrared temporarily reduces synaptic noise (see Chapter 3). Due to this trick, any evoked inputs greater than 10 pA could be detected above baseline in the PV-5 cell, as long as the synaptic noise was low. Noise increased (adaptation) after 1-2 minutes in the dark. To evoke an input to PV-5, the amacrine cell was depolarized from rest (-60 mV) to 0 mV for 1-2 seconds whilst holding the PV-5 cell at 20 mV so that only inhibitory conductances were measurable. If there was no connection, it was most likely that the amacrine cell was not an AII cell. Sometimes a widefield amacrine cell was patched (a so-called 'A17' amacrine cell type), and was never connected to PV-5, and had a slow sustained excitatory input at light ON and very thin radial processes extending beyond the field of view of the two-photon microscope. Since AII cells are homotypically coupled (Mills et al. 2001), it is unlikely that a patched AII within the dendritic field of the PV-5 cell could not evoke a direct or coupled inhibitory input. For pharmacological blockade of AII amacrine cell mediated inhibition, strychnine (an antagonist for glycine receptors) was applied by transferring the superfusion tubing to a separate bottle of Ringers solution that contained strychnine. A small air bubble was tracked to calculate the initial time of drug application, but the bubble had to be small enough to minimise any movement of the retina that could cause a loss of the patch clamp. Surprisingly, the amacrine cell patch was more stable than the ganglion cell patch. The former was less sensitive to tissue movement probably due to the buffering effect of the tunnel walls around the pipette. If the patch was lost for the ganglion cell during drug application, the PV-5 cell could be easily repatched with another pipette. If the amacrine cell was lost, it was not possible to repatch since the ganglion cell patch would be disrupted during removal of the amacrine cell pipette from the tunnel. Neurobiotin was included in the patch pipettes for *post-hoc* analysis. Occasionally, Lucifer Yellow, a fluorescent dye which also can be detected by an antibody, was added to the intracellular solution for the PV-5 cell instead of neurobiotin, to distinguish it from the amacrine cell.

Immunohistochemistry

The retina was immediately fixed after the experiment in cold 4% paraformaldehyde in phosphate buffered saline (PBS) at pH 7.4 for 30 minutes and incubated at 4^0C for >1 d. To allow greater antibody penetration, retinas were cryoprotected in 30% sucrose solution and rapidly freeze-thawed 3 times on a glass slide on tissue paper over dry ice (only for experiments in Chapters 2 and 3). For long term storage, the retina was embedded in 30% sucrose solution and kept at -80^0C. For vibratome sectioning, the retina was embedded in 2% agar in PBS and cut into 100-200 µm thick sections using a Leica VT 1000 S vibratome. For brain slices, the whole brain was embedded in 2% agar in PBS and vibratome sectioned to 200 µm thick sections. The antibody staining procedure for both wholemount and vibratome sections were the same and were carried out at room temperature. After 3 washes in PBS, the retina was blocked for 1 hour with a solution of 10% normal donkey serum (NDS) or 10% normal goat serum (NGS), 1% bovine serum albumin (BSA), 0.5% Triton X100 in PBS, and 0.02% sodium azide in PBS at pH 7.4. Next, the retina was incubated in primary antibody solution containing 3% NDS, 1% BSA, 0.5% Triton X100, and 0.02% sodium azide in PBS. For experiments in Chapter 1, the retina was incubated for 3 days. For Chapters 2 and 3, which used the choline acetyltransferase (ChAT) primary antibody, incubation was at least 6 days. The following antibodies and dilutions used were: rabbit anti-GFP 1:200 (or 1:500 for sections) which also binds EYFP (Molecular Probes), rabbit anti-RFP 1:200, sheep anti-GFP 1:200 (Biogenesis), rabbit anti-Melanopsin 1:5000 (gift from I. Provencio, Uniform Services University, Bethesda, MD, USA), goat anti-ChAT 1:200 (Chemicon), mouse anti-Calretinin 1:1000-2000 (Chemicon), mouse anti-Glutamine Synthetase 1:200 (Chemicon). After 3 washes in PBS, retinas were incubated in secondary antibody solution for at least 2 hours (same base solution as primary). The antibodies and dilutions used were: donkey/goat anti-rabbit/anti-sheep Alexa Fluor 488/633 1:200 (Molecular Probes), donkey anti-goat Alexa Fluor 555/633 1:200 (Molecular Probes), donkey anti-mouse/anti-rabbit Cy3/Cy5 in 50% glycerol 1:100 (Chemicon). After 3 washes in PBS, the retina was incubated overnight in a 0.5% Triton X100 in PBS solution with 2-10

mg/ml DAPI 1:200 (Roche Diagnostics) which labels cell nuclei, and Streptavidin conjugated to Alexa Fluor 555 or 568 1:200 (Invitrogen) which binds neurobiotin. If the retina did not include neurobiotin-filled cells, DAPI was added with the secondary antibody solution and the overnight step was skipped. After 3 washes in PBS, the retina was mounted ganglion cell layer facing up on a glass slide inside a parafilm window (a spacer to avoid crushing the retina; not used for early experiments) with ProLong antifade mounting medium (Invitrogen) and a coverslip. Slides were sealed with nail polish.

Confocal imaging and image quantification

A Zeiss LSM 510 Meta confocal microscope was used to generate images from antibody-stained retinas. The 405 nm, 488 nm, 543 nm and 633 nm lasers were used to excite DAPI (cell nuclei, marking borders of retinal nuclear layers), Alexa Fluor 488 (virus-labelled cells in Chapter 2 and PV cells in Chapter 2), Alexa Fluor 555/568 (neurobiotin-filled cell or sometimes ChAT marker), and Alexa Fluor 633 (ChAT marker) or Cy5 (Calretinin marker), respectively. For top-view morphologies, a 1.3 NA Plan-Neofluor 40X oil immersion objective was used without zoom with a 512 x 512 lateral pixel resolution. Z-stacks were acquired with 1 mm spacing for 2 mm optical slices with a linescan average of 2. Somata were saturated so that the dynamic range filled the pixel intensities of the dendrites. 2x2 to 4x4 xyz tile scans were carried out for very large cells or for several cells within one region (also for the tile scan in Fig. 1.2b). For side-view morphologies of PV cells (n > 145 cells, Chapter 2), a 1.4 NA Plan-Apochromat 63X oil immersion objective was used also with a 512 x 512 lateral pixel resolution but cropped to a region of interest (usually the proximal dendrites). Z-stacks were acquired with 0.35 mm spacing for 0.7 mm optical slices with a linescan average of 2. The scan region was between the GCL and the INL; these images were used for quantification of dendritic stratification (Fig. 2.2).

To determine the dendritic depths of PRV-labelled ganglion cells (Chapter 1), confocal stacks of 170 ganglion cells were acquired using an automatic stage controlled by Auto Time Series Macro software (Rabut and Ellenberg 2004).

In each imaging session 20-30 ganglion cells per retina were marked and confocal z-stacks were acquired at each location using the 63X, 1.4 NA objective lens. The z steps were 0.2-0.35 µm. The scan started at the ganglion cell layer and continued until the photoreceptor layer. The depth of dendritic ramification for each labelled ganglion cell was determined from the DAPI and Alexa 488 stacks (Viney et al. 2007). Briefly, the dendritic depths were automatically determined relative to the GCL border and the INL border using an algorithm written in Matlab (Math Works). The GCL border (0% depth) was defined as the depth of the peak DAPI fluorescence in the GCL (Fig. 1.1d), and the INL border (100% depth) was defined as the depth where the DAPI florescence was 66% of the maximum measured in the INL (Fig. 1.1d). Dendritic depths were calculated locally near each dendritic segment to eliminate artifacts caused by the fact that the retina is not entirely flat. In Chapter 2, depth quantification was based on the ChAT marker bands, which are independent of any artifacts (see below). To reconstruct the detailed 3D morphology of PRV labelled amacrines cells that were further away from the ganglion cell body, several overlapping image stacks were acquired and stitched together by an algorithm that calculated the correlation between neighbouring frames in the ganglion cell layer of DAPI labelled stacks. The stitching algorithm was implemented in Mathematica (Wolfram Research). 3D visualization for Fig. 1.1c was done using Imaris imaging software (Bitplane). Colocalisation of Calretinin and GFP in the INL (Fig. 1.5a) was quantified by the following algorithm in Mathematica: confocal scans were acquired at a number of locations in the INL for DAPI, Calretinin and GFP. From the DAPI scan the location of every cell nucleus was determined. Next, the GFP and Calretinin channels were thresholded and for each nucleus the number GFP and/or Calretinin positive pixels around the nucleus were counted in a fixed window and plotted in Fig. 1.5b. The horizontal axis shows the number of GFP positive pixels and the vertical axis shows the number of Calretinin positive pixels for each cell.

Confocal images of PV cells (Chapter 2) were analysed in Mathematica and ImageJ (National Institutes of Health). Using custom software written in Mathematica (Münch et al. 2009), peak pixel intensities from multiple small

regions of interest from the side-view morphology image stacks were quantified for DAPI, neurobiotin, and ChAT to find the relative dendritic stratification of the recorded neurobiotin-filled PV cell (Fig. 2.2). The quantification was normalised to the two ChAT marker bands, since these bands form two continuous strata within the IPL (Famiglietti 1983). The nuclear layers either side of the IPL (defined by DAPI) are discontinuous and therefore less reliable for quantification. The peak intensity of the ChAT band nearest the GCL was defined as 0% depth (ON ChAT band); that nearest the INL was defined as 100% depth (OFF ChAT band). The peak intensities of DAPI relative to the ChAT bands defined the GCL border (mean -135% depth) and INL border (mean 200% depth). To quantify relative dendritic stratification of the PV cell, the peak intensities of many proximal dendrites were measured, and the mean and standard error of the mean (SEM) were calculated. The thickness of each ChAT and Calretinin band (Fig 2.2a) was determined by interpolation, taking the full width at half the maximum of the fitted gaussian of each band from representative images. The thickness relative to the peaks of each ChAT band were estimated as: ChAT/Calretinin ON band -15 to 15%, Calretinin middle band 30 to 60%, ChAT/Calretinin OFF band 85 to 115% depth. The dendritic area of each recorded neurobiotin-filled PV cell was measured in ImageJ by fitting a polygon around the dendritic field from a maximum-intensity z-projection of the cell (Alexa Fluor 555 or 563 channel, top-view image stacks). For bistratified cells, separate z-projections were made for each stratum and measured independently. Two-dimensional clustering of stratification (s) and area (a) was calculated in Mathematica using Euclidean distance, $\sqrt{(\sum(s - a)^2)}$ and the agglomerative method of clustering with Ward's minimum variance dissimilarity.

To calculate the percentage of YFP-positive ganglion cells (the PV cells) in the PV retina, I counted YFP-positive somata in 325 x 325 mm confocal images of the GCL for 52 retinas (Alexa Fluor 488 channel, top-view image stacks). Based on my measurements and those of (Jeon et al., 1998), it is estimated that in the BL6 mouse strain (Williams et al., 1996), there are >8000 neurons in the GCL, and ~41% are ganglion cells. I converted the cell counts from the confocal scans into mm^2 and computed the percentage of

labelled cells versus unlabelled cells ± SEM (see Chapter 2). Data were taken from adult PV mice of both sexes between 6-20 weeks of age. Occasionally a PV mouse had an unusually large proportion of YFP-expressing cells; these outliers were not included in the statistics.

Physiological quantification

Several physiological parameters were used to quantify the light-evoked spiking activity and motifs of retinal ganglion cells (Chapter 2), based on flashed spot stimuli of different sizes (Fig. 2.3a). To calculate whether a cell was predominantly an ON-firing or OFF-firing cell, first the mean background firing rate was subtracted from the recording. Next the spikes were counted for light onset and light offset of each spot in the stimulus (black or white spots), and given a value between 1 and -1 based on which sign (onset or offset) had the most spikes. The firing index was calculated from the mean value over the entire stimulus set. The sustained-transient ratio was the ratio between the number of spikes within the first 500 ms of the spot stimulus and the last 500 ms. The surround inhibition ratio was calculated by dividing the number of spikes for the largest spot by the spot that evoked the maximum number of spikes. Calculation of the direction selective index was based on a method previously described (Taylor and Vaney 2002). I used the following function written in Mathematica (below), where *d* = direction selective index, *s* = list of spike counts for all directions, and *v* = direction of moving spot. A value of 0 indicates no direction selectivity (equal spike count in all directions), and 1 indicates full direction selectivity (all the spikes occurred for only one direction). Rise time for inhibition and excitation (Table 3) was calculated by fitting a half gaussian to the curve after the stimulus change and measuring the times at 10% and 90% of the peak.

```
d(s) = |∑Table[((Cos((v 2 π)/Length[s]) + Sin((v 2
π)/Length[s])) s[[v]])/∑s, {v, Length[s]}]|
```

Chapter 1: Local retinal circuits of melanopsin-containing ganglion cells identified by transsynaptic viral tracing.

Intrinsically photosensitive, melanopsin-containing retinal ganglion cells (ipRGCs) control important physiological processes including the circadian rhythm, pupillary reflex and suppression of locomotor behaviour (reviewed by Fu et al. 2005). The ipRGCs are also activated by classical photoreceptors, the rods and cones, through local retinal circuits (Belenky et al. 2003, Dacey et al. 2005). The ipRGCs can be transsynaptically labelled through the pupillary reflex circuit with the derivatives of the Bartha strain of the alphaherpesvirus pseudorabies virus (PRV) (Card 2000, Sollars et al. 2003) that express GFP (Jons and Mettenleiter 1997, Boldogkoi et al. 1999, Smith et al. 2000, DeFalco et al. 2001, Boldogkoi et al. 2002, Pomeranz et al. 2005, Yoon et al. 2005). Bartha strain derivatives spread only in the retrograde direction (Pickard et al. 2002). There is evidence that infected cells function normally for a while during GFP expression (Smith et al. 2000). Here I combine transsynaptic pseudorabies virus (PRV) labelling, two-photon laser microscopy and electrophysiological techniques to trace the local circuit of different ipRGC types in the mouse retina and record light-evoked activity from the transsynaptically labelled ganglion cells. First I show that ipRGCs are connected by monostratified amacrine cells that provide strong inhibition from cone-driven circuits. Second I show evidence that dopaminergic interplexiform cells are synaptically connected to ipRGCs. The latter finding provides a circuitry link between light-dark adaptation and ipRGC function.

PRV152 labels morphologically distinct retinal ganglion cell types

To transneuronally label ipRGCs via the autonomic circuits, I injected PRV152 into the anterior chamber of the right eye of mice (Fig. 1.1a, (Pickard et al. 2002, Sollars et al. 2003, Smeraski et al. 2004)). After 3.5-4.5 days I isolated

the retina from the left eye (n = 36 retinas), where several ganglion cells were brightly labelled with GFP (Fig. 1.1b).

Dendrites of mouse retinal ganglion cells of different morphological and physiological types (Sun et al. 2002, Kong et al. 2005, Coombs et al. 2006) ramify at different depths (strata) in the inner plexiform layer (IPL) (Masland 2001, Wässle 2004). All of 170 analysed GFP-expressing ganglion cells in the left retina were found to have dendrites in only two IPL strata at depths of 30% (± 4%) and 89% (± 6%) that were above and below the two outer strata labelled by the calretinin antibody ((Haverkamp and Wässle 2000), Fig. 1.1c, d) and in the same strata specifically labelled by melanopsin antibody (Fig. 1.1c, d). In the brain similar retinorecipient nuclei were labelled bilaterally (Fig. 1.1e) as described in hamsters and rats (Card et al. 1991, Pickard et al. 2002) including the Suprachiasmatic nucleus (SCN), the Intergeniculate leaflet (IGL), and the Olivary pretectal nucleus (OPN). The Dorsal lateral geniculate nucleus (dLGN) and the Superior colliculus (SC) were not labelled even at 5 days after injection (Fig. 1.1e). Ganglion cells in other retinal strata can be labelled from the Superior colliculus and Primary visual cortex (V1), ruling out the possibility that only certain types of ganglion cells have receptors for PRV (Fig. 1.2a). These experiments suggest that contralateral PRV152 infection into the anterior chamber labels specific types of mouse ganglion cells that project to the SCN, IGL and OPN, which are known targets of melanopsin-expressing ganglion cells (Hannibal and Fahrenkrug 2004, Hattar et al. 2006).

3.5-4 days after virus infection 99% (79/80 cells counted from two infected retinas) of the labelled cells were melanopsin positive whereas the fraction among all ganglion cells is estimated at 1-2% (Hattar et al. 2002, Sekaran et al. 2003), suggesting that at early times almost all labelled ganglion cells are ipRGCs. However, around 5 days after virus infection only 50% of the GFP expressing ganglion cells were positive for melanopsin (Sollars et al. 2003). One explanation is that these non-ipRGC types also project to the SCN, IGL and OPN since at 5 days the dLGN and the SC are not labelled (Fig. 1.1e). An alternative explanation is that PRV spreads through gap junctions to other types of ganglion cells (Sekaran et al. 2003).

The PRV-infected ipRGCs could be classified into three types based on their depth of dendritic ramification. Figure 1.1f shows examples of melanopsin and GFP double-stained ganglion cell types. Each type could be found at all eccentricities (Fig. 1.2b). Type 1 ipRGCs (n = 66) have dendrites close to the inner nuclear layer (INL); Type 2 ipRGCs (n = 69) have dendrites close to the ganglion cell layer (GCL); and Type 3 ipRGCs (n = 35) are bistratified, having dendrites in the same strata as Type 1 and 2 cells (Fig. 1.1f).

Figure 1.1. PRV152 retrogradely spreads from the right eye to specific types of ganglion cells in the left retina. (a) Simplified schematic of the PRV spread (Smith, Banfield et al. 2000; Pickard, Smeraski et al. 2002). Red arrows indicate the route of retrograde virus spread from the right eye to the contralateral retinal ganglion cells (RGCs). (b) Low-resolution confocal scan of the left retina 4 days after injection showing several GFP-labelled ganglion cells. Scale bar, 100 µm. (c) Confocal reconstruction from a 200 µm thick vibratome section. Calretinin antibody (blue) labels three strata in the IPL (CR1, CR2 and CR3). Cell nuclei are labelled with DAPI (red). Melanopsin antibody (yellow) labels two strata (MO1 and MO2). (d) The depths of dendritic ramification of PRV152-labelled ganglion cells are plotted as green dots. Monostratified cells are presented by one dot, bistratified ganglion cells as two dots. The fluorescence as a function of depth is plotted for calretinin (blue), DAPI (red) and melanopsin (yellow). X-axis shows the relative depth in the IPL, Y-axis shows normalised fluorescence. (e) Brain regions labelled 5 days after injection of PRV152 into the anterior chamber (AntC) of the right (R) eye and PRV614 (RFP expressing variant) to the left (L) visual cortex. PRV152 (green) labels the EWN, OPN, IGL, SCN and hypothalamic paraventricular nucleus (PVN) but not the Superior colliculus (SC) or Sorsal lateral geniculate nucleus (dLGN). PRV614 (red) labels the dLGN. Diagrams are taken from The Mouse Brain Atlas (Paxinos and Franklin). (f) GFP-labelled ipRGC types in the left retina 3.5-4 days after PRV152 injection into the anterior chamber of the right eye. Colocalisation with GFP (green) and melanopsin (red) antibodies is shown. Arrows indicate somata. Side views are shown below top views and indicate dendritic stratification in the IPL between the INL and GCL (marked by DAPI, blue). Scale bars, 20 µm.

Figure 1.2. Morphological types of retinal ganglion cells. (a) Examples of GFP-labelled ganglion cells 4 days after PRV152 injection into SC. Side views are shown below top views and indicate dendritic stratification in the IPL between the INL and GCL (marked by DAPI, red). Scale bars, 100 µm. (b) Confocal z-projection of a retina montage stained with melanopsin antibody (left). Scale bar, 500 µm. Note that Type 1 ipRGCs were the most intensely melanopsin stained cells. Right: magnification of two strata in the IPL closer to INL (above) and GCL (below). Both Type 1 and Type 2 cells covered and tiled the retina. Mean dendritic diameters were 410 ± 28 µm (Type 1) and 230 ± 52 µm (Type 2) with a mean distance between cell bodies of 250 ± 59 µm (Type 1 cells) and 95 ± 36 µm (Type 2 cells). The coverage factors for Type 1 and 2 cells were 2.5 and 4.8, respectively. Type 3 cells were not quantified.

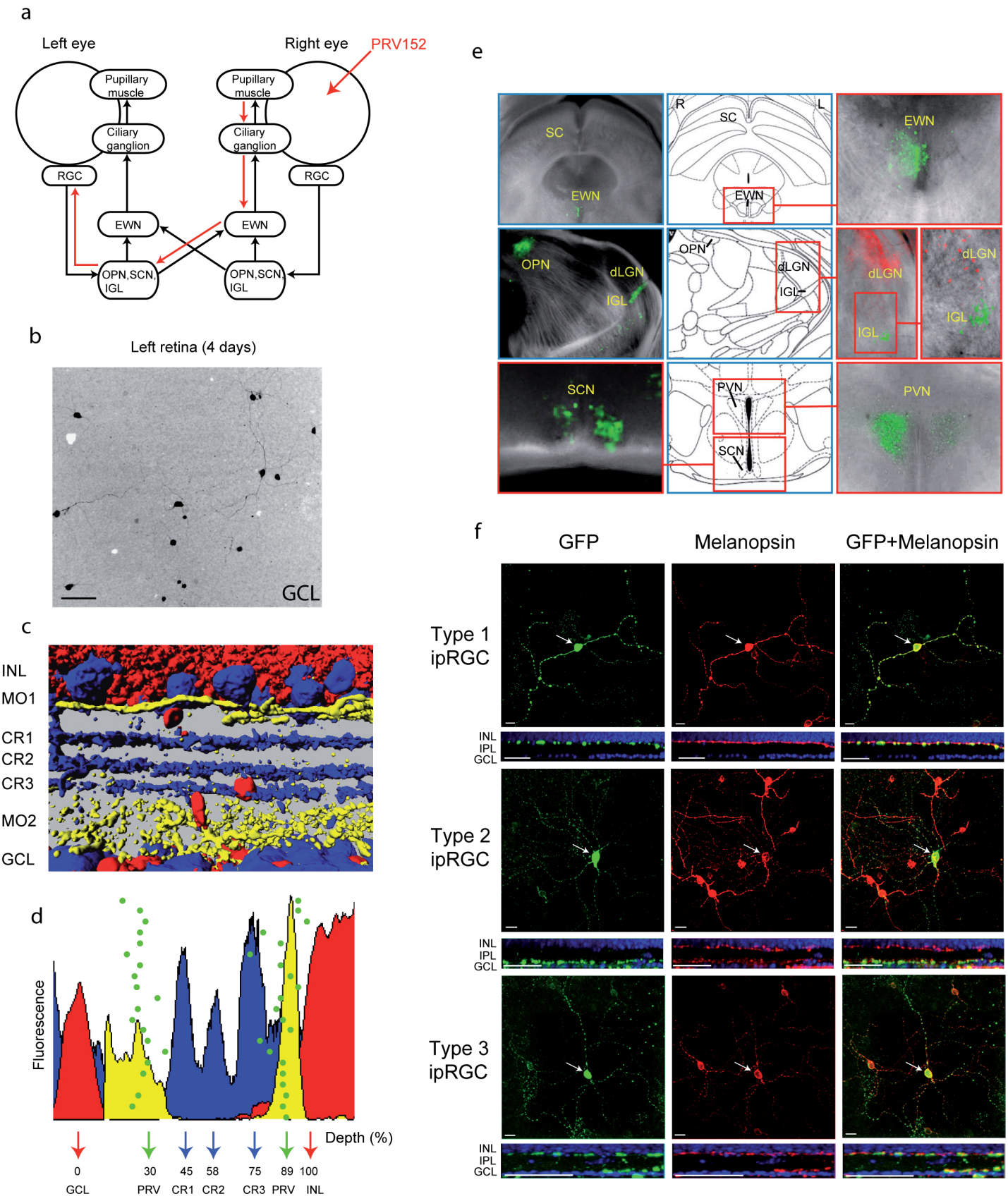
a
Left eye
Right eye
PRV152
Pupillary muscle
Ciliary ganglion
RGC
EWN
OPN,SCN, IGL
b
Left retina (4 days)
GCL
c
INL
MO1
CR1
CR2
CR3
MO2
GCL
d
Fluorescence
Depth (%)
0 GCL
30 PRV
45 CR1
58 CR2
75 CR3
89 PRV
100 INL
e
SC
EWN
R
L
OPN
dLGN
IGL
SCN
PVN
f
GFP
Melanopsin
GFP+Melanopsin
Type 1 ipRGC
Type 2 ipRGC
Type 3 ipRGC
INL
IPL
GCL

Figure 1.1

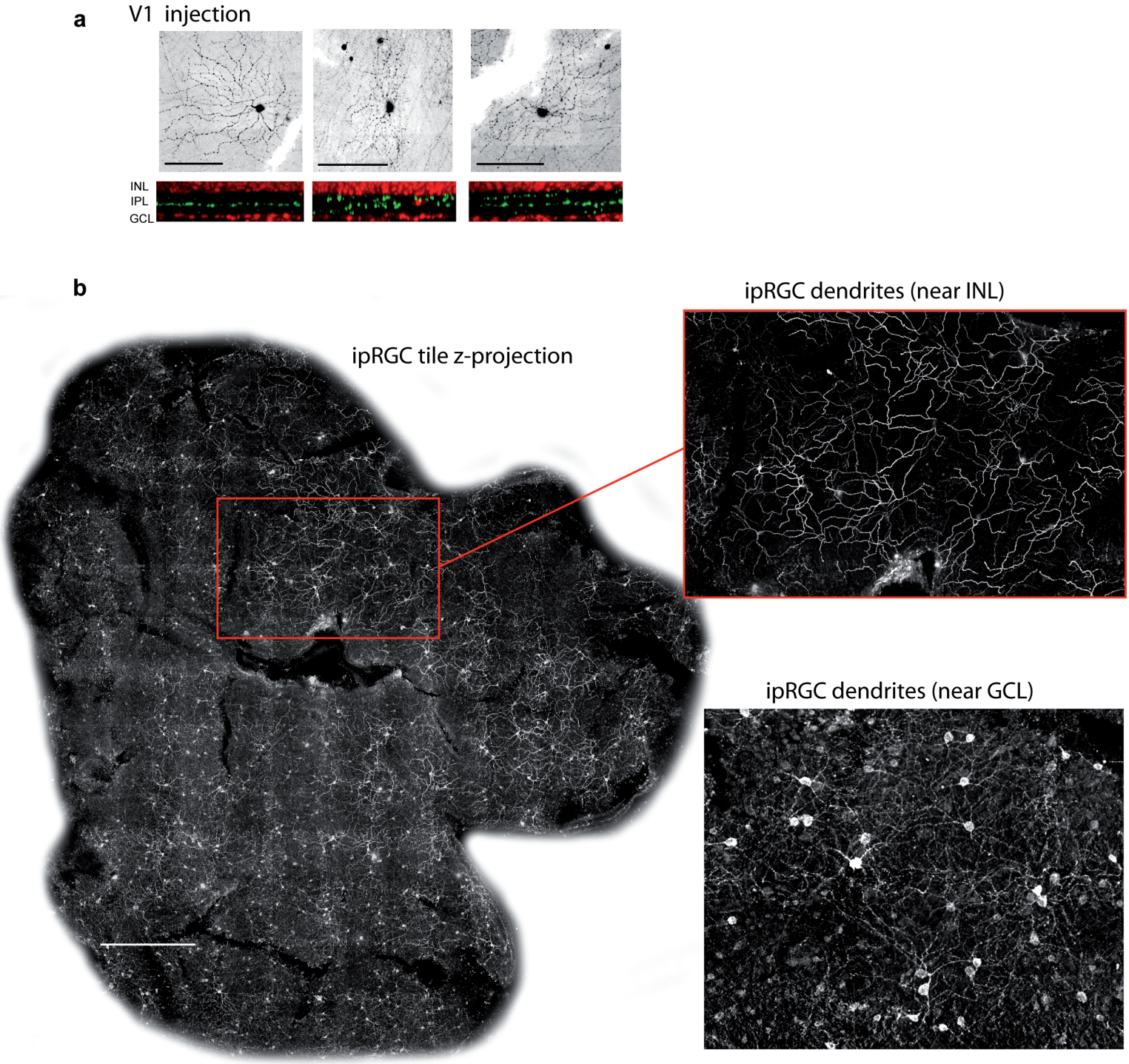
a
V1 injection
INL
IPL
GCL
b
ipRGC tile z-projection
ipRGC dendrites (near INL)
ipRGC dendrites (near GCL)

Figure 1.2

Common properties of local circuits of PRV152 labelled ganglion cells

The local circuits of the PRV152-infected ganglion cells can also be labelled. PRV152 was injected into the anterior chamber of the right eye (n = 32 retinas) as before, but in order to mark the cells in synaptic contact with the PRV152-infected ipRGCs I waited 5 days before dissecting the left retina. At this time, a number of other cells in the INL became intensely GFP positive (Fig. 1.3a). The newly-infected melanopsin-negative ganglion cells were not yet surrounded by cells in the INL suggesting that the passage of PRV from non-ipRGCs has not yet happened at this stage of infection. Most of the labelled cells in the INL were amacrine and Müller glia cells (Fig. 1.3a). Bipolar cells were labelled infrequently. Müller cell labelling was consistently observed solely near the cell bodies of infected ganglion cells, whereas labelled amacrine cells were scattered concentrically around them (Fig. 1.3a). Müller cells are easily identified from confocal stacks because their processes span the entire width of the retina. Their presence was further confirmed by staining the retina with antibody against glutamine synthetase, a marker specific to Müller cells (Fig.3b). Double-labelling with melanopsin and GFP showed that Müller cells were indeed in close proximity to ipRGCs (Fig. 1.3c). Surprisingly, however, no Müller cell labelling was seen in the retina when PRV152 was injected into V1 (Fig. 1.3d, e). In the INL, only the amacrine cells were GFP positive. This was true even at 5 days after injection to V1, at a time when large numbers of ganglion and amacrine cells are labelled. These results suggest that Müller cells make 'specialised contacts' with ipRGCs, but not with ganglion cells that project to the dLGN and subsequently to V1.

Amacrine cell labelling is unlikely to be caused by a release of PRV particles from Müller cells because infection of amacrine and Müller cells is temporally and spatially independent (Fig. 1.4). Further support for the idea that amacrine labelling is caused by transsynaptic release from ganglion cells comes from the finding that retinal strata juxtaposed to the GFP positive thin strata were not labelled (Fig. 1.5).

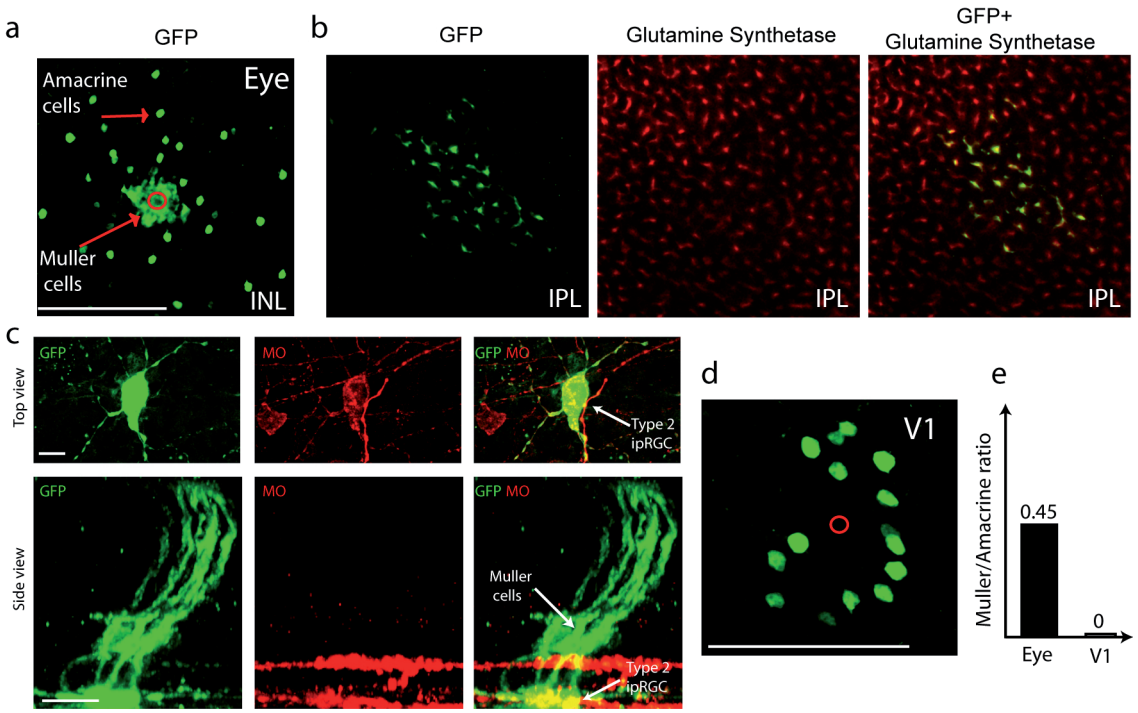

Figure 1.3. GFP-labelled local circuits 5 days after PRV152 injection into the anterior chamber of the right eye or right V1 cortical region. (a) GFP-positive amacrine and Müller cells in the INL. Red circle indicates position of the GFP-positive ganglion cell in the GCL. Scale bar, 100 µm. (b) Colocalisation of the Müller cell marker glutamine synthetase (red) and GFP (green) for cells which are GFP-labelled centrally near a GFP-positive ganglion cell. The depth of the scan is in the middle of the IPL. (c) Top views of a GFP-labelled Type 2 ipRGC with corresponding side views of labelled Müller cells. GFP (green) colocalises with melanopsin (MO, red). Scale bar 15 µm. (d) Confocal scan in the INL near to a labelled ganglion cell, 5 days after contralateral V1 injection, shows only GFP labelled amacrine cells and no Müller cells. The position of the ganglion cell body in the GCL is indicated by the red circle. Scale bar, 100 µm. (e) Proportion of the number of Müller and amacrine cells in the INL after contralateral eye and V1 injection at 5 days.

Figure 1.3

Figure 1.4. Time-lapse two-photon laser imaging of the PRV152 spread in the retina showing that infection of amacrine and Müller cells is temporally and spatially independent. Previously it was shown that PRV infection can spread from axons to glial cells that are in intimate contact with axons in the rat optic nerve, but does not spread from these glial cells to other neurons (Tomishima and Enquist 2002). Therefore glial cells have been proposed to be 'antiviral' and unable to propagate PRV infection to other cells. Here I tested the temporal order of amacrine/Müller cell PRV labelling to verify that amacrine cells are not labelled with PRV released from Müller cells. To rule this out, I argued that amacrine cells must either become GFP labelled earlier than Müller cells or labelled at the same time but separated in space. I isolated retinas from the contralateral eye 3.5-4 days after PRV infection. At this stage of viral spread only a few well-separated ganglion cells were labelled with GFP. The retina was maintained in an oxygenated superfusion chamber and two-photon confocal stacks were acquired (with 1 µm spacing) from regions around labelled ganglion cells every hour for 1-2 days using a two-photon laser microscope (See Materials and Methods). The left panel in (a) shows a schematic picture of a GFP-labelled circuit and its corresponding acquired confocal stack. Right, the images that were acquired for the GCL or INL are projected into the x-y plane and represent the GCL and INL, respectively (top views). The side view is the projection of the images on the x-z plane, where z represents the depth in the retina. Circuit 1 (b) shows the time-lapse imaging of GFP fluorescence. Each row shows a different time point (h, hour). The first two columns show top views (x-y projections) of the GCL and INL (as in (a)). On the first row, areas A and B are highlighted. The last two columns show side views (x-z projections) of the highlighted areas A and B. The INL and GCL are highlighted by yellow lines. Area A shows a ganglion cell in the GCL and later Müller cells in the INL (red arrows). Area B shows an amacrine cell in the INL (yellow arrows). This amacrine cell is labelled before the Müller cells appear at 11h. The amacrine cell loses GFP fluorescence at 14h. The lateral shift in position is due to slow movement of the retina. No temporal order between amacrine and Müller cell GFP expression was observed; occasionally amacrine cells became GFP positive before Müller cells. In other cases when amacrine cells became GFP positive after Müller cells the two cell types were spatially separated. Infection of amacrine and Müller cells is therefore temporally and spatially independent (b). This observation suggests that amacrine cells are not infected with PRV released from Müller cells.

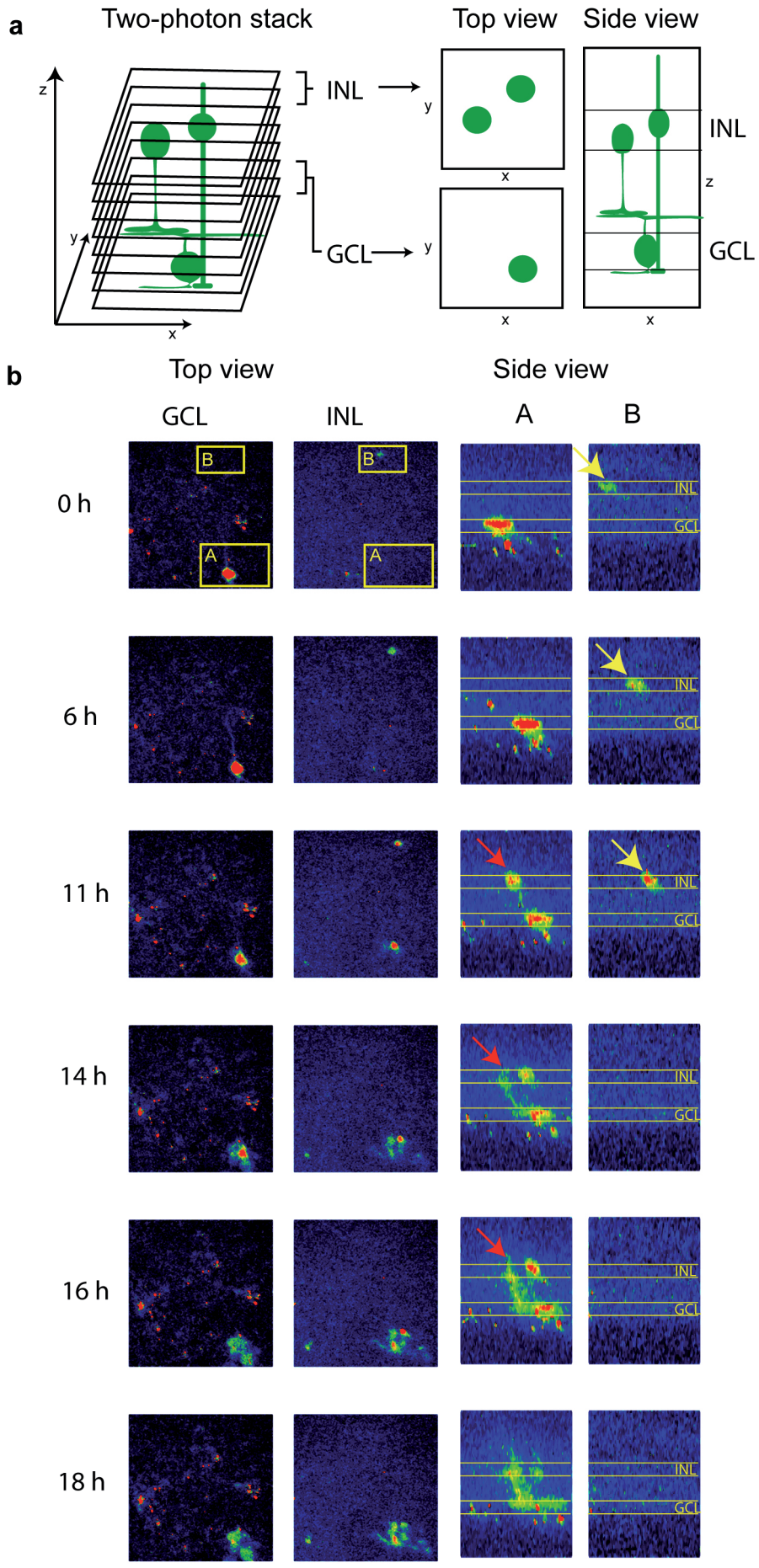
a
Two-photon stack
Top view
Side view
z
y
x
INL
GCL
INL
GCL
b
Top view
Side view
GCL
INL
A
B
0 h
6 h
11 h
14 h
16 h
18 h
B
A

Figure 1.4

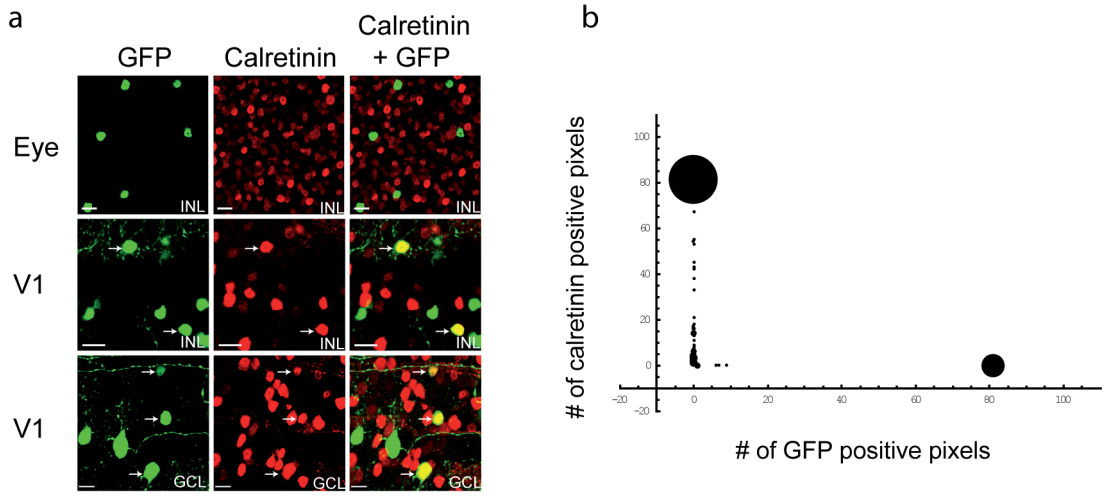

Figure 1.5. PRV infection from ipRGCs does not diffuse across retinal strata. To rule out the possibility that amacrine cells are infected by non-synaptic release of PRV152 from ganglion cells, I investigated GFP expression in amacrine cell types that occupied different strata than the PRV152 labelled ganglion cell dendrites. I used the finding that the antibody against calretinin labels a subpopulation of amacrine cells with processes in three distinct strata (Haverkamp and Wässle 2000). These calretinin strata are different from the strata where GFP positive ganglion dendrites ramify (see Fig. 1.1d). Therefore there are no calretinin positive amacrines that make synapses in the strata where the GFP labelled ganglion cell dendrites ramify. If the virus spreads only transsynaptically from ganglion cells to amacrine cells, all GFP positive amacrine cells should be calretinin negative. Conversely, if the virus is released from the ganglion cell dendrites non-synaptically, it could diffuse to neighboring strata and infect other cells in those strata. In this case one should find calretinin positive amacrine cells that are also GFP positive. To differentiate between the two possibilities I doubled labelled retinas, 5 days after infection from the contralateral eye (top row in a), with antibodies against GFP (green) and calretinin (red). None of the amacrines cells were double labelled, suggesting that PRV infection did not diffuse to neighboring strata from infected ganglion cell dendrites. To rule out the possibility that PRV152 infection interfered with calretinin expression, I also double stained retinas 4 days after V1 infection (middle and bottom rows in a). In this case a number of ganglion and amacrine cells were double labelled. The focal plane is shown in the bottom right corner of each image. Arrows point to double labelled cells. Scale bars, 15 µm. The calretinin and GFP colocalisation in the INL after virus injection to the contralateral eye was quantified based on confocal scans as in (a). The horizontal axis shows GFP staining and the vertical axis shows calretinin staining for each cell. Each point represents one cell or multiple cells if they have the same coordinates. The diameter of a point is proportional to the number of cells with the same coordinates. Cells with (0, 0) coordinates are not shown. No colocalisation is detected. These findings support the contention that amacrine cells are infected only by transsynaptic spread from ganglion cells.

Figure 1.5

There is a clear difference between the number of infected amacrine and bipolar cells in the retina, since very few bipolar cells become GFP positive through PRV spread from the contralateral eye. To show that this observation in my experiments was not due to the fact that some of the labelled ganglion cells contain their own photopigments and therefore might lack bipolar input, I investigated retinas retrogradely labelled with PRV152 from SC or V1. Similar to tracing from the contralateral eye, very few bipolar cells were detected after SC/V1 injection (results not shown). Other studies have also shown that melanopsin-expressing ganglion cells receive synaptic input from bipolar cells (Belenky et al. 2003, Dacey et al. 2005). This suggests that PRV152 spreads across unconventional, bipolar-to-ganglion ribbon synapses with low efficiency. Interestingly, the bipolar and amacrine cell GFP expression levels were the same, suggesting that differential expression from the cytomegalovirus (CMV) promoter of PRV is not the cause of inefficient bipolar labelling.

Monostratified amacrine cells provide inhibitory input to Type 2 ipRGCs

Next I investigated the structure and function of the local circuit of Type 2 ipRGCs. For this detailed circuit tracing I used low titer virus injections (10^3 PFU) that yielded sparse circuit labelling to avoid confusion of circuits belonging to neighboring ganglion cells. These ganglion cells have dendrites in the IPL close to the ganglion cell layer at 30% (± 4%, n = 57) depth. I generated 3D reconstructions from the processes of amacrines that surrounded Type 2 ipRGCs (Fig. 1.6a-c). For amacrine cells that were further away from the labelled ganglion cells a number of overlapping confocal stacks were acquired and then stitched together (Fig. 1.6d-e). All labelled amacrine cells studied this way (n = 20), independent of their distance from the ganglion cell body, were monostratified in the same stratum as the Type 2 ipRGCs. Although the GFP labelling of bipolar cells was rare (Belenky et al. 2003, Dacey et al. 2005), in some cases (n = 3) their their morphology could be reconstructed. As expected these bipolar cells costratified with Type 2 ipRGC dendrites (Fig. 1.6f). The structure of the Type 2 ipRGC's local circuit, based

on the detailed confocal reconstructions, is summarised in a circuit drawing in Figure 1.6g. The local circuit consists of three cell types: a Type 2 ipRGC, a Type 8 bipolar cell (based on Ghosh et al. 2004) and a monostratified amacrine cell. In this detailed morphological study I could not use melanopsin colabelling because the GFP-labelled fine amacrine dendrites were only visible with rabbit anti GFP, which was from the same species as the anti melanopsin antibody. I relied on the finding that at 5 days non-ipRGCs were newly infected (were not present at 4 days) and therefore the spread of the virus to amacrines most probably has not yet happened. This is supported by the finding that non-ipRGCs were not surrounded by amacrines at 5 days (see above).

To show more direct evidence that the identified monostratified amacrine cells are indeed connected to ipRGCs I isolated the retina at 3.5-4 days, at the time when 99% of the labelled ganglion cells are melanopsin positive. I determined the retinal coordinates of many labelled ganglion cells using two-photon microscopy and superfused the retina with oxygenated Ringers solution for an additional day. In these experiments I used a new PRV strain (Viney et al. 2007) that expressed a membrane-bound GFP that labelled more clearly the dendrites and axons. One day after isolation (5 days after infection) I fixed the retina and stained the circuit with rabbit anti GFP antibodies and analysed the circuits at the marked coordinates. The analysed circuits are therefore, with 99% probability, local circuits of ipRGCs. The morphology of the labelled amacrines was identical to those described above (Fig. 1.6h).

Figure 1.6. Local circuit and physiology of Type 2 ipRGCs. (a) Confocal scan in the proximal part of the IPL in the left retina at 5 days after PRV152 injection to the right eye. A GFP-labelled (green) Type 2 ipRGC is shown. (b) Confocal scan of the same area as in (a) but in the INL. The GFP-labelled cells are amacrine cells. Cell nuclei labelled by DAPI are shown in red. (c) An x-z projection of a high-resolution scan of the yellow box shown in (a) and (b). An amacrine cell (AC) in contact with the dendrites (D) of the Type 2 ipRGC is shown. (d) Five confocal scans were stitched together to show the dendritic arbor of two amacrine cells (AC) and of a Type 2 ipRGC (GC2). A Type 1 ipRGC is also shown (GC1), although its dendrites are not visible because they are in a different depth. (e) x-z projection of the stack shown in (d). Here the dendrites of the two amacrines as well as the Type 1 ipRGC are shown. Red arrows point to the two amacrine cell bodies. (f) An x-z projection of a high-resolution scan from another Type 2 ipRGC shows a Type 8 cone bipolar cell (CB 8). (g) The identified cell types in the local circuit of Type 2 ipRGCs based on the viral tracing. (h) The same as (c) except that this amacrine cell was from an experiment where the retina was isolated at 4 days and kept in a superfusion chamber for one day (see main text). Scale bars represent 10 µm for all figures. (i) Light-evoked inhibitory currents from 3 different Type 2 ipRGCs. Inhibition cannot be detected after light OFF. The currents were measured in voltage clamp at a holding potential of 0 mV (Roska and Werblin 2001). The stimulus was a 1 mm diameter bright spot. The timing of the stimulus is indicated by black bars. (j) Light-evoked inhibitory currents from 5 different types of ON ganglion cells in the rabbit retina. Light evokes inhibition both at light ON and OFF in 4 out of the 5 cell types (names shown to the right of each). The OFF response is indicated by arrows. Stimulus is the same as in (i). Scale bars represent 100 pA.

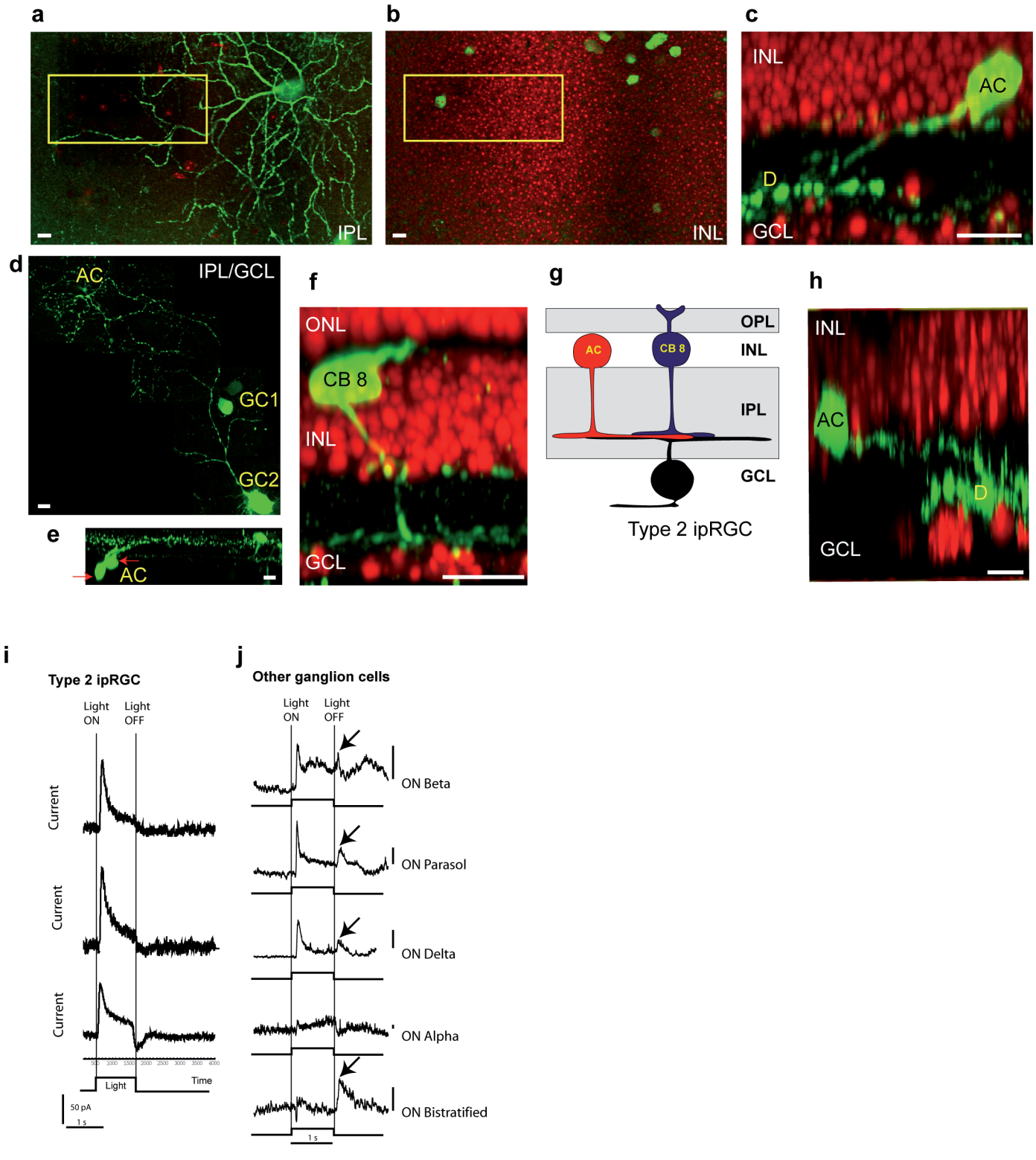
a
IPL
b
INL
c
INL
AC
D
GCL
d
AC
IPL/GCL
GC1
GC2
e
AC
f
ONL
CB 8
INL
GCL
g
OPL
AC
CB 8
INL
IPL
GCL
Type 2 ipRGC
h
INL
AC
D
GCL
i
Type 2 ipRGC
Light ON
Light OFF
Current
Current
Current
Light
Time
50 pA
1 s
j
Other ganglion cells
Light ON
Light OFF
ON Beta
ON Parasol
ON Delta
ON Alpha
ON Bistratified
1 s

Figure 1.6

The labelled circuit gave very strong predictions about the direct, amacrine cell mediated, inhibitory input to Type 2 ipRGCs. In most vertebrates (except in zebrafish, (Connaughton et al. 2004)) and in all mammalian species studied the IPL is roughly divided into two major regions. Strata close to the GCL (sublamina B) incorporate axon terminals of ON bipolar cells; strata close to the INL (sublamina A) embody axon terminals of OFF bipolar cells (Famiglietti and Kolb 1976, Ghosh et al. 2004). Since amacrine cells receive excitation from bipolar cells, the reconstructed amacrines must receive excitation only at light ON. Most amacrines are inhibitory cells. If the Type 2 ipRGCs receive inhibitory input only from the reconstructed amacrines, inhibition should arrive only at light ON but not at light OFF. Inhibition at light OFF would suggest a multi- or bi-stratified amacrine cell because OFF activity should travel vertically in the IPL from sublamina ‘a’ to sublamina ‘b’ (Roska and Werblin 2001). To test these predictions, light-evoked inhibitory currents were recorded (Roska and Werblin 2001) from PRV infected, GFP labelled, Type 2 ipRGCs with two-photon-targeted whole cell patch clamp, in the voltage clamp configuration after 4 days of infection (see Materials and Methods). As mentioned before, at that time only ipRGCs were labelled. The resting membrane voltage was -58 mV ± 4 mV (n = 8). Inhibition in Type 2 ganglion cells was only evoked at light ON (n = 10) when stimulated with a 1 mm diameter white spot (Fig. 1.6i), as predicted by the structure of the PRV labelled local circuit elements. This finding is in strong contrast with inhibitory currents evoked in most other ON ganglion cells in the mammalian retina (Fig. 1.6j); in the rabbit retina only one type of ON ganglion cell receives inhibition only at light ON. These results suggest that Type 2 ipRGCs receive a strong, fast inhibitory input at light onset from a single morphological type of amacrine cell.

Dopaminergic interplexiform cells are synaptically connected to Type 1 ipRGCs

Similar to Type 2 ipRGCs, Type 1 ipRGCs were surrounded by GFP positive amacrine cells (Fig. 1.7a). These amacrine cells had processes in the same stratum as Type 1 ipRGCs. Because the morphology and stratification of the labelled INL cells were very similar to a well described cell type, the

dopaminergic interplexiform/amacrine cells (Gustincich et al. 1997), I triple labelled retinas for tyrosine hydroxylase (TH), GFP and melanopsin. Figure 1.7b-e shows that a number of amacrine cells around a melanopsin and GFP positive Type 1 ipRGC (Fig. 1.7e) were both GFP and TH positive. Figure 1.7c-d shows that TH positive processes and melanopsin positive dendrites of ipRGCs cofasciculate in the IPL. Since the virus spreads in the retrograde direction, from ganglion cells to amacrine cells, these results suggest that dopaminergic cells provide synaptic input to Type 1 cells.

Figure 1.7. Type 1 ipRGCs are synaptically connected to dopaminergic amacrine/interplexiform cells. (a) Confocal scan of a region in the INL-IPL border around a GFP positive Type 1 ipRGC. A descending dendrite of the ipRGC is shown by the white arrow. Red arrows point to a number of GFP positive cell bodies in the INL. (b) Colocalisation of GFP (green) and TH (red) in amacrine cells around a Type 1 ipRGC in the INL. Arrows point to double labelled cells. (c) Triple staining for TH (red), melanopsin (green) and GFP (blue) at the IPL-INL border. Arrow points to TH and GFP positive amacrine cell. (d) Higher magnification of a region in (c). Arrows point to cofasciculating TH and melanopsin positive processes. (e) Triple staining for TH (red), melanopsin (green) and GFP (blue) labels a Type 1 ipRGC (cell labelled as '1') and two dopaminergic amacrines (two cells labelled as '2') in close proximity. Top views are on the left and side views are on the right. (f) Top: confocal scan of a region in the IPL-ONL border shows a labelled horizontal cell body (left) and axon terminal (right). Bottom: z-axis view of the yellow window region from the upper panels. Scale bars represent 15 µm for all figure panels.

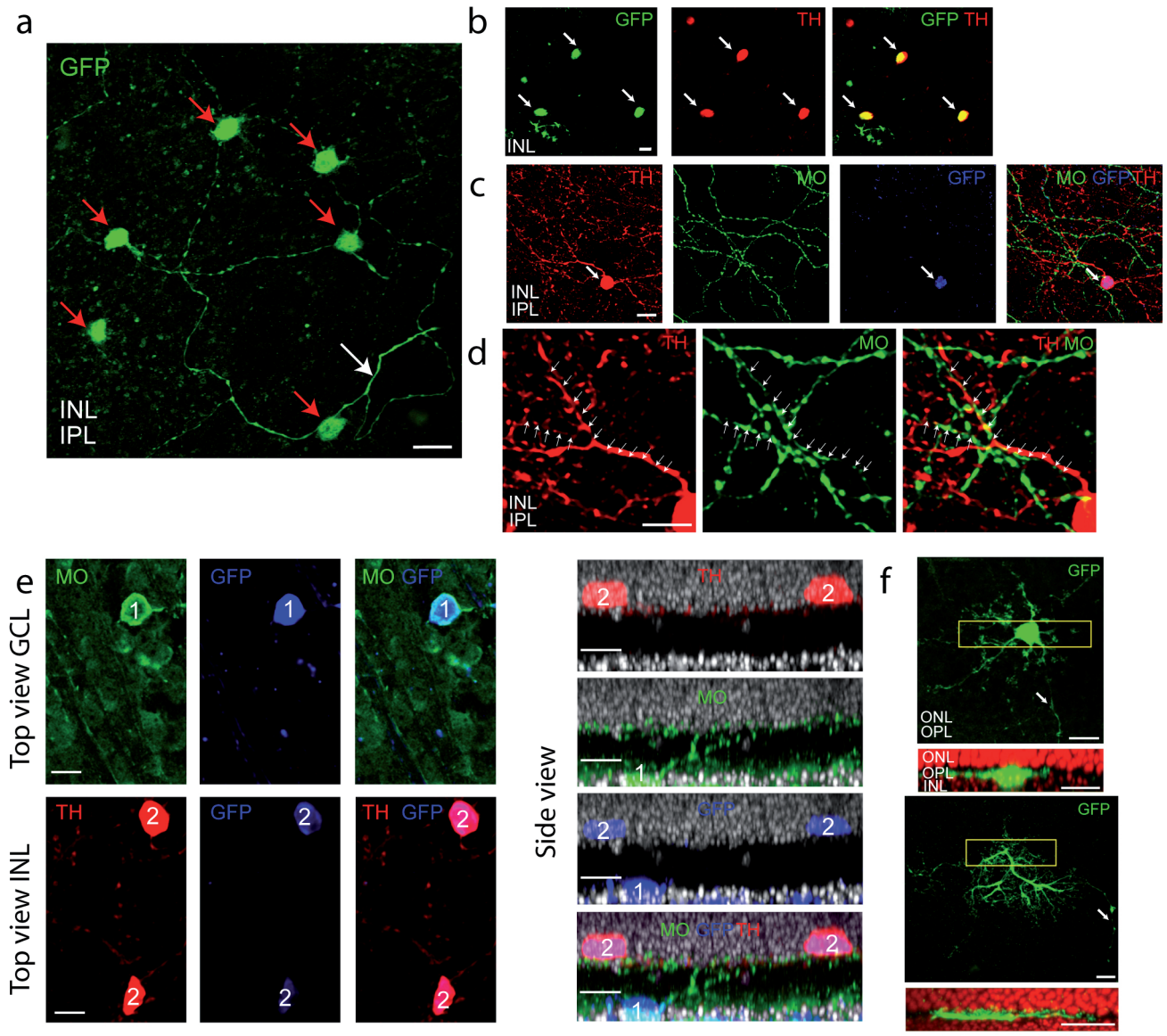
a
GFP
INL
IPL
b
GFP
TH
GFP TH
INL
c
TH
MO
GFP
MO GFP TH
INL
IPL
d
TH
MO
TH MO
INL
IPL
e
Top view GCL
MO
GFP
MO GFP
1
Top view INL
TH
GFP
TH GFP
2
Side view
TH
MO
GFP
MO GFP TH
1
2
f
GFP
ONL
OPL
INL

Figure 1.7

Dopaminergic amacrine cells in the mouse retina are interplexiform cells that have processes in the IPL and in the outer plexiform layer (OPL) (Dowling and Ehinger 1975, Marc and Liu 1984, Mangel and Dowling 1985, Gustincich et al. 1997). 5.5-6 days after contralateral virus infection a number of horizontal cells become labelled with GFP (Fig. 7f). The PRV labelling of horizontal cells suggest that these cells are not only postsynaptic targets (Lasater and Dowling 1985) of but also presynaptic to dopaminergic interplexiform cells. The finding that PRV152 very inefficiently passes to bipolar cells and the fact that no bipolar cells were detected in the vicinity of the labelled horizontal cells (result not shown) indicates that the virus spread from interplexiform cells to horizontal cells. Interestingly, even after 7 days of infection we could not detect rods or cones which reinforced our conclusion that PRV152 very inefficiently crosses ribbon synapses.

Dopamine is a neurotransmitter in the retina that controls light adaptation (Witkovsky 2004). Dopaminergic cells of the mouse retina are GABAergic (Gustincich et al. 1997). These cells make conventional synapses and also release neurotransmitter extrasynaptically (Puopolo et al. 2001, Contini and Raviola 2003, Witkovsky 2004). In an earlier study the control of melanopsin expression in ipRGCs was shown to be modulated by dopamine through D2 receptors indicating that classical photoreceptors may modulate the transcription of melanopsin (Sakamoto et al. 2004, Sakamoto et al. 2005). Further evidence linking dopamine and ipRGCs was provided by a study in D2 receptor null mice that showed a markedly deficient suppression of locomotor behavior by light, called the light masking response, indicating that D2 receptor mediated signalling is an essential component of the neuronal pathways leading to light masking of circadian rhythms (Doi et al. 2006). In Xenopus both light and dopamine phase-shift the retinal circadian clock in a phase-dependent manner (Steenhard and Besharse 2000). In rats ipRGCs and dopaminergic amacrine cells show a very similar superior-inferior difference in density in the retina (Hannibal et al. 2002).

My experiments suggest that dopaminergic cells are in synaptic contact with Type 1 ipRGCs. The synapse between dopaminergic cells and ipRGCs are either GABAergic or dopaminergic or both. It is possible that similar to the

synapse between dopaminergic cells and AII amacrine cells (Contini and Raviola 2003) both GABA and dopamine are released but the postsynaptic receptors are positioned at different distances from the release site. In either case however, the synaptic contact between interplexiform cells and ipRGCs suggest that activity of dopaminergic cells synaptically influence the activity and/or gene expression in ipRGCs. Therefore, these results suggest a circuitry link between light-dark adaptation and ipRGC function.

Chapter 2: Precise timing of inhibitory-excitatory motifs in eight genetically-identified neural cell types.

I investigated how inhibition and excitation interact in time within identified neural circuits. First I quantified morphological and physiological properties of genetically-identified neurons in the 'PV retina' and identified 8 distinct neural cell types, which are all ganglion cells, the output neurons of the retina. Next I compared the inhibitory and excitatory inputs to each identified neuron and discovered that the timing of the interactions is very precise, and that each type has a temporal signature, or 'motif,' that describes its neural circuit and offer clues to its function. It is the change in excitation relative to inhibition that causes the neuron to fire. Finally I measured the interactions during 'natural' visual stimulation and found evidence that the precision of spikes from each ganglion cell type, which represent the parallel output channels of the retina, is determined only by the time points when inhibition is not interacting with excitation. In other words, inhibitory pathways appear to act as 'irrelevance' detectors, only allowing the output neuron to fire when something in the receptive field of the cell becomes 'relevant' - when excitation changes faster than inhibition.

Precise timing is critical for the functions of the central nervous system (CNS). Spiking neurons are thought to provide a temporal code, with millisecond precision spike events (Berry et al. 1997, Meister and Berry 1999, Gollisch and Meister 2008). Inhibition has been shown to modulate spike timing in many different brain regions, and the brain state - the frequency of the local field potentials that emerge from the synchronised firing of neuronal populations - is finely-tuned by inhibitory interneurons (Klausberger et al. 2003, Klausberger et al. 2004, Crowley et al. 2009, Cardin et al. 2009). Different types of inhibitory neurons are known to have different roles in shaping the activity within local circuits (Klausberger et al. 2005, Roska et al. 2006, Eggers and Lukasiewicz 2010). The difficulty of studying the role of

inhibition in the CNS is that it is often very hard to define all the synaptic connections to the principle spiking neuron of interest, or even the direction of information flow. Furthermore, there is an enormous diversity of interneurons (Thomson and Lamy 2007, Ascoli et al. 2008, MacNeil and Masland 1998). The major limitations are usually that the neurons studied are poorly defined; most of their synaptic connections remain unknown, and recordings are often done in experimental conditions that differ greatly from work *in vivo* (such as in brain slices or cultures). Even *in vivo* work has its limitations due to the effects of anaesthesia on cortical oscillations, but now recent studies are being carried out in awake behaving animals (Harvey et al. 2009, Gentet et al. 2010). In order to understand the role of timing for inhibitory-excitatory interactions across parallel neural circuits, I argue that the dataset must comprise a definitive quantitative description of cell type that is based on parameters of the local circuits that the neurons of interest belong to, rather than qualitative descriptions of particular morphological or physiological properties. Furthermore, my aim was to perform experiments as close to *in vivo* conditions as possible. To achieve this goal I used the mouse retina, where the direction of information flow is known, it is straightforward to isolate, and can be kept intact and alive *ex vivo* for many hours without the need for anaesthesia. Furthermore, I used a transgenic mouse line that had fluorescently labelled neurons, reducing the time spent targeting cells of the same type in the same and different experiments. From 600 targeted recordings, I characterised the interactions between excitation and inhibition to gain insight into the role of inhibition in spike-timing for defined types of central neurons.

The PV retina contains a class of targetable genetically-identified neurons

A subpopulation of neurons in the Parvalbumin-Cre x Thy1-Stop-EYFP transgenic mouse line express YFP. In the retina of this mouse line, which I refer to as the 'PV retina', YFP labels a single class of neurons of the CNS, the retinal ganglion cells (Fig. 2.1a). This class is defined by their axons, which project to the optic disk and on to higher brain regions via the optic nerve. Within the ganglion cell class, more than a dozen distinct cell types

have been described so far in mammals, and are classically defined by their dendritic trees (morphology) (Boycott and Wässle 1974, Sun et al. 2002, Rockhill et al. 2002) or responses to visual stimulation (physiology) (Levick 1967, DeVries and Baylor 1997, Zeck and Masland 2007). The greatest understanding is gained from studies that map physiology with morphology on a cell-type basis (Bloomfield and Miller 1986, Isayama et al. 2000, Roska and Werblin 2001, O'Brien et al. 2002, Pang et al. 2003, Roska et al. 2006). It is currently unknown how many ganglion cell types exist, especially since there are often disagreements between independently identified physiological and morphological cell types (Rodieck and Brening 1983). Approximately 41% of neurons in the so-called ganglion cell layer (GCL) of the mouse retina are of the ganglion cell class (Jeon et al. 1998, Williams et al. 1996), the remainder being mostly inhibitory interneurons known as amacrine cells. In the PV retina, 11.4% (± 0.70%, n = 52 retinas) of ganglion cells express YFP (see Materials and Methods), which I call the 'PV cells'. There is also a small proportion of PV cells in the inner nuclear layer (INL), a multilayer of somata that consist mostly of amacrine cells and excitatory bipolar cells. However these PV cells are 'misplaced' ganglion cells since each cell also possesses an axon that projects through the inner plexiform layer (IPL) and GCL to the optic disk, and dendrites that terminate in the IPL with all other ganglion cell dendrites (data not shown). The density of labelled cells (approximately 380 PV cells mm^{-2}) is low enough for single-cell targeting but high enough for screening the population. Two-photon imaging of the PV retina reveals a variety of soma sizes and dendritic tree arbourisations (Fig. 2.1b). To determine the number of labelled cell types, I targeted 600 PV cells (Fig. 2.1c) with microelectrodes in 211 PV retinas and quantified light-evoked spiking activity, excitatory and inhibitory conductances, and dendritic tree properties (Fig 2.1d-h).

Figure 2.1. Targeting a class of genetically-identified neurons in the PV retina. (a) YFP expression in a Parvalbumin-Cre x Thy1-Stop-EYFP (PV) retina (epifluorescence excitation). Left, *in vivo* image through the lens of the eye. Right, *ex vivo* wholemount image. Filaments are axons extending to the optic disk (centre). Scale bars: 250 µm. (b) Maximum intensity z-projection of a two-photon image series of a region of a wholemount PV retina. 1.0 NA objective, 1024 x 1024 pixel resolution. Scale bar: 20 µm. (c) Infrared image of the GCL (greyscale) of the same region in (b) with a 2D overlay of the two-photon signal (green). Scale bar: 20 µm. (d) Light-evoked spiking from the YFP-positive PV cell in (b) and (c) (indicated by an asterisk). Visual stimulus (below): 200 µm black then white spot on a grey background, aligned to dendritic field centre. Dashed lines indicate the onset or offset of the spot. Black bars: spike trains. Below, discrete firing-rate (in Hz, 25 ms time bins). (e) Voltage steps during whole cell voltage clamp of the same PV cell (left) and corresponding current-voltage (I-V) curves (right). Left, 10 mV steps from -110 to 30 at two time points during the recording. Right, mean current taken from light-grey region from voltage steps, plotted against the voltage at each step (I-V curve). Black, 0 min after break-in (QX314 has not blocked the voltage-dependent sodium currents). Grey, 20 min after break-in. (f) Whole cell voltage clamp of same the PV cell measuring inward currents (excitation, black trace) and outward currents (inhibition, grey trace), respectively. Same stimulus as in (e). (g) Maximum intensity z-projections of confocal images in the fixed, antibody-stained PV retina. Left, the recorded PV cell, filled with neurobiotin (magenta). Axon show in top left. Middle, region from (b) and (c) shown in rotated white box, with same PV cell marked with an asterisk; anti-GFP (green). Right, merge showing GFP-positive neurobiotin-filled PV cell. Scale bar: 20 µm. (h) Maximum intensity yz-projection of the IPL region for the PV cell. Left, dendrites of the PV cell in the IPL, filled with neurobiotin (magenta). Middle, ChAT marker antibody labelling two bands (cyan). Right, merge showing bistratified PV cell colocalising with the ChAT bands. Scale bar: 20 µm.

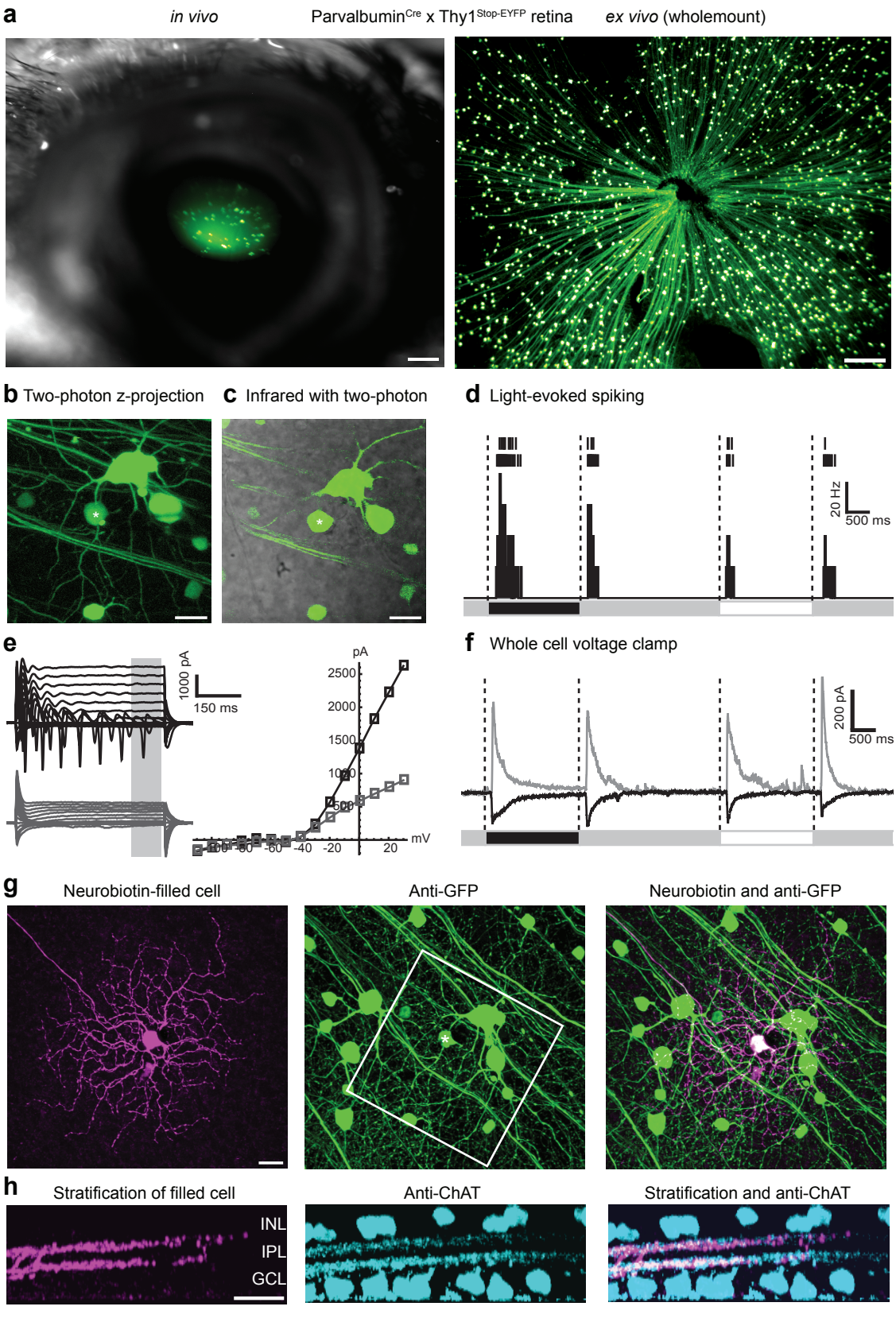
a
in vivo
Parvalbumin^Cre x Thy1^Stop-EYFP retina
ex vivo (wholemount)
b Two-photon z-projection
c Infrared with two-photon
d Light-evoked spiking
20 Hz
500 ms
e
1000 pA
150 ms
pA
2500
2000
1500
1000
500
-80
-60
-40
-20
20
mV
f Whole cell voltage clamp
200 pA
500 ms
g
Neurobiotin-filled cell
Anti-GFP
Neurobiotin and anti-GFP
h
Stratification of filled cell
Anti-ChAT
Stratification and anti-ChAT
INL
IPL
GCL

Figure 2.1

Figure 2.1 shows the steps used to characterise a single PV cell from the PV retina. After cleaning the GCL in the region of the two-photon targeted cell (see Materials and Methods and Fig. 2.1b,c), the loose on-cell patch configuration was used to record spiking activity during visual stimulation of the photoreceptors (Fig. 2.1d). Since the retina contains both ON and OFF pathways (which correspond to parallel neural circuits that are active for light increments and light decrements respectively), black and white spots (of 50% contrast relative to the grey background) were presented to the underlying neural circuit of the targeted PV cell to identify the pathways involved. In the example, the PV cell fired after light increments (brightening: light ON, grey-to-white or black-to-grey) and after light decrements (dimming: light OFF, black-to-grey or white-to-grey) (Fig 2.1d), indicating that the underlying neural circuitry involves both ON and OFF pathways. Only uniform spots - presented to the dendritic field centre - were used for this characterisation, which act on all photoreceptors within the area of the spot. This ensured that so-called 'ON-centre' and 'OFF-centre' circuit activity was measured (at the resolution of spikes), rather than measurement of antagonistic effects from the 'surround' (outside the central spot area, activated by presenting an annulus) (Küffler 1953).

To investigate the circuitry beyond the resolution of spikes, whole-cell voltage-clamp was used to isolate the underlying synaptic conductances responsible for the spiking activity: the excitatory and inhibitory inputs to the cell (Fig 2.1e,f). First, the current flowing across the cell membrane was measured at different holding potentials in rapid 10 mV steps to generate a current-voltage (I-V) curve (Fig. 2.1e). The I-V curve provided an estimate of the reversal potential and input resistance. Two-to-three minutes after break-in, voltage-dependent sodium currents were blocked by QX314 in the intracellular solution and remained blocked for the duration of the recording (Fig 2.1e). Given that ganglion cells receive excitatory input from bipolar cells and inhibitory input from amacrine cells (Werblin and Dowling 1969), voltage clamping the cell to the equilibrium potential of chloride (-60 mV) isolated the bipolar-mediated input, and voltage clamping to +20 mV (above the reversal potential of nonselective cations, 0 mV) isolated the amacrine-mediated input.

Under the same visual stimulus conditions as in Fig.2.1d, the example PV cell received both excitatory and inhibitory input at light ON and at light OFF (Fig. 2.1f). This suggests that the neural circuit includes at least two types of bipolar cells and at least two types of amacrine cells. Clearly inhibition is interacting with excitation at both changes of contrast (light ON and light OFF) to produce transient 'ON OFF' spiking activity. The question as to how the timing of these inhibitory-excitatory interactions affects spiking is addressed later.

The recording pipette contained neurobiotin, so that the morphology of the PV cell could be analysed after the experiment and correlated with the physiology. The PV cell had a symmetrical dendritic field (Fig. 2.1g, left), with a mean diameter of 183 ± 7 µm and an area of 106 mm^2. The recorded PV cell was identified from the surrounding pattern of YFP positive neurons (compare Fig. 2.1g, centre, with b and c). In this example, there was one large and one medium soma next to the recorded PV cell. The dendrites of the PV cell have a specific depth, or stratification, in the IPL. This neuron was bistratified (Fig. 1.1h, left), and colocalised with the marker for cholinergic amacrine cells, ChAT (Fig. 2.1h). The physiological 'ON-centre OFF-centre' characterisation of the cell that suggested contributions from both the ON and OFF pathways (Fig. 2.1d) and was highlighted by the dual excitatory and inhibitory inputs (Fig. 2.1f), conveniently corresponds to the morphology: two independent dendritic trees, each receiving input from separate populations of bipolar cells and amacrine cells. Furthermore, it is known that the IPL has a vertical organisation, such that ganglion cells that fire at light ON stratify in the innermost portion of the IPL (towards the GCL) and those that fire at light OFF stratify in the outermost portion (towards the INL) (Bloomfield and Miller 1986, Roska and Werblin 2001). This organisation reflects the excitatory input - the ON and OFF bipolar cell types - whose axon terminals stratify so that they synapse with the corresponding ON, ON OFF and OFF ganglion cells (Ghosh et al. 2004, also see Introduction). Taken together, the PV cell in Figure 2.1 resembles an 'ON OFF direction selective' ganglion cell type, which has been characterised in the mouse and other species where it has a conserved morphology and physiology (Barlow et al. 1964, Weng et al. 2005). Thus it is

possible to construct a putative neural circuit, complete with excitatory and inhibitory components, from single two-photon targeted YFP-labelled genetically-identified ganglion cells.

Quantification of PV cell morphology forms 8 groups

Given the variety of soma sizes and dendritic arbours identified in the two-photon scans, and given that a particular 'morphology' can correspond to a particular 'physiology', can the labelled PV cells be grouped by morphology alone? Is the position of the dendritic tree in the IPL sufficient to predict a cell type, such as the ON OFF direction selective cell identified in Figure 2.1? To address this I quantified the depth of stratification in the IPL relative to the two strata marked by the ChAT antibody for >135 recorded two-photon targeted neurobiotin-filled PV cells (Fig. 2.2). As with the cortex, the retina is laminated, but here the divisions are more clearly defined since there are alternating layers of nuclear and synaptic layers, with the somata defining the borders (see Introduction). The innermost synaptic layer, the IPL, has been classically subdivided into two sublayers or 'sublamina', roughly corresponding to bipolar cells and ganglion cells of the OFF pathways and ON pathways (Masland 2001). However, due to differences in retina preparation (such as fixation and mounting) and the fact that the somata at the borders of the INL and GCL are not flat, it is often difficult in the literature to compare stratification of cell types when expressed as a function of percent IPL depth. To circumvent this discrepancy, I divided the IPL into 'biological' sublayers based on well-known marker proteins, Calretinin and ChAT (Haverkamp and Wässle 2001). Calretinin marks three strata within the IPL, and ChAT marks two that colocalise with Calretinin (Fig. 2.2a). Due to greater efficiency of labelling, only ChAT is shown for ganglion cell stratification images. From the biological strata, which make seven sublayers, I quantified PV cell stratification in *relative* percent IPL depth, where 0% is the ON ChAT band (closer to GCL) and 100% is the OFF ChAT band (closer to INL). The relative depths of stratification for 135 PV cells are shown in Fig. 2.2b. Note that the middle Calretinin band is not precisely in the middle of the two other bands. All PV cells were monostratified, except those that stratified at 0% and 100%, which were the bistratified ON OFF direction selective ganglion cells (Fig. 2.1). From

stratification alone, the PV cells formed a continuum that ranged from -60% depth to 154% depth relative to the two ChAT strata.

Stratification refers to the vertical organisation of the retina; it is purely an indication as to which presynaptic bipolar cell types might be included in the neural circuit of the ganglion cell, and thus offers clues as to which pathway or pathways are involved (ON or OFF or both). However, the inhibitory interneurons - amacrine cells - act both vertically and laterally in the IPL, which is indicated morphologically by the existence of narrowfield and widefield groups of amacrine cells (MacNeil and Masland 1998). Based on this notion, I included a second parameter of quantification for each PV cell: the dendritic field area. This would take into account both the lateral and vertical components of the neural circuitry of each ganglion cell, since the dendritic field is the morphological equivalent of 'visual space' (which is linked to the receptive field of a ganglion cell in the physiological description). Upon plotting stratification as a function of dendritic field area, the monostratified PV cells formed seven groups (Fig 2.2c). Each group is plotted as a different colour, which was determined by a clustering algorithm (see Materials and Methods) and black represents the bistratified group where each point has a corresponding point in the other stratum. In total the PV cells formed eight morphological groups based on two 'biological' parameters. The smallest PV cell had a mean dendritic area of 4 mm^2 (74 µm diameter) and stratified at 46.2 ± 2.7% depth (colocalising with the middle-Calretinin band), and the largest PV cell from the plot had a mean area of 80 mm^2 (318 µm diameter) and stratified at -42.9 ± 7.2% depth (Fig 2.2c). Interestingly, a small number of the bistratified PV cells (at 0% and 100% depths) had very large spatially-offset dendritic fields suggesting the existence of 'giant' direction selective neurons (discussed below). A comparison of a very small and a very large PV cell is shown in Fig. 2.2d. The very large PV cell was in fact the largest PV cell ever recorded (dendritic area 116 mm^2, diameter 384 µm, depth -45.5 ± 8.7%), and is not plotted in Fig 2.2c since it is an outlier and would have altered the plot range (but is a member of the cyan cluster - the only group with negative percent depth). The very small PV cell (dendritic area 91 mm^2, diameter 107 µm, depth 154.3 ± 11.0%), from the blue cluster (smallest area

group with depth greater than 100%) had a strongly asymmetric dendritic field relative to the soma, and due to the fact that neurobiotin diffuses through gap junctions, was shown to be coupled to axonless cells (probably amacrine cells) within or very close to its dendritic field. Coupling, and similarities to previously described cell types, is discussed below. The range of dendritic areas is comparable to the range of dendritic depths; the advantage of the PV retina is that only 8 groups were identified. It is worth mentioning that these groups only arose due to both parameters (depth and area) being quantified. A single parameter (such as depth, Fig. 2.2b), does not identify all groups. This highlights that different 'groups' of cells can exist within the same IPL stratum, suggesting that describing cell types by stratification alone is insufficient.

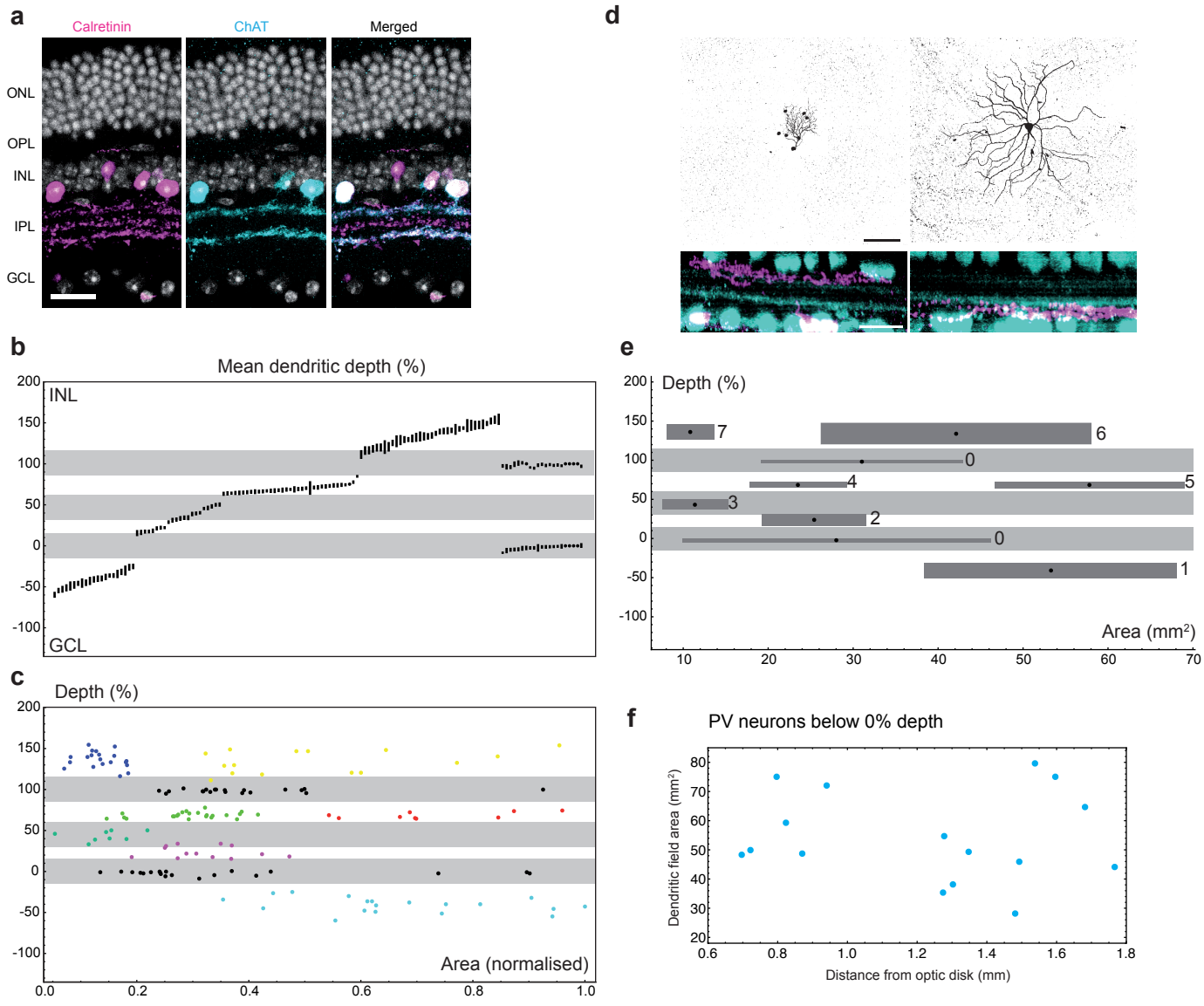

Figure 2.2. Morphological quantification of PV cells into 8 groups. (a) Vertical section of the retina with Calretinin (magenta) and ChAT (cyan) markers. DAPI (greyscale) labels cell nuclei. ONL, outer nuclear layer; OPL, outer plexiform layer; INL, inner nuclear layer; IPL, inner plexiform layer; GCL, ganglion cell layer. (b) Mean dendritic depth of PV cells relative to the ChAT bands (light-grey boxes: -15 to 15% for ON ChAT band, 85 to +115% for OFF ChAT band; middle box is the middle Calretinin band, 30 to 60%). Each black bar represents the dendrites of a PV cell (n = 135 neurons). The length of the bar (% depth) represents ± SEM. Bistratified cells are shown on the right (two bars per cell). The depth range is plotted between the mean GCL (-136%) and INL (202%) borders. (c) Two-dimensional cluster of PV cells (n = 127) for k = 7 clusters (colours) excluding bistratified cells (black, every spot is from a pair). Y-axis, depth as in (b); x-axis, dendritic field area normalised to the area of the largest PV cell (80 mm^2). (d) A very small PV cell (left) and the largest PV cell (right). The latter is an outlier and not included in (c). Mean dendritic depth, 154.3 ± 11.0% (left) and -45.5 ± 8.7% (right); dendritic field area 91 mm^2 (left) and 116 mm^2 (right). Top views, neurobiotin (greyscale), scale bar 100 µm; side views, neurobiotin (magenta) and ChAT (cyan), scale bar 20 µm. Same scale for both cells. (e) Mean (black spots) and standard deviation (dark grey boxes) of each cluster, including both strata from bistratified cells at 0 and 100% depth. Marker bands are light-grey. Clusters are marked as Groups 0-7 (see Table 1). (f) Dendritic field area (mm^2) plotted against distance of soma from optic disk (mm). Data from PV cells that stratify less than 0% depth (between GCL and ON ChAT band), n = 17.

Figure 2.2

The eight groups are summarised in Fig. 2.2.e and displayed in Table 1. Setting aside any hindsight that one group (the bistratified cell group) contains ON OFF direction selective ganglion cells, it is important to stress that these 'groups' do not necessarily correspond to any particular cell type, since the divisions are based on only two properties of neural circuits, and those properties are derived from a purely morphological method of quantification. The notion of cell type must be reserved for a 'more complete profile' of each PV cell, which must include physiologically-derived information (see below). Coupling patterns were not taken into account. Nevertheless, several interesting findings resulted from the eight groups. First, groups that overlap in area do not overlap in depth, such as the three groups with the largest mean areas, 1, 5 and 6 (Fig. 2.2e and Table 1). Second, groups that overlap in depth do not overlap in area, such as the two groups that stratify at ~68% depth (Fig. 2.2e). Third, the ON dendritic trees of the independent bistratified group (group 0min, mean depth -2.2%) have the largest standard deviation of the area (18 mm^2) out of all the groups. The OFF dendritic trees (group 0max, mean depth 98.5%) had less variation (12 mm^2), which was also less than three other monostratified groups. This reinforces the finding that within the population of bistratified PV cells, there are several neurons with spatially-offset dendritic fields, since the ON and OFF standard deviations for area are not equal. Three neurons with large ON dendritic trees are shown in Fig. 2.2c, yet only one of these neurons has a comparably large OFF dendritic tree. If the three 'outliers' are removed, the mean areas for the ON and OFF dendritic trees become 21 and 27 mm^2 with a similar standard deviation of 7 and 6 mm^2, respectively.

Group	Mean depth (%)	S.D.	Mean area (mm^2)	S.D.	Mean diameter (µm)
0 min	-2.2	2.3	28	18	189
0 max	98.5	1.8	31	12	199
1	-40.8	9.3	53	15	260
2	23.9	7.2	25	6	180
3	43.3	6.2	11	4	121
4	68.8	3.5	24	6	173
5	68.4	4.0	58	11	271
6	134.0	13.8	42	16	232
7	136.3	10.0	11	3	118

Table 1. The eight morphological groups of PV cells in the PV retina. Bistratified PV cells, group 0 (0min and 0max for both dendritic trees). Monostratified PV cells, groups 1-7.

In many mammals, the area of a given ganglion cell type is related to its lateral position in the retina (referred to as its retinal eccentricity). Could the variation of PV cell dendritic tree areas within each stratum be to due retinal eccentricity? I measured the distance from the optic disk to soma for 17 PV cells from group 1 (those neurons with negative percent stratification and which had a wide range of dendritic field areas) (Fig 2.2f). There was no correlation between dendritic field area and distance. Mammals with a fovea or visual streak do show a correlation dependent on retinal eccentricity, but since the mouse is afoveate, each ganglion cell type is thought to have a fairly constant dendritic field area independent of position (Badea and Nathans 2004, Sun et al. 2002). Therefore, in the mouse retina (PV retina), area is not

determined by eccentricity, supporting the conclusion that depth alone does not indicate cell type and that the PV retina contains eight morphological groups of PV cells.

Quantification of PV cell physiology forms 8 groups

Is the morphological diversity of the PV retina linked to a similar physiological diversity? For example, do the two morphological groups whose dendrites stratify at the same depth (groups 4 and 5) have a different spiking output? Given that different bipolar cell types provide excitatory input to different ganglion cells dependent on IPL depth (Roska and Werblin 2001), it is reasonable to speculate that within the PV retina, cells from different groups but a similar depth may receive the same excitatory input. However, inhibition to the ganglion cell excitatory circuit, via amacrine cells, is dependent on the excitatory input to those amacrine cells, which can arise from many different bipolar cell types and modulate the spiking output of the ganglion cell. Therefore, as a readout of the underlying neural circuitry, I recorded light-evoked spiking activity from 600 PV cells and quantified the number of spikes and compared the statistics to the known morphological groups. For physiological quantification, I chose two parameters that in some respects mirrored the morphological parameters by emphasising biological traits. First, I used visual stimuli consisting of black and white spots on a grey background, reflecting the OFF and ON pathways that relate to OFF and ON bipolar cells and their axon terminal stratification in the IPL. Second, I used different spot diameters to map the receptive field of the PV cell, which takes into account both the dendritic field area (the 'centre', which integrates the direct bipolar cell input as well as amacrine cell input) and the contributions from the 'surround' (beyond the dendritic field area, involving only amacrine cell input) (Fig. 2.3a). These two parameters, spot contrast and spot diameter, resemble dendritic depth (IPL organisation) and dendritic area (visual space of the ganglion cell) respectively, allowing a direct comparison with the morphological groups.

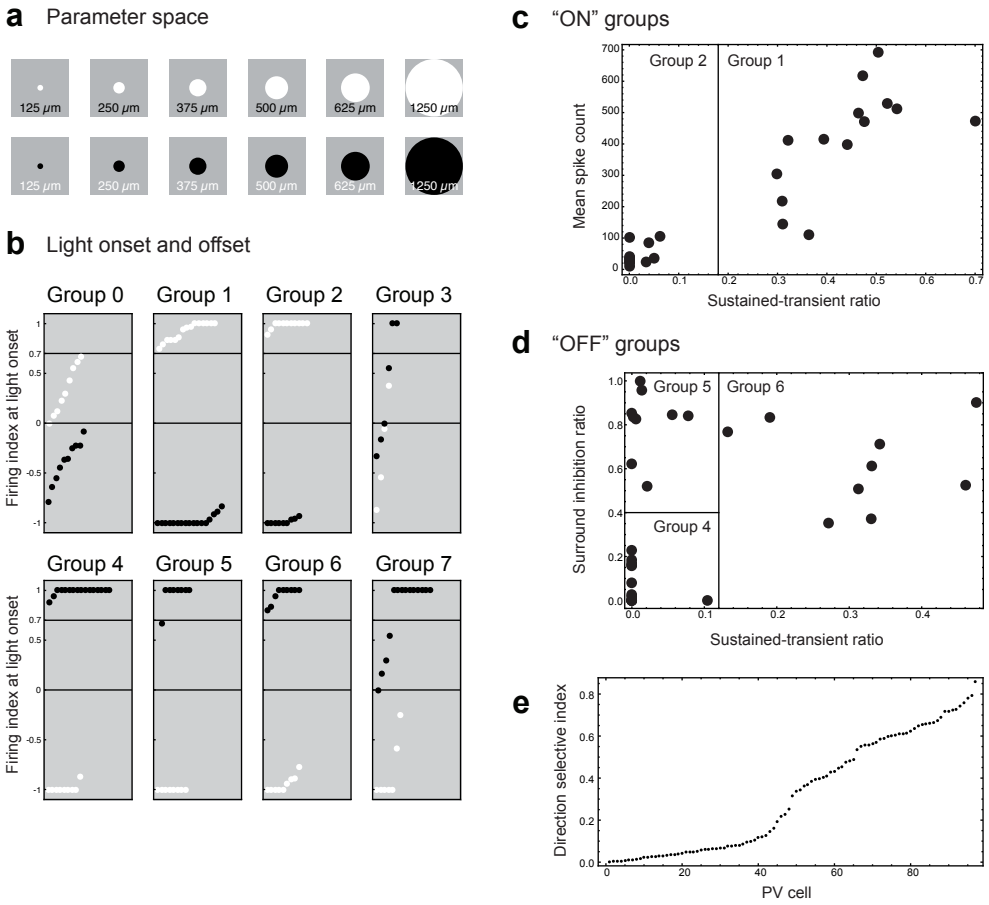

Figure 2.3. Physiological quantification of PV cells into 8 groups. (a) Parameter space used for quantification. Spots aligned to the receptive field centre of each recorded PV cell, each presented for 2 seconds on a grey background. Both black and white spots were used, with a range of sizes from 125 μm to 1250 μm in diameter. (b) Index of PV cell firing at onset of spot stimulus for all spot sizes, organised by morphological groups from Fig.2.2e. Each point represents a PV cell where the morphology has been quantified and grouped. White and black points indicate the spiking index during presentation of a white spot and a black spot, respectively (see Materials and Methods). For many cells, there are recordings for both white and black spots. +1 indicates that the cell always fires during the onset of the stimulus. -1 indicates that the cell never fires during the onset of the stimulus. A threshold of 0.7 is marked by black bars, representing divisions between predominantly 'OFF' or 'ON', or 'ON OFF' cells. (c) Separating all 'ON' cells from (b) by the ratio of sustained and transient firing rates for the white spot stimulus in (a). Sustained-transient ratio is plotted against mean spike count during the entire stimulus, and a threshold of 0.18 is marked by a black bar, dividing the cells into two groups. (d) Separating all 'OFF' cells from (b) by the sustained-transient ratio and the ratio of spikes during the largest black spot and the spot that evoked the maximum number of spikes ('surround inhibition ratio'). A threshold of 0.12 is used to separate more 'sustained' cells, and 0.4 to separate the transient cells by the surround inhibition ratio. (e) Direction selective index for 98 random PV cells, where 0 is non-direction selective and 1 is entirely direction selective. The majority of 'group 0' PV cells had an index above 0.5.

Figure 2.3

Spot contrast was quantified for all PV cells and formed three physiological groups based on a threshold of 70% for the firing index for the onset of the spot stimuli (Fig 2.3b). The three groups comprised cells that always fired at light ON (from morphological groups 1 and 2), cells that fired at light OFF (from morphological groups 3-7), and mixed firing cells (from morphological groups 0, 3 and 7). Evidently, spot contrast alone did not reveal a similar number of physiological groups to morphological groups. Ganglion cells fire at different rates for different lengths of time, dependent on the stimulus (Gollisch et al. 2008, Roska et al. 2006). ON-firing cells formed two groups based on the ratio between 'sustained' and 'transient' firing following stimulus onset (Fig 2.3c and see Materials and Methods). These groups corresponded to the two morphological 'ON' stratifying groups (Fig. 2.2e). For the OFF-firing cells (Fig. 2.3b), those that fired at high rates formed three groups based on the sustained-transient ratio and the 'surround inhibition' ratio. The latter refers to the phenomenon that the firing rate of ganglion cells is reduced in the surround from widefield inhibitory cells (Flores-Herr et al. 2001). These effects were measured using stimulation with the largest spot sizes versus the spikes evoked by the smaller spot sizes (Fig 2.3a). The three groups corresponded to the three morphological 'OFF' stratifying groups (Fig 2.2e). Groups 4 and 5 have the same stratification but a different dendritic field area, which reflects the same firing probability to black spots but a different firing rate in the surround. The mixed firing cells (Fig 2.3b) and the remaining OFF-firing cells with low firing rates could not be separated into groups that corresponded with the morphological groups 0, 3 or 7 with the same methods used for the other cells. However, the majority of cells corresponding to morphological group 0 were strongly direction selective, with an index of at least 0.5, based on a separate moving-spot stimulus (Fig. 2.3e and see Materials and Methods). Cells corresponding to morphological group 7 did not have a receptive field centered about the soma. Before stimulating cells with the spots shown in Fig. 2.3a, black squares of 100 µm length were flashed sequentially in a 9x9 grid about the soma, to map the receptive field centre. All 'group 7' cells had an offset receptive field centre, by which the maximum spikes were evoked for a black square other than the central square (data not shown). All other PV cells showed maximum evoked spikes for the central square. Finally, cells

corresponding to morphological group 3 had the highest (and more sustained) firing rate for the smallest spot stimulation, compared to other mixed or low-firing OFF cells. This suggests a very small receptive field, which also correlates with the morphology of group 3 (Table 1, mean dendritic field area). In summary, all quantified PV cells could be divided into physiological groups that matched the morphological groups, using various characteristics of their firing rate properties, so that morphological groups 0-7 correspond to physiological groups 0-7.

Morphological and physiological characteristics of PV cell types

The morphological and physiological groups were resolved to form eight PV cell types (denoted PV-0 to PV-7, matching the groups). This enabled all subsequent PV cell recordings to be classified as one of the eight PV cell types based either on physiology or morphology or both, with a high success rate. A third and important feature of the PV cell type was its two-photon imaging reconstruction (Fig. 2.1b). From a single z-stack scan, the PV cell type could be identified based on its soma size and pattern of primary dendrites. The mean firing rates for the spot stimuli, comprising all PV cells within each physiological group, are plotted in Figure 2.4. Here the physiological differences between each group are more evident, and reflect the morphological diversity (Fig. 2.5). The area-response profile (Fig. 2.4c) shows the firing rate as a function of spot size. PV cells from groups 0, 2 and 4 have a similar peak firing rate (250 µm), reflecting a similar receptive field/dendritic field size (Fig. 2.1g, 2.5b,d, and Table 1). PV-1 and PV-2 are the only cell types that receive input from only the ON pathway, which is reflected by firing at light ON (Fig. 2.4b) and stratifying at depths less than 30% (Table 1, Fig. 2.5a,b). However, PV-1 has a significantly higher firing rate than PV-2 (Fig. 2.4c) and a similarly larger dendritic field area (Table 1). Two other cell types with high firing rates and large dendritic fields are PV-5 and PV-6, two OFF-firing cell types (Fig. 2.4, 2.5e,f). Similarly, the two cell types with the smallest dendritic areas, PV-3 and PV-7, have the lowest firing rates, with PV-7 being by far the lowest (Fig. 2.4, 2.5c,g). Interestingly, both cell types are able to fire at light ON and at light OFF, even though PV-3 is monostratified and PV-7 stratifies near the INL (discussed below).

Nevertheless, these data demonstrate that PV cell types - the genetically-identified ganglion cell types of the PV retina - have specific physiological properties that mirror the morphological properties, indicating that the two 'independent' descriptions of cell type are intimately linked.

Figure 2.4. Physiological profile for spiking in the 8 PV cell types. (a,b) Summary of physiological groups for black (a) and white (b) spot stimuli. The spot sizes, represent by bars, are ordered as in (Fig. 2.3a). Firing rate is in 25 ms time bins for the mean of all PV cells of each group. (c) Area response profile for each group. The spike rate (spike count within first 1 second of spot stimulus) for each spot size from (Fig. 2.3a). All black spots, except groups 1 and 2, which are for white spots. Horizontal grey bars represent zero Hz for each group.

Figure 2.5. Morphology of the identified PV cell types in the PV retina. (a-g) PV-1, PV-2, PV-3, PV-4, PV-5, PV-6, PV-7 cell types, top views (greyscale) and side views (dendrites, magenta; ChAT bands, cyan). Side views orientated as in Fig. 2.1h, with the ON and OFF ChAT marker bands as 0% and 100% depth. (h) Rare 'giant' PV-0 cell (called PV-0G), with top view of filled cell in magenta, and other YFP-positive PV cells in green for comparison. Right two panels, top views of ON- and OFF-stratifying dendrites of the cell. 'Common' PV-0 cell type is shown in Figure 2.1. Scale bar, 50 µm, representing all images, except two right panels in (h), which are scaled down by 50%.

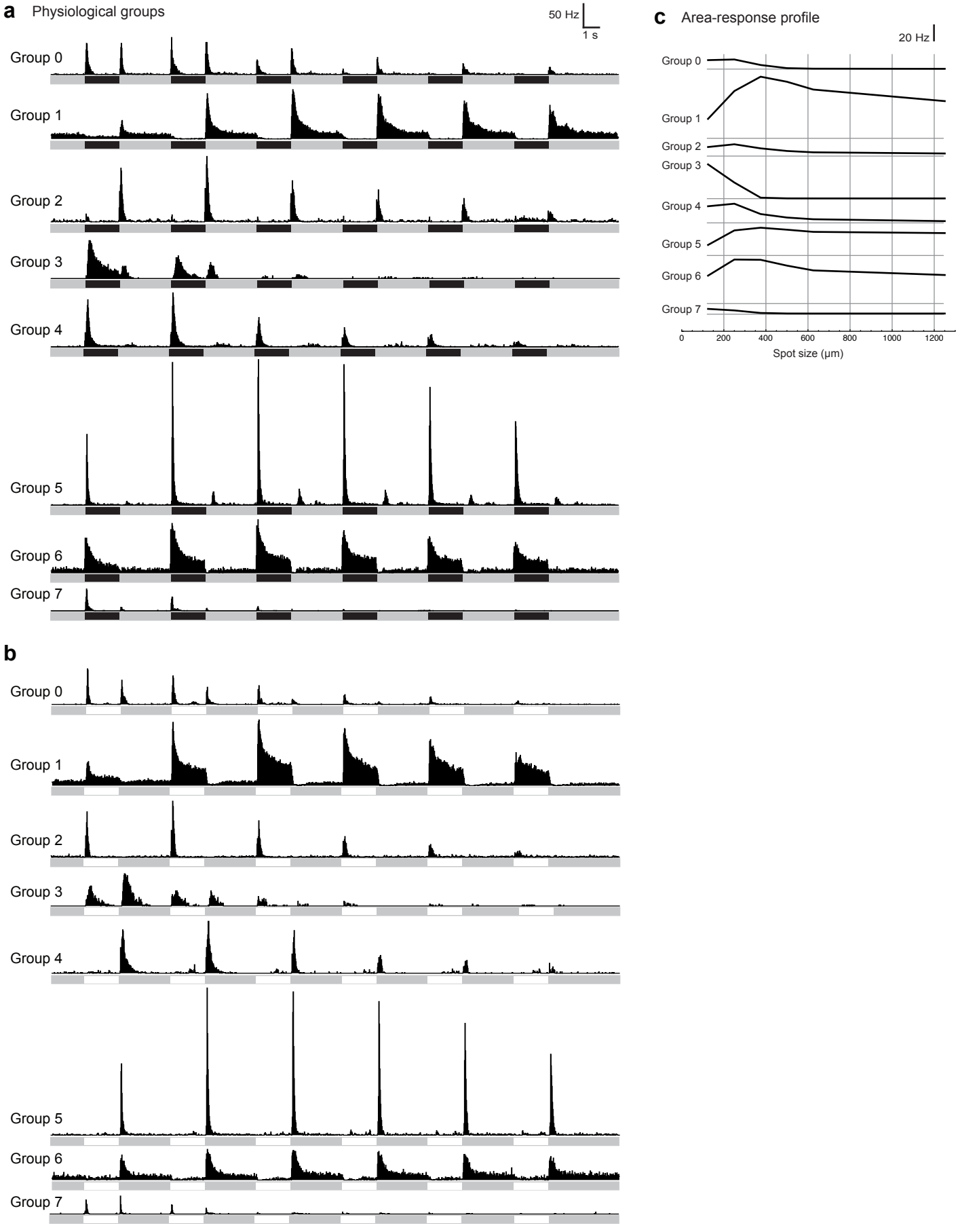
a
Physiological groups
50 Hz
1 s
Group 0
Group 1
Group 2
Group 3
Group 4
Group 5
Group 6
Group 7
b
Group 0
Group 1
Group 2
Group 3
Group 4
Group 5
Group 6
Group 7
c
Area-response profile
20 Hz
Group 0
Group 1
Group 2
Group 3
Group 4
Group 5
Group 6
Group 7
0
200
400
600
800
1000
1200
Spot size (µm)

Figure 2.4

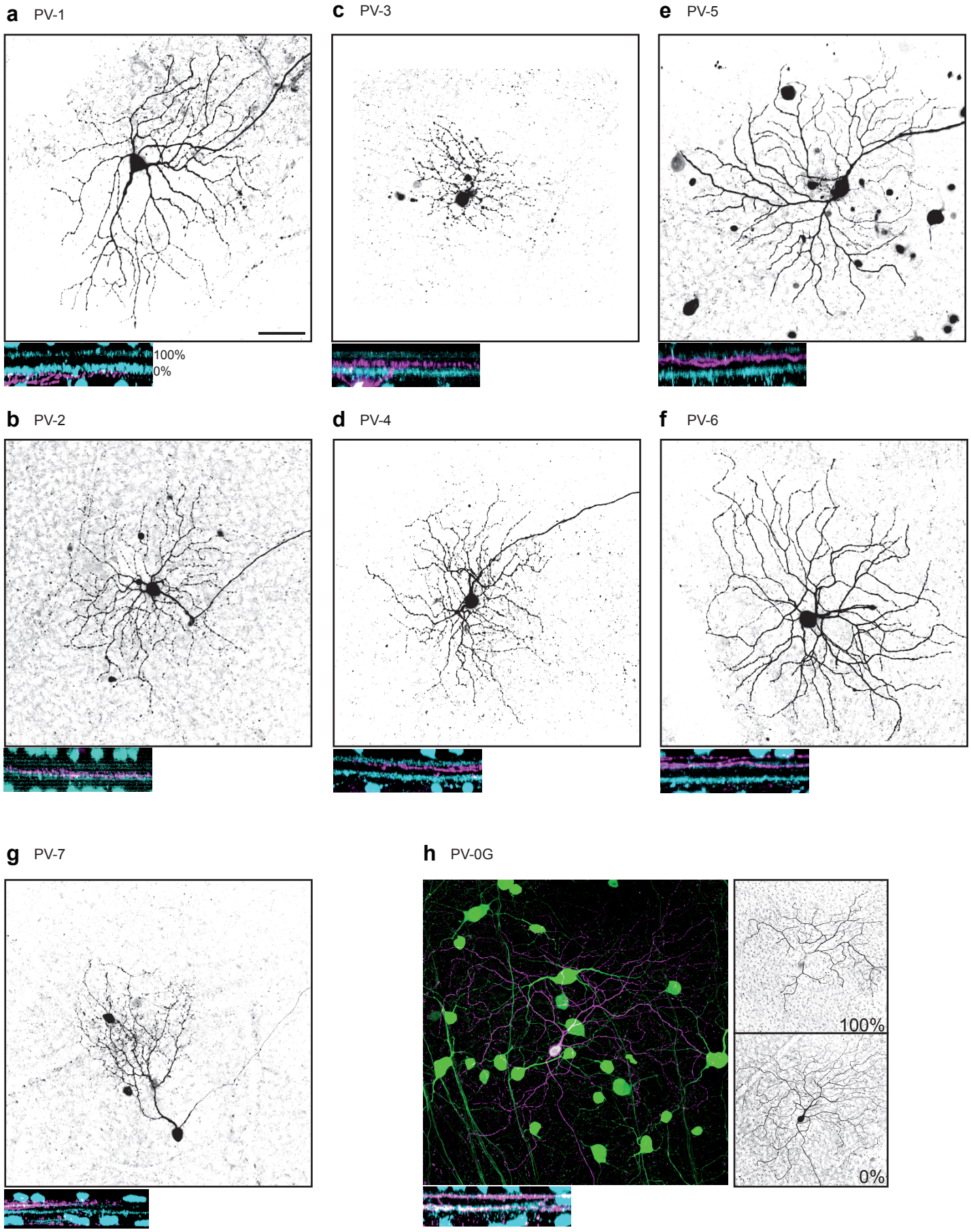

Figure 2.5

The motifs of 8 genetically-identified PV cell types

Firing rate is dependent on the interactions between inhibition and excitation that occur during visual stimulation at the photoreceptor level within the receptive field of the ganglion cell. To determine the nature of the temporal interactions that lead to cell-type-specific firing, I performed whole cell voltage clamp on 286 PV cells to isolate the excitatory and inhibitory input. I used the same spot stimulus (Fig. 2.3a) to determine the input pathways, this time at the level of the bipolar cells. Each PV cell type received a unique combination of excitatory and inhibitory input that interacted dynamically in time (Fig. 2.6). These dynamic interactions were termed 'motifs' and each PV cell type could be identified by its motif. The input from the ON and OFF pathways is summarised in Table 2. Motifs were also quantified, by measuring the time to reach 10% to 90% of the peak of the input (rise time). Rise time was chosen since it is an indication of how the input dynamically changes over time, irrespective of the timing of the onset of the stimulus. These data are displayed in Table 3. Two values were taken as representative rise times of the motifs: input for the 250 μm spot (a 'centre' stimulus) and input for the 625 μm spot (a 'surround' stimulus).

Figure 2.6. Motifs of the 8 identified PV cell types in the PV retina. (a) Motifs for PV-0, PV-1, PV-2, PV-3 ganglion cell types, and (b), motifs for PV-4, PV-5, PV-6, PV-7 ganglion cell types, displayed at high temporal resolution. Each PV cell type motif is shown as a column. Top row: light onset (grey to spot stimulus). Bottom row: light offset (spot stimulus to grey). First 600 ms after stimulus event is shown for the six spot sizes from Figure 2.3a. Red traces: discrete firing rate in 25 ms bins, normalised to peak rate (value below each column). Black and grey traces: excitation ± SEM (dark grey band) and inhibition ± SEM (light grey band), normalised to peak value (amplitude in pA below each column). Excitation has been flipped for comparison with the relative timing of inhibition.

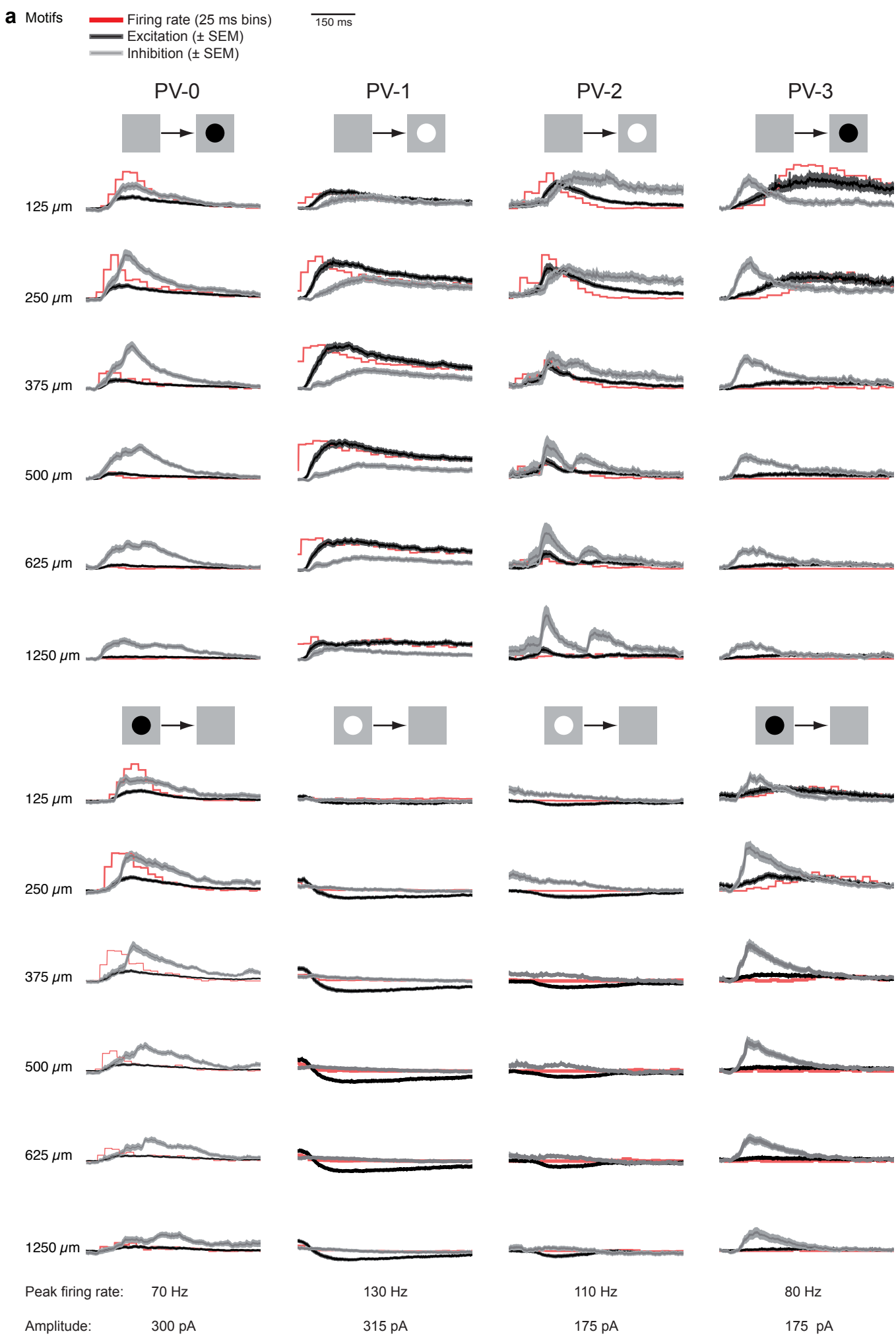
a Motifs
Firing rate (25 ms bins)
Excitation (± SEM)
Inhibition (± SEM)
150 ms
PV-0
PV-1
PV-2
PV-3
125 μm
250 μm
375 μm
500 μm
625 μm
1250 μm
Peak firing rate: 70 Hz 130 Hz 110 Hz 80 Hz
Amplitude: 300 pA 315 pA 175 pA 175 pA

Figure 2.6

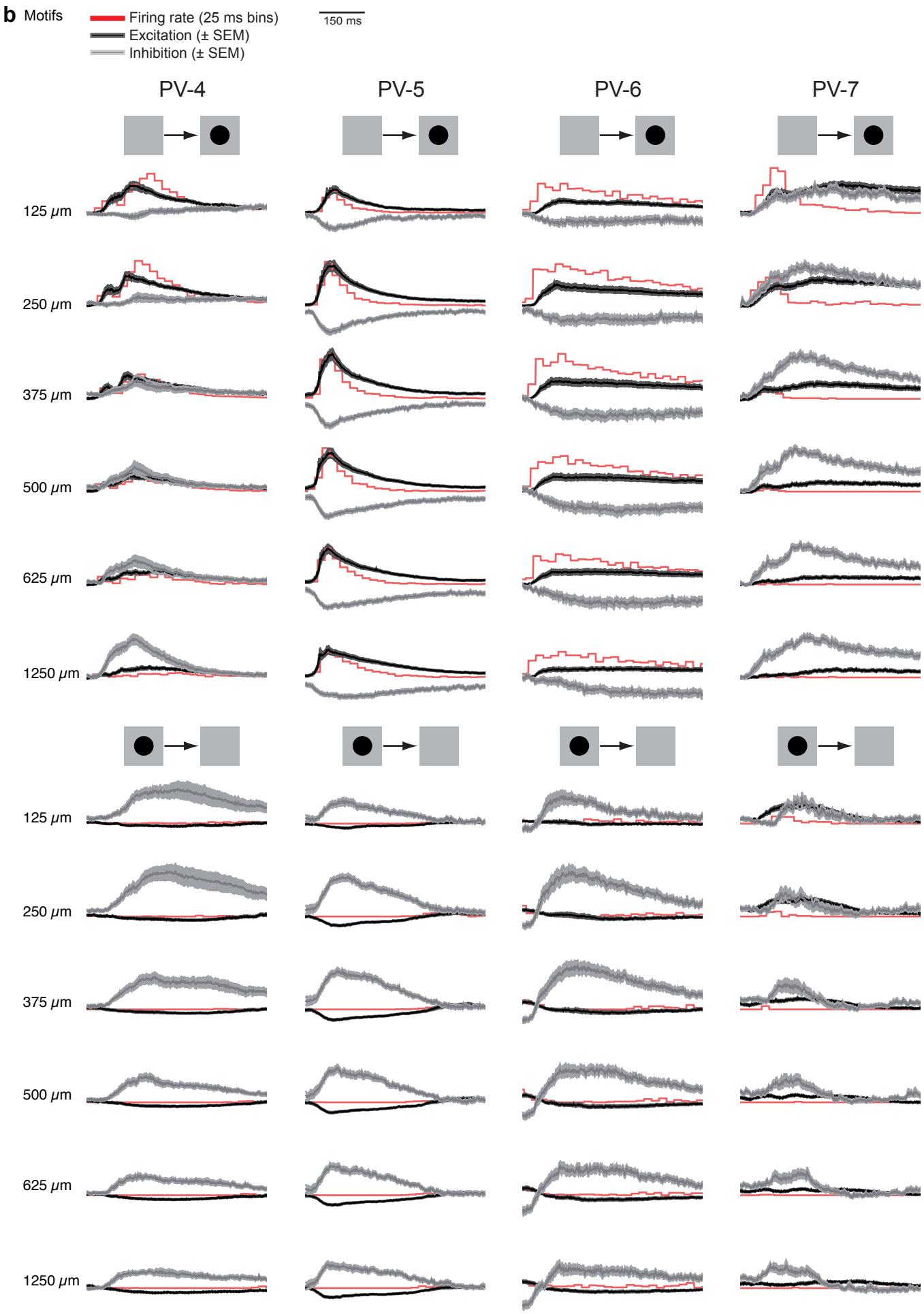
b Motifs
Firing rate (25 ms bins)
Excitation (± SEM)
Inhibition (± SEM)
150 ms
PV-4
PV-5
PV-6
PV-7
125 μm
250 μm
375 μm
500 μm
625 μm
1250 μm
Peak firing rate: 110 Hz 290 Hz 110 Hz 40 Hz
Amplitude: 175 pA 320 pA 185 pA 65 pA

Figure 2.6

PV cell	Excitation at onset	Excitation at offset	Inhibition at onset	Inhibition at offset
PV-0	OFF	ON	OFF	ON
PV-1	ON	-	ON	-
PV-2	ON	-	ON	-
PV-3	OFF	ON	OFF	ON
PV-4	OFF	*	OFF	ON
PV-5	OFF	*	-	ON
PV-6	OFF	-	-	ON
PV-7	OFF	ON	OFF	ON

Table 2. Summary of excitatory and inhibitory input to the PV cell types shown in Figure 2.6 for black spots (white spots for PV-1 and PV-2). *Occasionally inward currents were measured after the offset of black spots for PV-4 and PV-5; these are not excitatory but due to a 'rebound' effect from inhibition, which occurs 'out of phase' of excitation and can cause the cell to fire (see main text).

PV cell	Onset (excitation)	Onset (inhibition)	Offset (excitation)	Offset (inhibition)	Bias
PV-0	(76, -)	(49, 157)	(73, -)	(44, 116)	Inhibition
PV-1	(84, 133)	(140, 145)	-	-	Excitation
PV-2	(35, 27)	(103, 36)	-	-	Excitation
PV-3	(195, -)	(48, 71)	(122, -)	(23, 35)	Inhibition
PV-4	(72, 169)	(-, 103)	-	(195, 93)	Excitation
PV-5	(41, 33)	-	-	(105, 53)	Excitation
PV-6	(57, 196)	-	-	(113, 96)	Excitation
PV-7	(233, -)	(168, 125)	(246, -)	(59, 205)	Inhibition

Table 3. Precise timing of inhibition and excitation in the eight identified PV cell types. Rise time (10% to 90% of peak in ms) for onset and offset of (250 μm, 625 μm) spots, from Figure 2.6. PV-0, and PV-3 to PV-7 show rise times for black spots (OFF); PV-1 and PV-2 are for white spots (ON). 'Bias' indicates which input arrived first, based on the spot stimulus.

The standard error of the mean was small for all cell types for both excitation and inhibition (Fig. 2.6), suggesting that timing is very precise. I found several 'rules' that applied to all motifs. One, the spiking rate followed the rise time of excitation rather than arising from the peak (Fig. 2.6, compare black and red traces; Table 3). Two, the timing of inhibition was generally different in the centre and surround (except for PV-1) (Table 3). Three, inhibition and excitation did not change at the same rate (no motif had similar excitatory and inhibitory rise times). These rules suggest that the spot stimuli themselves bear no relevance to function. For example, for PV-5 and PV-6 (and to a lesser extent, PV-4), inhibition occurs 'out of phase' with excitation (also observed in the rabbit retina, see Introduction). What is the relevance of inhibition to these cell types? In another example, PV-3 receives a 'sluggish'

slow-rising excitatory input at light OFF and at light ON, yet inhibition changes approximately 4-5 times faster. Why is inhibition required when the firing rate simply follows excitation? These findings suggest that the motifs are purely 'hints' or 'clues' as to how inhibition and excitation interact during 'natural' visual stimulation. Since inhibition lowers the probability of the cell to fire by hyperpolarizing the cell (or by short-circuiting/shunting excitation), the ON and OFF pathways identified by the motifs (Table 2) for inhibition refer to those time points during visual stimulation when something is 'irrelevant'. The excitatory pathway(s) therefore must be taken as the 'default' visual channel of each cell type. When the interaction between excitation and inhibition is low (such as for the 'out of phase' motifs), this stimulus could be said to be one of the 'relevant' components that the ganglion cell type (parallel channel) is receptive to in visual space. When the interaction is high - when excitation and inhibition overlap - this could be considered the greatest 'null' stimulus, since the default excitatory visual channel that would cause the cell to fire is now 'blocked' (shunted/cancelled out) by inhibition. Each PV cell type thus has a different motif, based on specific excitatory and inhibitory input pathways (Table 2). The motifs, displayed in the time domain after onset or offset of the stimulus, provide a simple readout of the neural circuitry that leads to cell-type-specific firing. An alternative method to describe these inhibitory-excitatory interactions - the dynamics of each neural circuit - is to compare each time point of inhibition with each time point of excitation.

Precise inhibitory-excitatory interactions are a signature for cell type

Figure 2.7 shows how both components of the motif interact, for every PV cell type for each spot size. As the spot diameter increases, more inhibitory input is recruited (surround inhibition, reduction of firing rate for large spots, Fig. 2.4). In the parametric plots (Fig. 2.7), inhibition in most of the cell types changes faster than excitation, shown by a shift to the left of the plot for large spots. This is most apparent for PV-4 (Fig. 2.7a), which receives an in-phase form of inhibition in the surround (Fig. 2.6b). For PV-5 and PV-6 (and for the 'centre' stimulation for PV-4), inhibition does not interact for the spot stimuli. The 'out of phase' motif is clearly demonstrated by the lack of change of

inhibition for the change of excitation (Fig. 2.7b). The reason for the negative loops for light onset (PV-5 and PV-6) is due to the slight inward currents measured when attempting to clamp at inhibitory potentials (Fig. 2.6b). Similarly, at light offset for PV-5 and PV-6, inhibition is dominant, and changes without a change in excitation (vertical white loops, Fig. 2.7b). For PV-0, the only bistratified PV cell type (Fig. 2.1), inhibitory-excitatory interactions are mirrored for the ON and OFF pathways, shown by similar loops at onset and offset (Fig. 2.6b). Interestingly, inhibition changes slightly faster than excitation, due to the loops shifted to the left, suggesting that for these particular 'spot stimuli', which are simple flashes without movement, the PV-0 neural circuits are close to their 'null' stimulus parameter (discussed below). Note that this applies to 'centre' stimulation, within the receptive field of the ganglion cell. In the 'surround', in which the ratio of inhibitory circuits to excitatory circuits is larger, only inhibition changes, which reduces the probability of the cell firing. In the case of PV-1 and PV-2, inhibition and excitation only interact for light onset (white loops, Fig. 2.7a). Except for the smallest spots for PV-2, excitation changes faster relative to inhibition in PV-1 but slower in PV-2, when comparing the majority of spot sizes. However, if spot stimulation greater than 1250 μm were used, eventually a larger pool of inhibitory surround would be present to dominate PV-1. The difference between the receptive fields (and dendritic fields) of the PV-1 and PV-2 cell types simply emphasises the large central pool of direct excitatory input to the PV-1 cell. Furthermore, both cell types show wide loops (compared to PV-4 or PV-0, for example), suggesting that the input follows a sustained time course. Finally, PV-3 and PV-7, which have the smallest areas (Table 1), both show dynamic interactions for the two smallest spots (which dominate their dendritic field - 'centre' stimulation), corresponding to the highest firing rates (Fig. 2.4). However, PV-3 has a striking fast change in inhibition at the onset of the small spot stimuli, not present in PV-7. Excitation gradually takes over in PV-3, after the peak, as inhibition falls, indicated by the 'triangular' loops (Fig. 2.7a). Again only inhibition dominates the surround, shown by vertical loops to the left of the plots. These inhibitory-excitatory interactions, when displayed parametrically, suggest a 'signature' of each cell type, which may prove useful when analysing more 'natural' input to their circuits.

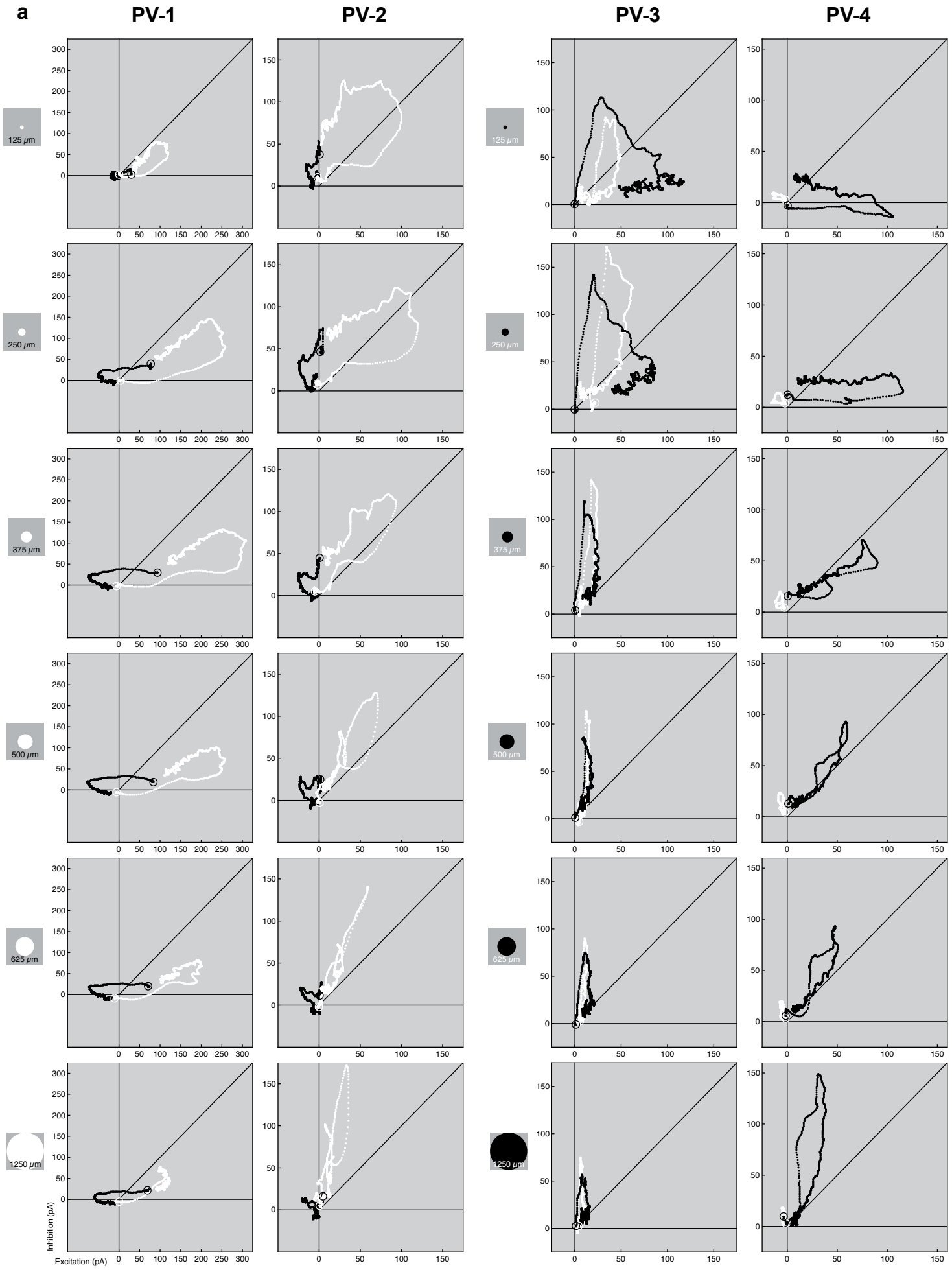
a
PV-1
PV-2
PV-3
PV-4
125 μm
250 μm
375 μm
500 μm
625 μm
1250 μm
Inhibition (pA)
Excitation (pA)

Figure 2.7

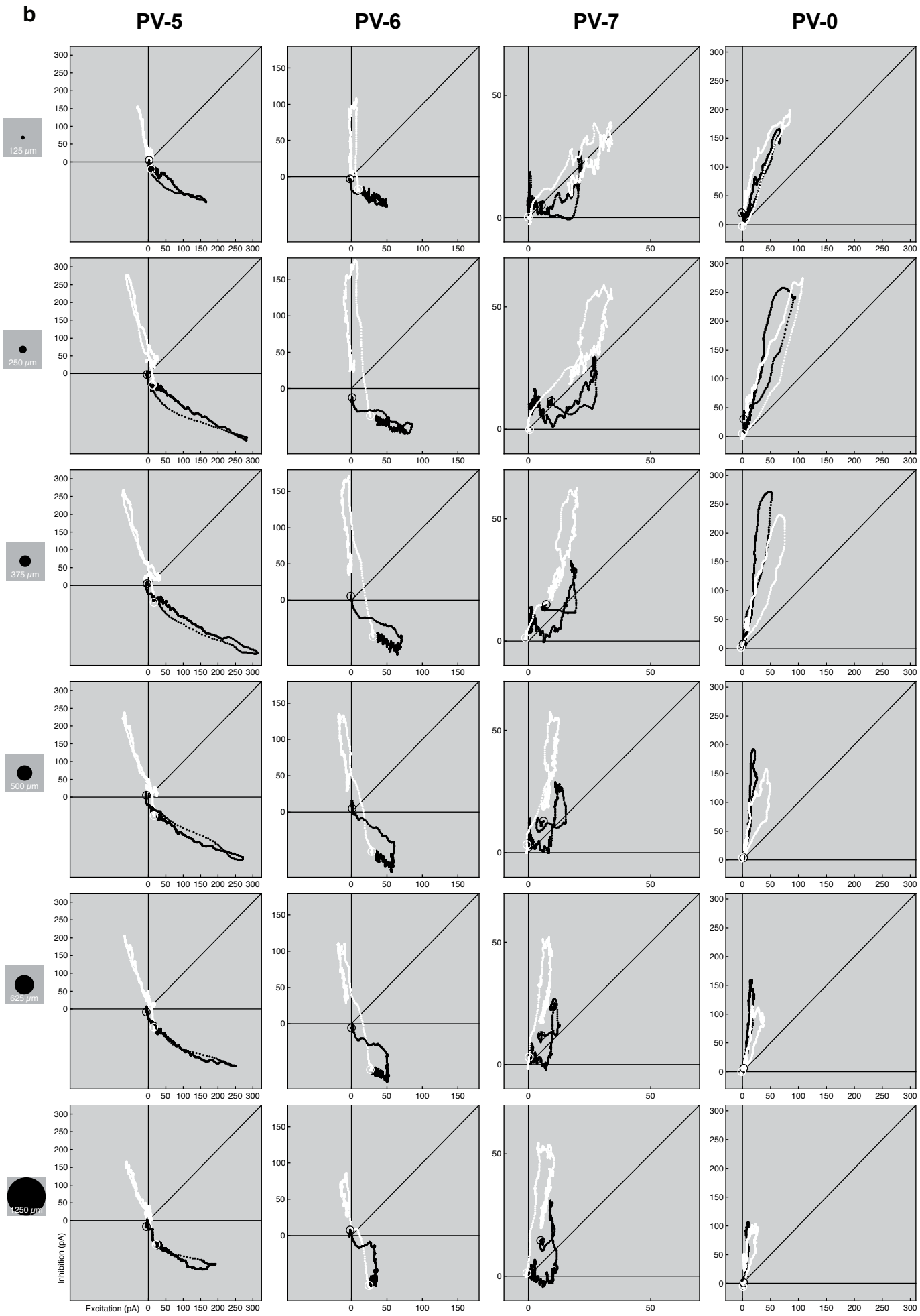
b
PV-5
PV-6
PV-7
PV-0
125 μm
250 μm
375 μm
500 μm
625 μm
1250 μm
Inhibition (pA)
Excitation (pA)

Figure 2.7

Figure 2.7. Inhibitory-excitatory interactions for all PV cell types during visual stimulation. (a,b) Motifs from Fig. 2.6 displayed as parametric plots, with each time point of inhibition (y-axis, pA) plotted against excitation (x-axis, pA). PV-1 and PV-2 are shown for white spot stimuli. PV-3 to PV-7 and PV-0 are shown for black spot stimuli. Black points represent inhibitory-excitatory interactions at light OFF (offset of white, or onset of black); white points represent interactions at light ON (onset of white, or offset of black). A ring indicates the first time point after the stimulus change. Interactions are plotted for the first 1000 time points (1 sec after stimulus change). Unity line artificially divides regions of excitatory and inhibitory dominance.

The role of inhibition during natural visual stimulation

To demonstrate the role of inhibition in parallel circuits, I targeted different PV cell types and compared their spiking patterns during 'natural' visual stimulation, consisting of movies acquired from a camera mounted to a cat's head whilst it explored a wood (see Materials and Methods). These natural scenes included a wide range of contrasts and movement, mimicking natural vision (Betsch 2004). First, to demonstrate parallel processing, I asked whether PV cells of the same type have the same spiking patterns to natural stimulation, and cells of different types have different spiking patterns. Second, I targeted cells that had the same dendritic depth but different dendritic areas, PV-4 and PV-5 (Fig. 2.2). These PV ganglion cells might receive input from the same types of bipolar cells and amacrine cells. But due to both the independent morphological groupings (Fig. 2.2e, groups 4 and 5) and physiological groupings (Fig. 2.4, groups 4 and 5), I classified them as different cell types. Therefore, what similarities and differences would there be in the 'naturally evoked' firing patterns from these two cell types, which have different motifs (Fig. 2.6, 2.7)? I chose a region of the PV retina with several labelled 'OFF'-stratifying PV cells (Fig. 2.8a), and recorded their light-evoked spiking activity to identify the cell type (Fig. 2.8b). I found four PV-4 cells (cells 1-4) and two PV-5 cells (cells 5-6), none of which stratified in the inner IPL (Fig. 2.8a, middle image). I also recorded a PV-1 cell (cell 7) for comparison with the OFF-firing cells, which did stratify in the inner (ON) IPL (Fig. 2.8a). The cells are grouped by type (Fig. 2.8b), but were patched in the following order: 1, 5, 2, 6, 3, 7, 4. They were also patched with the same cleaning pipette (see Materials and Methods), meaning that there was little time

between recordings when the retina was illuminated with infrared light. Interestingly, the supposedly 'OFF-firing' cells (which both stratify in the OFF IPL, at ~68% relative depth (Table 1)), were also able to fire at light ON (offset of black spots). The first two recorded cells (cells 1 and 5, top row Fig. 2.8b) matched the physiological groupings by firing at light OFF (Fig. 2.4a). The second row of cells (cells 2 and 6) showed spiking activity at light OFF and at light ON. However, the spikes at light ON had a latency of 0.5 seconds and were less than half the rate of the OFF spikes. Cells 3 and 4, which were patched afterwards, also displayed this delayed-ON-spiking behaviour, this time with the same latency but with a firing rate that matched the OFF spikes (Fig. 2.8b, lower rows). Cell 7, a PV-1 cell, did not show spiking activity at light OFF, reflecting its physiological grouping (Fig. 2.4b). Since for the majority of the experiment the retina was illuminated with visible (bright) light, it is reasonable to suggest that the network state of the retina – the degree of adaptation to light - was different for the last recorded cells than it was for the first recorded cells. All other conditions were equal, including the pipette, temperature, and stimulus set. In most experiments, the algorithm was to target a PV cell, record light-evoked spiking activity, then approach with a new pipette for whole cell voltage clamp recording. In these experiments, the retina was under infrared illumination for most of the experiment. Here, the retina was illuminated with visible light for more than 90 minutes, with brief intervals under infrared for targeting the next cell. Therefore, under these conditions, the retina could be said to have become 'fully light adapted'. Consequently, a new source of spikes appeared in the two OFF PV cell types, PV-4 and PV-5. What is the origin of this? It most likely arises from the inhibitory pathway, which is an ON pathway in both PV-4 and PV-5 (discussed below).

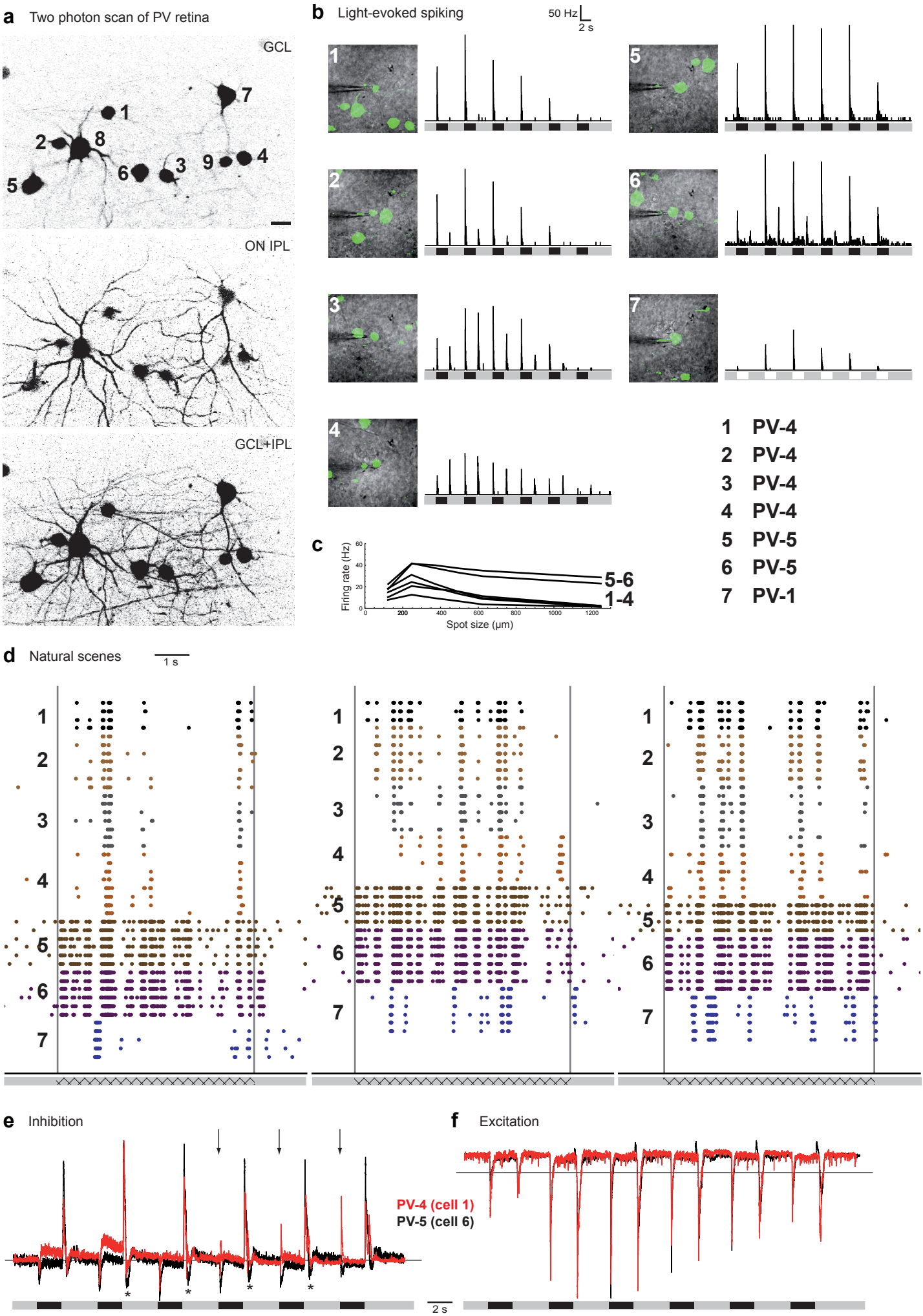
a
Two photon scan of PV retina
GCL
ON IPL
GCL+IPL
b
Light-evoked spiking
50 Hz
2 s
1 PV-4
2 PV-4
3 PV-4
4 PV-4
5 PV-5
6 PV-5
7 PV-1
c
Firing rate (Hz)
Spot size (μm)
5-6
1-4
d
Natural scenes
1 s
e
Inhibition
f
Excitation
PV-4 (cell 1)
PV-5 (cell 6)
2 s

Figure 2.8

Figure 2.8. Parallel processing in the PV retina demonstrated by different PV cell types. (a) Two-photon maximum intensity z-projections of a region of the PV retina at two different levels: GCL (ganglion cell layer), ON IPL (innermost inner plexiform layer), and below the full z-projection (GCL with full IPL). Numbers indicate each targeted PV cell. Scale bar, 20 µm. (b) Light-evoked spiking activity of PV cells from (a), for increasing-size spot stimulus from Fig. 2.3a. Left of each recording is a two-photon overlay (green) with the patch pipette on the PV cell in the GCL (greyscale). (c) Area-response profiles as in Fig. 2.4c, for PV cells 1-6. PV cells 5 and 6 have a higher firing rate in the surround (large spots). Right, PV cell type for each recorded cell, identified by two-photon imaging (morphology-based) and the spiking profile from the spot stimuli (physiology-based). (d) Three natural scenes presented to all 7 targeted cells (scenes were centered about the soma). Each line represents a single recording. Horizontal bars represent the onset and offset of each movie, with uniform grey as background before and after. Each point is a spike, and each cell is given a different colour. Some movies were presented more times to some cells than others. (e,f) Whole cell voltage clamp of a PV-4 cell (cell 1, red), and a PV-5 cell (cell 6, black) for the same stimulus as in (b), recorded at the end of the experiment and normalised to their own peaks (PV-4 had the smaller amplitude). (e) Inhibition (+20 mV holding potential), with arrows showing surround 'OFF' inhibition in PV-4, and asterisks indicating putative post-inhibitory rebound inward currents. (f) Excitation (-60 mV holding potential).

After characterising the cell type with the increasing spot stimuli, and showing that the two PV-5 cells were separate from the four PV-4 cells (Fig. 2.8c), three natural movies were presented and spiking activity was recorded (Fig. 2.8d). The firing patterns were repeatable in each cell. Furthermore, the firing patterns were identical within the same cell type and different to the other cell types (PV-4 cells 1-4; PV-5 cells 5-6, PV-1 cell 7). The only ON cell (cell 7, PV-1) fired at times when all the OFF cells did not fire, suggesting that all ON-pathway cell types complement OFF-pathway cell types. There was also a similarity between PV-4 and PV-5. Each spike event from PV-4 correlated with a spike event from PV-5, even though PV-5 also fired at other time points. This suggests that cell types that stratify at the same depth might receive the same excitatory bipolar input and therefore be receptive to similar components of the visual scene. What are the differences in the input pathways to PV-4 and PV-5 under the same conditions in the same region of the PV retina? I chose one cell of each type (cells 1 and 6) and recorded inhibition and excitation using whole cell voltage clamp (Fig. 2.8e,f). In these fully light adapted conditions, both cell types received a transient ON inhibitory input that followed the same time course (Fig. 2.8e). The only difference was

that PV-4 received an additional OFF inhibitory input in the surround (arrows). This could be responsible for the sparser firing patterns of PV-4 compared to PV-5 (Fig. 2.8d). Alternatively, the sparser patterns could be due to a smaller dendritic field area (Table 1), pooling less excitatory input than PV-5. After the ON inhibition in both cell types, an overshoot was observed (asterisks). This overshoot, or post-inhibitory rebound, could be responsible for the additional inward currents measured at light ON (light offset) at -60 mV (Fig. 2.8f), matching the ON spikes (Fig. 2.8b). Excitation was time-locked for both cell types in these conditions (since both cells were patched in whole cell mode after recording spiking from all other cells), further suggesting that they receive the same type of bipolar cell input (Fig. 2.8f). Interestingly, the ON spikes from PV-1 in the natural scenes (Fig. 2.8d) did not coincide with any spikes from the PV-4 or PV-5 cells, suggesting that the ON spikes measured in these 'OFF firing' cell types for spot stimuli were either not evoked during natural stimulation (due to inhibition interacting with excitation), or still had a longer latency, and arrived slightly after PV-1 ON spikes (Renterìa et al. 2006). In the case of PV-1 and PV-5, the transient/sparse firing patterns observed during natural scenes is in contrast to the more sustained firing patterns evoked during simple spot stimulation. The remaining PV cells from the same region of the PV retina were also identified (Fig. 2.8a). Cell 8 had the same stratification as cell 7 and was a PV-1 cell. Cell 9, adjacent to cell 4, was a PV-7 cell, identified by its single polarized primary dendrite that extends into the outer IPL (OFF layers) (Fig. 2.8a and Fig. 2.5g). In fact distance between cells of the same type is an important parameter for identifying cell type, and is discussed below. Every PV cell could be identified as a specific type within the region scanned in Fig. 2.8a. This is further evidence for the existence of eight main PV cell types in the PV retina, although it is not possible to rule out more types. The natural scenes data show that each ganglion cell type responds in parallel to different components of a dynamic visual scene, with ON-pathway cells firing at the opposite contrast to OFF-pathway cells (excitatory pathways), and that cell types that receive similar or the same excitatory input share many spiking output events. Inhibition may modulate the sparseness of the spiking events by interacting with excitation at time points when the information content in the visual scene is 'irrelevant'

(about the ideal 'null-stimulus', which is defined and determined by the central and surrounding inhibitory input). The next step would be to quantify the inhibitory-excitatory interactions during natural scenes to further explore the role of inhibition in these identified circuits.

Features of the PV retina

Within the PV retina, eight specific cell types have been identified, yet each cell type, representing the integration of local excitatory and inhibitory circuits in parallel, has specific features unique to that type. One main criterion briefly mentioned above - distance between cells of the same type - is key to defining the cell type. To act as parallel visual channels, the ganglion cell types must independently tile the retina (Wässle and Riemann 1978), so there must be a minimum distance between each cell of a given type. I therefore used the PV retina to measure the minimum distance between identified cell types. From multiple two-photon z-projections, I quantified the distances between cells of known types. This was possible for PV-7 due to the single polarized primary dendrite (Fig. 2.5g confocal example). In many two-photon images there were several labelled PV-7 cells, each with their primary dendrite pointing in the same direction. The minimum distance between any two PV-7 somata was approximately 50 µm (Fig. 2.9a). It was also possible to quantify the minimum distance for PV-1, which is identified from two-photon images by its several thick primary dendrites extending immediately from the soma into the innermost IPL (Fig. 2.8a, middle image, cells 7 and 8). PV-1 is the only negative-stratifying cell type (mean depth -40.8%, Table 1). The minimum distance measured between PV-1 somata was ~100 µm (Fig. 2.9a), and given a mean dendritic diameter of 260 µm (Table 1), this value indicates that PV-1 cell dendritic fields overlap by more than 50%. These minimum distances for PV-1 and PV-7 suggest that these cell types independently tile the retina. Is this true for all identified PV cells in the PV retina?

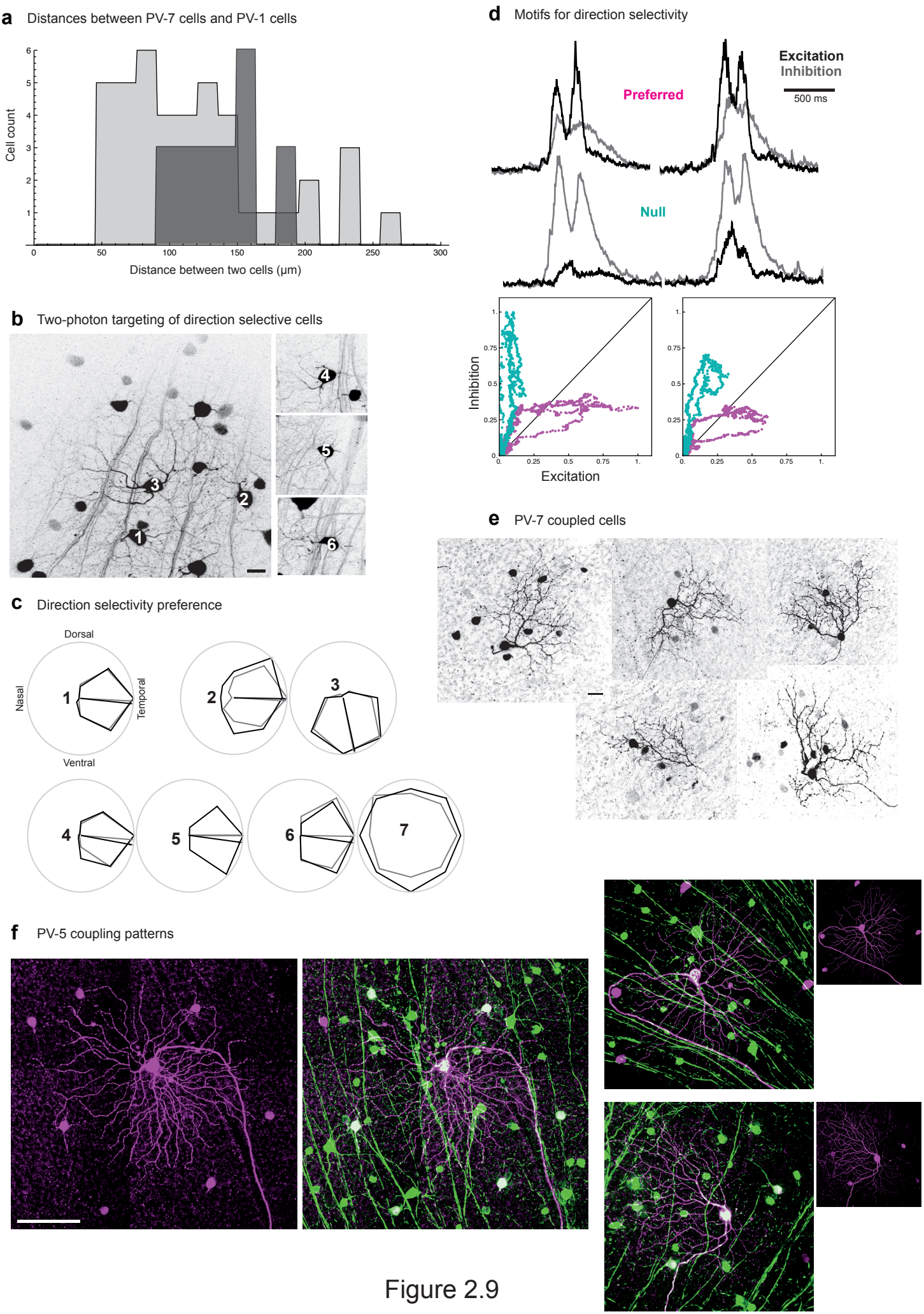
a
Distances between PV-7 cells and PV-1 cells
Cell count
Distance between two cells (μm)
b
Two-photon targeting of direction selective cells
c
Direction selectivity preference
Dorsal
Nasal
Temporal
Ventral
d
Motifs for direction selectivity
Excitation
Inhibition
500 ms
Preferred
Null
Inhibition
Excitation
e
PV-7 coupled cells
f
PV-5 coupling patterns

Figure 2.9

Figure 2.9. Cell-type-specific properties within the PV retina. (a) Histograms of distances between PV-7 cells (light grey bins) and separately PV-1 cells (dark grey bins) from two-photon images (n = 20 and 13). (b,c) Direction selectivity of PV cells. (b) Two-photon maximum intensity z-projections of a region of the PV retina. Numbers refer to different targeted cells. Scale bar, 20 µm (c) Direction selectivity preference for PV cells targeted in (b). (d) Motifs for a PV-0 cell (excitation, normalised, black; inhibition, normalised, grey) during presentation of a 200 µm diameter white spot moving across the receptive field at 900 µm sec^{-1} on a grey background. Top two traces represent motifs during two 'preferred' directions, when the cell fires. Middle two traces are motifs during 'non-preferred' motion (null stimulus), when the cell does not fire. Bottom panels are corresponding parametric plots for the two motif sets. Magenta loops represent inhibitory-excitatory interactions during preferred motion; teal loops represent interactions during non-preferred motion. Unity lines represent bias for inhibition (left) and excitation (right). (e) Five PV-7 cells (top view z-projections, neurobiotin), showing coupled cells with somata in the GCL. Scale bar, 20 µm. (f) Coupling patterns in three PV-5 cells (top view confocal z-projections). Magenta, neurobiotin (filled cell). Green, GFP (labelled PV cells). Left two panels, tile scan showing seven coupled cells, 6/7 are GFP-positive. Top right panel, PV-5 cell is coupled to four ganglion cells in the GCL, all GFP negative, and two small cells with their somata in the INL within the dendritic field of PV-5. Bottom right panel, PV-5 cell is strongly coupled to two ganglion cells and weakly coupled to three ganglion cells. All are GFP positive. Right panels show adjacent neurobiotin channel scaled down by 50%. Scale bar, 100 µm.

PV-0 cells, although having round somata and strongly labelled with YFP, cannot be as easily identified in the two-photon scans. Fortunately, they are highly direction selective compared to all other PV cells, so that it is possible to screen for PV-0 cells by two-photon targeted patching. PV-0 is not part of the 'monostratified' cell type classification scheme, hence the '0' designation. It can be considered separate because it is bistratified, meaning that it receives two independent forms of input - one local circuit from the ON pathway and another from the OFF pathway. This is in contrast to PV-3 (see below), which is monostratified yet also receives input from both ON and OFF pathways. In this case, input to PV-3 from both pathways may directly interact, since signals must be integrated on the same stratum. 100% of recorded PV-0 cells were direction selective, having a high direction selective index (Fig. 2.3e, Fig. 2.7b). Furthermore, by marking the orientation of the retina prior to isolation, the vast majority of PV-0 cells were found to be temporal-preferring (Fig. 2.7c). The exception was the third cell, which was

ventral-preferring (Fig. 2.7c). What is the difference between these cells? Between the temporal-preferring PV-0 cells, the minimum soma-soma distance was calculated to be ~110 µm (and with a mean diameter of ~195 µm, this indicates that these cells do not overlap but may just touch the proximal dendrites). Any direction selective cell less than this distance had a different preference, such as cell 3 in Fig. 2.9b,c. Interestingly, this example was one of the rarely encountered 'giant' PV-0 cells (Fig. 2.5h), also indicated by the thicker radial dendrites in the two-photon image (Fig. 2.9b). It is already known that several cell types can exist within the same IPL stratum. For instance, there have been seven cell types characterised that costratify with the ON ChAT band (0% depth in PV retina nomenclature). These are three types of so-called 'ON direction selective' cells (Levick 1967, Oyster 1968, Sun et al. 2006, Yonehara et al. 2008, Yonehara et al. 2009) and four types of 'ON OFF direction selective' cells (Barlow et al. 1964, Taylor and Vaney 2002, Weng et al. 2005). The ON OFF cells are bistratified. Each cell type has a different directional preference. Clearly, the majority of PV-0 cells in the PV retina represent the temporal-preferring cell type. However, the 'giant' PV-0 cell type, termed PV-0G, could be considered as a valid ninth PV cell type, based on the definitions described in this chapter. Due to the low number (n = 5, mostly only morphology), the cell has not been analysed further. Interestingly, two of the giant cells showed strong coupling to unknown cells in the GCL. What is the role of the 'giant' direction selective cell? Given that there are four directions, are there other (non-labelled) giant direction selective cells within the retina for the nasal, temporal and dorsal directions? In any case, a rule emerges whereby for any given cell type, if there is a PV cell less than the minimum distance, that cell will be of a different type. This applies to PV-0 and PV-0G cells, as well as for any combination of cell types. Even though the four ON OFF direction selective cell types are morphologically identical, they each independently tile the retina. This rule fits with the concept that all ganglion cell types independently cover the retina as an array, and may be used as a parameter in a targeting algorithm in the PV retina.

To summarise the main PV-0 neural circuitry, this cell type is one of the so-called direction selective cell types, previously characterised and conserved in mouse and rabbit (Barlow et al. 1964, Sun et al. 2002, Rockhill et al. 2002, Roska and Werblin 2003, Famiglietti 2005, Roska et al. 2006, Weng et al. 2005). It receives glutamatergic input from excitatory bipolar cells, acetylcholinergic excitatory input from starburst amacrine cells, and inhibitory GABAergic input from the same amacrine cells, which are responsible for its direction selectivity (Fried et al. 2002). Given that the interaction between inhibition and excitation is strong for simple flashing spot stimuli (Fig. 2.7b), how does inhibition interact for moving spots? Due to the fact that inhibition interacts with excitation for the stationary spots already suggests that this stimulus is close to its 'null function'. In two examples from the PV-0 cell type, when a spot is moved across the receptive field, one direction reveals that excitation changes faster than inhibition (Fig. 2.9d, top traces), and another direction reveals inhibition changing faster than excitation (Fig. 2.9d, middle traces). Differences in magnitude are due to both pre- and post-synaptic inhibition (Fried et al. 2002). The double peaks are due to the ON and OFF pathways being activated (first peak, ON pathway, from onset of white spot - leading edge. Second peak, offset of white spot - trailing edge). When the inhibitory-excitatory interactions are shown in a parametric plot, the role of inhibition for the preferred and null directions is more evident (Fig. 2.9d, bottom plots). When excitation is changing faster than inhibition, the loops shift to the right, where the cell fires (preferred). When inhibition changes faster than the change in excitation (null), inhibition has hyperpolarized the cell (and inhibited bipolar cell release) and blocked firing. The role of inhibition is therefore to block any 'irrelevant' motion, i.e. all other 'non-preferred' directions except the preferred direction. The next step would be to quantify these interactions in the parametric plots, to predict the behaviours of a given ganglion cell. Similar interactions seen in PV-0 are likely to be occurring during natural stimulation.

Another advantage of the PV retina is that many biological questions can be addressed. For example, given that there are left and right retinas, are the majority of PV-0 cells all temporal-preferring in both retinas? If they were the

same, this would suggest a common 'molecular profile' of each cell type, even from those closely related by function. Another cell type that has 'directional' information is PV-7 (Fig. 2.5g, 2.2d left). In each PV retina, PV-7 cells are pointing in the same direction. They are also weakly direction selective, having a direction selective index between 0.1 and 0.3 (Fig. 2.2e). If they were found to have the same *orientation*, then they would be a useful tool - a molecular compass - for the PV retina. The orientation marker would also benefit the studies of the PV-0 direction selective ganglion cells, since the direction preference could be correlated with PV-7. A recently identified cell type has been shown to be an 'upward motion preferring' cell (Kim et al. 2008, also randomly labelled by Sun et al. 2002). PV-7 is probably the same or a related cell type, depending on which direction it points, and suggests a function in the domain of direction selectivity. Interestingly, the motif of PV-7 shows input from both ON and OFF pathways (Fig. 2.6b), even though it stratifies in the 'OFF' region of the IPL (Fig. 2.2c,e), suggesting only OFF bipolar input. However the single-labelled cell type similar to PV-7 was found to overlap minimally with ON bipolar cells (Kim et al. 2008), and given that ON bipolar cell axons must pass through the 'OFF' region of the IPL, it is also possible that there are ectopic synapses between ON bipolar cells and OFF-stratifying ganglion cells (Dumitrescu et al. 2009). In fact the same 'reporter line', Thy1-Stop-EYFP was used to generate both their transgenic line and the PV mouse line described here. However, PV-7 contains an additional component that cannot be revealed by a purely transgenic approach. The neurobiotin used in the patch pipettes is able to pass through gap junctions, therefore, each recorded PV cell that is electrically coupled was revealed *post-hoc*. 100% of PV-7 cells were coupled to small YFP-negative cells, with their somata in the GCL within the dendritic field of the PV-7 cell and processes costratifying with the PV-7 dendrites, above 100% depth (n = 21). This was similar to another recently described asymmetric coupled ganglion cell (Völgyi et al. 2009). No coupled cell had a resolvable axon, suggesting that they are amacrine cells. Five examples are shown in Fig. 2.9e. Since electrical coupling is sign-conserving, coupled cells influence the ganglion cell output. For this reason, I did not exclude the neurobiotin-streptavidin-Alexa Fluor 555 signal from coupling observed in the immunostained tissue when

quantifying the stratification of PV-7 cells. This contributed to the large standard deviation (10%) of depth: coupled cells form a dense band above 100% depth and should be considered an integral part of the PV-7 circuitry. A similar cell type has been characterised in the rabbit retina, also coupled (Roska and Werblin 2003, Roska et al. 2006).

PV-7 cells were not the only cell types to be coupled. Both PV-5 and PV-2 cells were often coupled, but the coupled was not observed as frequently as for PV-7. PV-5 has an 'out-of-phase' motif (Fig. 2.6b, 2.7b, and compare to rabbit motif in Introduction Fig. III). PV-5 has a 'fast' form of inhibition when presented with a spot that stimulates both the centre and surround, with a mean rise time of 53 ms (Table 3). The role of inhibition in the PV-5 local circuit is described in Chapter 3. PV-5 has been previously described in different mammalian species including mouse, cat and guinea pig, and is often named 'OFF alpha' or 'OFF alpha transient' due to its large soma, large dendritic field and 'transient' firing patterns based on simple spot stimulation (Sun et al. 2002, Pang et al. 2003, Völygi et al. 2005, Kong et al. 2005, Manookin et al. 2008, Huberman et al. 2008, van Wyk et al. 2009). In the cat it has been described physiologically as a 'phasic W-cell' but more often simply as an alpha cell (Stanford 1987, Boycott and Wässle 1974), and grouped with other ganglion cell types that bear no resemblance in circuitry save for having large dendritic fields. In the PV retina, it is classified based on combined physiological and morphological parameters that separate it from other 'OFF-firing' cells such as PV-4 and PV-6. The coupling patterns observed are most likely mediated by Cx36-expressing gap junctions (Schubert et al. 2005). I observed two groups of coupled cells: ganglion cells in the GCL (mostly homotypic coupling) and small cells in the INL (most likely amacrine cells) (Fig. 2.5e, example of a full z-projection of GCL-IPL-mid-INL, and Fig. 2.9f). Coupling was not always observed and may reflect diffusion time of neurobiotin or experimental conditions (such as network state). The homotypic coupling observed in the GCL was based to two features. One, many of the coupled cells were also PV cells (expressing YFP, labelled by anti-GFP antibody) (Fig. 2.9f). In one example, all coupled cells except one were PV cells (Fig. 2.9f, left panel), and these coupled PV cells were PV-5

cells, based on previous identification from two-photon scans, and in some cases, electrophysiology. Two, there is a minimum distance between coupled somata (175 ± 33 µm). The mean dendritic diameter of PV-5 cells is 271 µm (Table 1), giving a 30% overlap of the dendritic fields. This is consistent with previous findings in the 'OFF alpha' cell (Völgyi et al. 2005). However, in the example (Fig. 2.9f, left), there was one outlier, which had a minimum distance of 84 µm from the other coupled cells, and did not fit the symmetry. This cell happened to be the only GFP negative cell. These data suggest that PV-5 is homotypically coupled (Völgyi et al. 2005, Schubert et al. 2005), but may also be heterotypically coupled, and that PV-5 constitutes a single ganglion cell type in the PV retina. Furthermore, since not every symmetrical coupled cell to PV-5 is always YFP positive (a PV cell) (Fig. 2.9f, right), this provides further evidence that only a subset of each PV cell type is labelled in the PV retina. In contrast to PV-5, PV-4 cells were never observed to be coupled, and since they have share their dendritic depth with PV-5 (68-69%, Table 1), coupling could also be used as a valid parameter to define cell type. The next step would be to record from homotypically coupled cell pairs, such as the PV-5 cells, and study the influence on one cell by independently stimulating the other cell, for instance with a spot of light or electrically with the electrode.

The PV-1 cell type (Fig. 2.5a and 2.2d right), which resembles the previously described mammalian 'ON alpha' ganglion cell type due to its ON-firing and large soma and dendritic field (Sun et al. 2002, Pang et al. 2003, Roska and Werblin 2003, Wässle and Boycott 1991, Coombs et al. 2006, Rockhill et al. 2002, Manookin et al. 2008, Kong et al. 2005, van Wyk et al. 2009), was not coupled in the PV retina, based on my experimental conditions. There was only one exception (1 out of 17 PV-1 cells quantified), where a single small soma in the GCL was labelled within the primary dendritic field area of the PV-1 cell. This general lack of labelling probably represents the strength of coupling in my experimental conditions (which were generally photopic conditions), since diffusion time of neurobiotin was approximately the same as PV-5, which was found to be coupled and also has an extensive large-volume dendritic arbour (Table 1). Nevertheless, amacrine cell coupling has been found in mouse ON alpha cells (Schubert et al. 2005, Völgyi et al. 2005).

What is the role of PV-1 in vision? It receives both excitatory and inhibitory at light ON, and no input at light OFF (Fig. 2.6a), i.e. it has a pure ON motif. For the spot stimuli, excitation changes faster than the change in inhibition (Fig. 2.7a), and the cell fires at a high rate, with a transient component and a sustained component (Fig. 2.4 group 1). This is due to inhibition having less influence, indicated by the excitation-dominated (right shifted) loops for the excitatory-inhibitory interactions (Fig. 2.7a, white loops). What is the role of inhibition? It is possible that it has a role in processing speed. Similar to the PV-0 cell, where inhibition changes faster than the change in excitation during movement in the null direction (Fig. 2.9d), perhaps inhibition would 'catch up' with excitation when the inhibitory pool surrounding the PV-1 cell is stimulated before the centre, which would be the case for very slow movement (and have a comparable interaction to that in Fig. 2.9d, lower plots, teal/null loops). Fast movement would not give inhibition time to change faster than excitation. Probably what is observed for the flashing spot stimuli (Fig. 2.6/2.7 motifs), is the equivalent of a very fast moving object. And since PV-1 has a very large dendritic field, the inhibitory surround would be even larger (not measured based on the spot stimuli used in Fig. 2.4 and 2.6). Another characterised group of ganglion cell types, not labelled in the PV retina, is the so-called 'ON direction selective' cell types, of which there are three, and are responsible for providing feedback to the vestibular system for the three dimensions of head movement (Oyster 1968). These respond optimally to slow movement and also have very large dendritic fields (Yonehara et al. 2009). Therefore these cell types sample a large visual angle, in much the same way as PV-1, and have a large inhibitory surround. Perhaps the function of PV-1 is to behave as a speed *predictor*. It could act as an indicator of how fast the organism is moving through the visual scene, which would explain why the natural scenes (Fig. 2.8d, cell 7) show sparse spiking patterns, since the movies are from a cat moving and exploring over a small area. PV-1 fires at higher rates when the movement of the scene is at high speeds (excitation changes faster than inhibition, as for flashed spots), but gradually at lower rates for progressively lower speeds (where inhibition catches up with excitation and strongly interacts).

Apart from PV-1 and PV-5, the third large dendritic field cell type identified in the PV retina is PV-6 (Fig. 2.5f). This cell type has also been found in the mouse, guinea pig and rabbit, and is likely to have been named as a 'delta' cell or as another 'alpha' cell (Stanford 1987 (cat tonic W-cell, also Q cell), Wässle and Boycott 1991 (cat delta cell, OFF-centre sustained), Pang et al. 2003 (mouse sOFF alpha), Roska et al. 2006 (rabbit OFF delta), Manookin et al. 2008 (guinea pig OFF delta), and possibly the 'OFF-S' cell in van Wyk et al. 2009). This cell type is often described physiologically as 'OFF sustained' due to its sustained firing patterns during simple spot stimuli (same as PV-6, Fig. 2.4, a mirror of the PV-1 cell). During natural scenes, the cell also fires sparsely, suggesting that inhibition is changing faster than excitation for the irrelevant components in the natural scene, much like PV-1. This brings further support to the notion that the physiological descriptions 'transient' and 'sustained' only apply to specific stimuli, usually flashed spots. An interesting feature of PV-6 is its unusual stratification. The more proximal regions of the dendritic tree ramify at 100% depth (OFF ChAT band), then the same dendrites switch to greater depths (up to 150%) before the distal parts extend back to 100%. This accounts for the large standard deviation of depth (Table 1), and from a side view of the IPL, the cell appears multistratified (Fig. 2.5f, here only a region of interest is shown, so each dendrite is cropped). In fact these are single dendrites that switch to both strata. From the top view, the dendrites appear to overlap, and are not avoiding each other like in PV-5 (compare Fig. 2.5f and e). This is a criterion for distinguishing PV-5 and PV-6 from a two-photon scan: PV-6 has a greater depth and the dendrites 'criss-cross', whereas PV-5 has a shallower depth and arbourises with separated primary and secondary dendrites. Therefore it is possible that PV-6 receives input from different populations of amacrine and bipolar cells, including the OFF starburst amacrine cells (marked by the ChAT antibody), but integrates the input on the same dendrites. Since PV-6 also has an 'out of phase' motif for flashed spots (Fig. 2.7b, compare PV-6 to PV-5), it may fulfill a related role to the detection of dark objects relative to a brighter surround (see Chapter 3).

PV-3 is monostratified, with a mean depth of 43.3%, colocalising with the middle Calretinin marker band (Table 1, Fig. 2.2), and is also positive for the

Calretinin marker (not shown). However it receives both ON and OFF input pathways (Table 2), so must integrate input on the same dendrites, much like PV-6, but in this case also from excitatory ON-pathway bipolar cells and OFF-pathway amacrine cells (Fig. 2.6a). This suggests that the contrast of the object presented is not the relevant information. Due to its small dendritic field (121 µm diameter, Table 1, Fig. 2.5c), a very small proportion of visual space in represented by this ganglion cell type for each cell, suggesting that the relevant stimulus is fine details. Assuming that this cell type tiles the retina, then there must be a large number of PV-3 cells, each with an inhibitory surround that spans several PV-3 cells. This small cell type has been described as a 'local edge detector' in rabbit (Famiglietti 2005, Roska and Werblin 2003, Roska et al. 2006, van Wyk et al. 2006). Even though the mouse does not contain a visual streak or fovea - a region of high visual acuity - the PV-3 cell type only fires for small details, and therefore only small spot stimuli (Fig. 2.4), and is characterised by the slow onset excitatory input in its motif (Fig. 2.6a). For the inhibitory-excitatory interactions, stimulation with spots larger than the dendritic field result in strong surround inhibition, shown by a shift of the loops to the left (Fig. 2.7a). This is consistent with the equivalent cell type in rabbit (van Wyk et al. 2006). For all changes in contrast, especially within the dendritic field where it interacts with excitation (i.e. only centre stimulation), inhibition has an extremely fast rise time (~30 ms, Fig. 2.6a, Table 3). This is sufficient to interact with the rise time of excitation to cause a 'delay' in the firing of PV-3 (Fig. 2.6a). Consequently, there is a triangular-like loop in the interactions, where the change in inhibition is replaced by the change in excitation after the peak inhibitory input (Fig. 2.7a). The role of inhibition therefore might be to suppress the temporal changes and allow the cell to fire only for the small spatial changes in the visual scene.

The remaining two cell types, PV-2 and PV-4 are somewhat mirrors of the ON and OFF pathways. Morphologically, they are both inside the two ChAT bands in the middle third of the IPL: PV-2 at 23.9% depth next to the ON ChAT band (Table 1, Fig. 2.5b), PV-4 at 68.8% depth next to the OFF ChAT band (Table 1, Fig. 2.5d). Both have similar dendritic field areas (24-25 mm^2), qualitatively

share the same dendritic arbourisation (Fig. 2.5), and therefore sample the same visual space. The only difference apart from stratification is coupling. PV-2 was found to be consistently coupled to small cells with somata in the INL (at least 5 per PV-3 cell) and weakly coupled to small cells with somata in the GCL. PV-4 was never observed to be coupled. In terms of physiology, both cell types have transient firing rates based on the spot stimuli (Fig. 2.4a and 2.3c,d) and similar area-response profiles (Fig. 2.4c). The firing rates are governed by similar inhibitory-excitatory interactions where inhibition becomes more dominant (changes faster than excitation) when the spot size increases (Fig. 2.7a). For the 375 µm spot, inhibition and excitation appear to overlap (Fig. 2.7a). In the mouse retina, 1 degree of visual angle is 31 µm on the retina (Remtulla and Hallett 1985). This suggests that each PV-4 and PV-2 cell fires optimally to less than 12 degrees. The difference between PV-2 and PV-4, is that for centre stimulation, inhibition is present for PV-2, much in the same way as for PV-1 (Fig. 2.7a), but not enough to shift the loop from the excitatory region at the onset. Therefore even with this difference, PV-2 also fires transiently like PV-4, where inhibition has no influence for the small spot stimuli. Inhibition in PV-2 is also unusual due to its double-peak at light OFF, suggesting input from at least two populations of amacrine cells or a form of feedback (Fig. 2.6a). In rabbit, the equivalent cell types might be the ON and OFF 'parasol' cell types (Roska and Werblin 2003, Roska et al. 2006), and possibly those described in the primate (Jacoby et al. 1996, Trong and Rieke 2008). Interestingly, in the primate, ON parasol cells are coupled (like PV-2), but OFF parasols are not (like PV-4) (Trong and Rieke 2008), suggesting that coupling patterns may also be conserved in mammals. PV-4 is also the most commonly encountered cell type in the PV retina (for example Fig. 2.8).

In this chapter I have described eight genetically-identified retinal ganglion cells, based on combined morphological and physiological parameters. There are several points I believe to be of interest. First, given the definition for cell type described here, it is possible for several different cell types to exist within the same IPL stratum and even share some common input pathways. This definition is based on not only quantification of morphology and physiology, but also rules such as tiling (and that for any given PV cell, the nearest PV cell

will always be a different cell type). The four ON OFF direction selective ganglion cell types appear identical, even at the resolution of electron microscopy, yet have different motifs for the same stimulus (based on moving spots in one direction), and tile the retina independently. Therefore, although it is possible that quantification of PV-4 and PV-5 dendrites beyond the resolution of the light microscopy used here might separate them into different strata, they could still be different cell types even with identical stratification. This chapter extends and hopefully consolidates the definition of cell type. Second, timing within the neural circuits is very precise (Fig. 2.6), highlighted by the small standard error for both excitation and inhibition. It is important to stress that this precision was only revealed once each cell type was identified as being a distinct type. This suggests caution when comparing responses of different cells that have not been defined quantitatively. Third, motifs could be considered as a signature of cell type. The parametric plots highlight the two forms of input that each ganglion cell receives (Fig. 2.7). These inhibitory-excitatory interactions are based on the simple flashing spot stimuli often used by other researchers, but may be extended to other forms of stimulation, for example, direction selectivity or natural scenes. The motifs could be used as a 'starting point' to gain intuition into how different ganglion cell types integrate their input to produce the specific firing patterns sent to the rest of the brain. To consolidate the notion of cell type based on the spiking activity observed during natural visual stimulation, my physiological definition of cell type would be that if two ganglion cells are of the same type, then they will have identical firing patterns for *any* visual stimulus. Forth, the PV retina could be a resource for the retina community, to compare and contrast identified cell types. Recently, there have been several mouse lines with fluorescently-labelled cells (Yonehara et al. 2008, Huberman et al. 2008, Kim et al. 2008), however these are usually single cell types. These may be useful for tracing studies and single cell analysis, but do not allow the direct comparison with other types. The PV retina contains eight genetically-identified cell types, most labelled within each region of the ganglion cell layer. This enables the rapid identification of different cell types within the same preparation (such as in Fig. 2.8), which may be useful for dual patching experiments and fast confirmation of the recorded cell type. Furthermore, since it is only one mouse

line that contains several labelled cell types, less space and resources are required for the maintenance of the line, compared to the numbers required for keeping different single-labelled transgenic lines. Fifth, the PV retina can be used as an indication the diversity of ganglion cell types that exist in the mouse. If the minimum distance was found for all PV cell types, it would be possible to estimate the total number of ganglion cell types, from these values and the total number of ganglion cell somata in the GCL (Jeon et al. 1998; Williams et al. 1996). Taking into account the number of distinct cell types stratifying in the ON ChAT band alone, the number of ganglion cell types in the retina is likely to consist of at least 60 types. Finally, the analysis in this chapter suggests that within each ganglion cell circuit, inhibition plays a vital role in how components of the visual scene are conveyed through the retina. 'Irrelevance' is constantly filtered by the inhibitory pathways, so that only in those brief moments when the excitatory input changes faster, is the ganglion cell integrating 'relevant' input and subsequently fires. In the next chapter, I will look specifically at the ganglion cell circuit of the PV-5 cell type, and ask what is the specific role and mechanism of inhibition.

Chapter 3: The mechanism of fast inhibition in a neural circuit for the detection of approaching objects.

The detection of approaching objects, such as looming predators, is necessary for survival. Which neurons and circuits mediate this function? The PV-5 cell type from the PV retina (Chapter 2) was discovered to be sensitive to approaching motion but not lateral motion (Münch et al. 2009). I became interested in the underlying circuitry, and by what mechanism this approach detection was computed. The answer is that the neural circuit of PV-5 has an essential building block: a rapid inhibitory pathway that selectively suppresses responses to non-approaching objects. This rapid inhibitory pathway, which includes AII amacrine cells connected to bipolar cells through electrical synapses, was previously described in the context of night-time vision. In the daytime conditions of the experiments described here, the same pathway conveys signals in the reverse direction. The dual use of a neural pathway in different physiological conditions illustrates the efficiency with which several functions can be accommodated in a single circuit.

In animals (Schiff et al. 1962, King et al. 1992a, Waldeck et al. 1995, King et al. 1999, Ishikane et al. 2005) and humans (Ball et al. 1971, King et al. 1992b), approaching motion, such as that of looming objects, elicits well-documented behaviours, such as startle and protective motor responses. The relevance of approaching motion to survival, the requirement for rapid action upon the detection of an approach event and the stereotypical nature of motor responses all suggest the existence of dedicated neural hardware for the detection of approaching motion. Neurons have indeed been identified in locust (Hatsopoulos et al. 1995, Gabbiani et al. 1999, Gabbiani et al. 2005) and in pigeon (Sun and Frost 1998) that respond selectively to approaching motion stimuli. These are found in higher visual areas and seem to achieve a

sophisticated whole-field computation that predicts the collision time of the looming object. An approach-sensitive neuron in the mammalian retina, a mouse ganglion cell type, has been described and the elements of its afferent circuit have been elucidated (Münch et al. 2009). I show how these elements allow the approach-sensitive behaviour of the ganglion cell. An important component of the circuit is a rapid inhibitory pathway that relies upon an electrical synapse. Experiments in frog (King et al. 1999, Ishikane et al. 2005) have suggested that approach detection may occur in the retina, but the mechanism there (King et al. 1999, Ishikane et al. 2005) seems to be different from the one explored here.

The PV-5 ganglion cell type is sensitive to approaching motion

I targeted and recorded from PV-5 cells in the light-adapted PV retina, this time presenting visual stimuli that included 'approach motion' (Münch et al. 2009). The dendritic tree of each PV-5 cell extends over a large area (diameter 270 μm, n = 20; Fig. 2.2c,e, 2.5e and Table 1), covering ~10 degrees of the visual field. The dendrites of this neuron arborize in the IPL at 68.8 % (n = 20; Fig. 2.2 and Table 1) relative to the two strata marked by the antibody to choline acetyltransferase (ChAT) (Haverkamp and Wässle 2000, Manookin et al. 2008). The inhibitory-excitatory motif of PV-5 is 'out of phase', since it receives only excitatory input at light OFF and only inhibitory input at light ON (Fig. 2.6b). Consequently, for simple presentations of dark objects, PV-5 fires only at light OFF (Fig. 2.4). For which occasions would the cell integrate these two temporally-separate inputs to become sensitive to approaching motion?

To demonstrate that PV-5 was approach sensitive, I presented PV-5 cells with a set of stimuli (Münch et al. 2009) that mimicked approaching motion (an expanding bar), lateral motion (a drifting bar) and receding motion (a shrinking bar) of a dark object within the dendritic field (Fig. 3.1a). All stimuli began with the presentation of a black bar at the centre of the dendritic field. After a 2 second pause during which the image was held fixed, the two edges of the bar moved at different velocities to the left or to the right, drawn randomly from a set of velocities (Fig. 3.1a,b). Spiking responses were evoked

preferentially by expanding bars compared to either drifting or shrinking bars (n = 7), at all velocities of the bar edges tested (Fig. 3.1a). The absent (or greatly reduced) response to non-approaching motion was not due to an overall change in the responsiveness of the cell during the course of the experiment, as the response to the onset of the black bar was similar for all stimuli (Fig. 3.1b). The peak spiking rate increased monotonically with edge velocity, while the spike count during motion was roughly invariant (Fig. 3.1c). In summary, within the array of stimuli I used, PV-5 cells favoured approaching motion over lateral and shrinking motion. Since approach motion results in overall dimming, the ON inhibition would not be required. This leads to the following question: what is the role of ON inhibition in the PV-5 neural circuit?

ON inhibition is required for approach sensitivity

Since inhibition occurs only at light ON (i.e. through an ON pathway), this inhibitory activity could be responsible for suppressing the response of PV-5 cells to non-approaching motion, i.e. when brightening occurs at the same time as dimming, as is the case for lateral motion (the leading edge of a black bar results in dimming whereas the trailing edge results in simultaneous brightening). Perhaps simultaneous brightening and dimming of lateral motion would 'cancel out' the spiking response since inhibition would interact with excitation at this time.

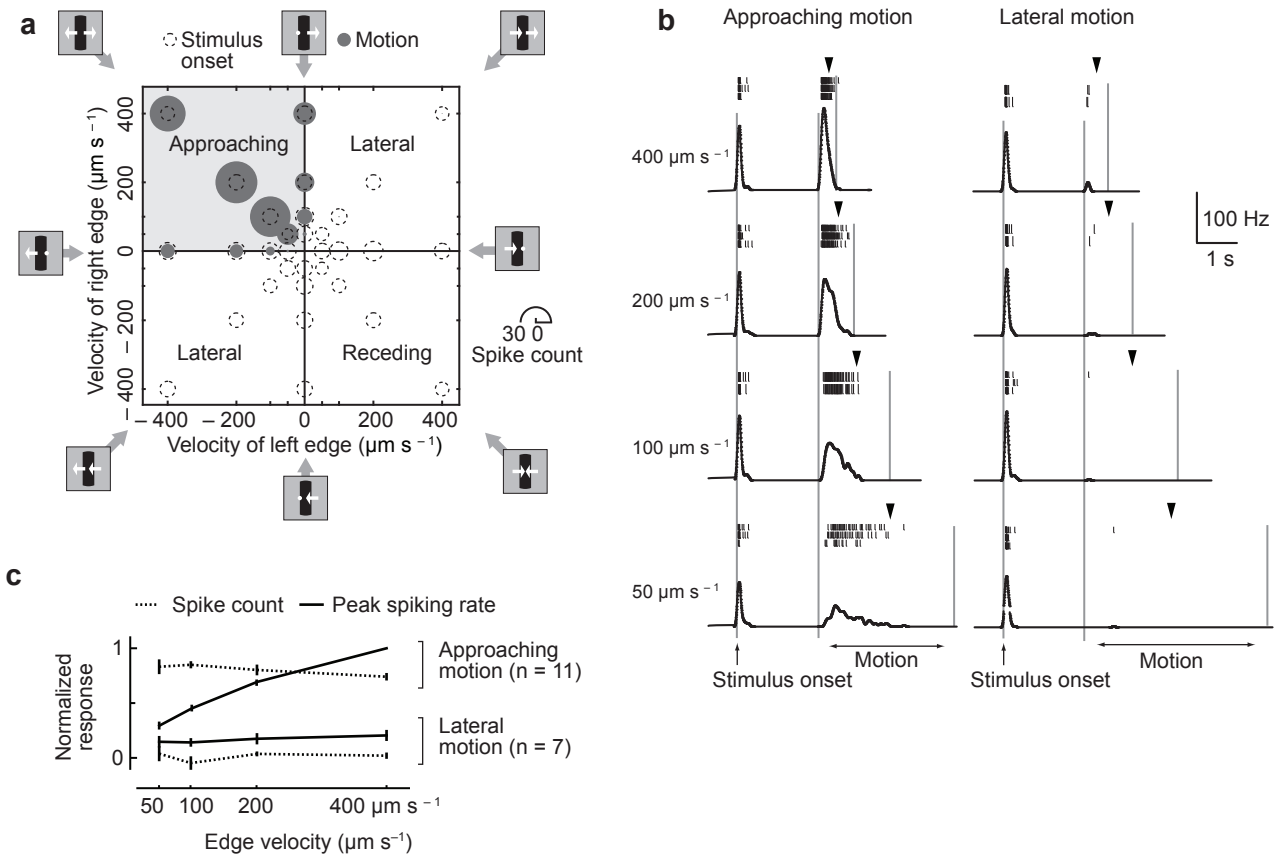

Figure 3.1. PV-5 ganglion cells are sensitive to approaching motion. (a) Overview of spiking responses of a PV-5 cell to different motion stimuli in the parameter space. A 60 µm black bar was turned on within a 400 µm diameter mask in the center of the dendritic field ('Stimulus onset'). After a 2 second pause, the left and the right edges of the bar began to move at velocities drawn at random from a number of values ('Motion'). Radii of dotted circles and gray disks are proportional to the average spike count after the onset and during the motion of the bar, respectively. Scale radius is shown at lower right. The quadrant that corresponds to approaching motion is shaded in light gray. (b) Responses to expanding ('Approaching motion') and drifting ('Lateral motion') bars for different edge velocities. Ticks, individual spikes; black traces, average spiking rates. Black arrowheads, times at which the moving edges exit the dendritic field of the cell. (c) Spike count and peak spiking rate during motion as a function of edge velocity, for expanding ('Approaching motion') and drifting ('Lateral motion') bars. Error bars, s.e.m.

Figure 3.1

To test whether the ON inhibition is required for approach sensitivity, I recorded from PV-5 cells during approaching motion (expanding black bars) and lateral motion (drifting black and white gratings) in the presence and absence of 10 mM APB (L-(+)-2-amino-4-phosphonobutyric acid), which blocks the ON pathway (Slaughter and Miller 1981) (n = 5, for both spiking and inhibition). As expected, the firing rate of PV-5 increased during approaching motion in the presence and absence of ABP (Fig. 3.2a top). This was consistent with the lack of inhibitory input, since during approaching motion there is no brightening to activate the ON pathway (Fig. 3.2a bottom), only dimming, which involves only the OFF pathway. However, during lateral motion in control conditions, the firing rate was low compared with that of approaching motion even though the drifting grating contained dimming information (Fig 3.2b top). Examining the underlying synaptic currents revealed an inhibitory input that was initiated by the onset of lateral motion (Fig 3.2b bottom). In the presence of ABP, inhibition was blocked, and a burst of spikes appeared at the onset of lateral motion (Fig 3.2b). Interestingly, the spike burst under ABP was time-locked with the inhibitory input measured in control conditions. In the putative PV-5 neural circuit, ABP blocked the ON bipolar cell input to the amacrine cell responsible for PV-5 ON inhibition but kept the direct excitatory bipolar cell OFF pathway intact (Fig 3.2c). These results suggest that the precise timing of inhibition is required for maintaining approach sensitivity in the PV-5 neural circuit, indicated by ON inhibition serving to suppress responses of PV-5 cells to lateral motion. The suppression was robust: it was observed for a variety of spatial frequencies, grating contrasts and drifting velocities (Münch et al. 2009).

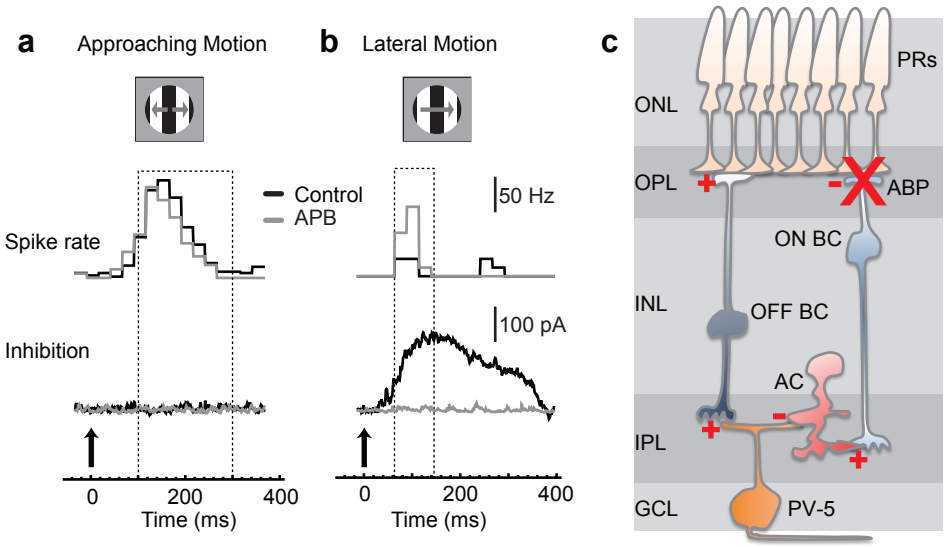

Figure 3.2. PV-5 ganglion cells receive ON inhibition that suppresses responses to lateral motion. (a,b) Responses to approaching (a) and to lateral (b) motion in control conditions and with APB (10 mM). The stimulus, presented within a 300 µm diameter mask, was a black-and-gray grating (100 µm bar width) with edges moving at 500 µm s^{-1}. Dashed boxes, duration of the burst of spikes; arrows, motion onset. Control conditions were restored after wash-out of ABP (data not shown). (c) Simplified diagram of putative ON and OFF pathways in the PV-5 neural circuit, inferred from Chapter 2. OFF bipolar cells (OFF BC) make sign-conserving synapses (+) between photoreceptors (PRs) and the PV-5 ganglion cell, providing direct excitatory input at light OFF. A putative inhibitory amacrine cell (AC) provides inhibitory input (-) to PV-5 at light ON via the ON pathway, which is represented by an ON bipolar cell (ON BC) that makes a sign-inverting synapse (-) with the photoreceptors and a sign-conserving synapse (+) with the AC. Red X shows site of action of ABP in the ON pathway.

Fast ON inhibition is responsible for approach sensitivity in PV-5 but not in PV-6

Next I asked whether approach sensitivity was restricted to the PV-5 neural circuit or was a general property of other OFF cells. Another PV cell type, PV-6, also has an 'out-of-phase' inhibitory-excitatory motif, since it receives OFF excitation and fires at light OFF, yet receives inhibition only at light ON (Fig. 2.6b and Table 2). Its putative neural circuit would therefore be similar to that shown in Figure 3.2c for PV-5. It also has a similarly wide dendritic field (diameter 232 μm, but stratification at 134 %, n = 14, Fig. 2.2, 2.5f and Table 1). However, due to the difference in stratification, it receives input from a different type(s) of bipolar cell, which is demonstrated by a more sustained response than that recorded in PV-5 (Fig. 2.6b). Nevertheless, PV-6 responded both to approaching and lateral motion (Fig. 3.3a,b), which by definition means it is not approach sensitive. Given that both PV-5 and PV-6 have 'out-of-phase' motifs, what is the mechanism behind the differences in motion sensitivity (Fig. 3.3b)? To answer this question, I measured the dynamics of inhibition in PV-5 and PV-6 and found that inhibition (via the ON pathway) was faster in PV-5 than in PV-6 (Fig. 3.3c,d). Therefore, PV-5 inhibition contains a 'fast component' that is lacking in PV-6, which gives rise to approach sensitivity since inhibition is fast enough to cancel out excitation during lateral motion.

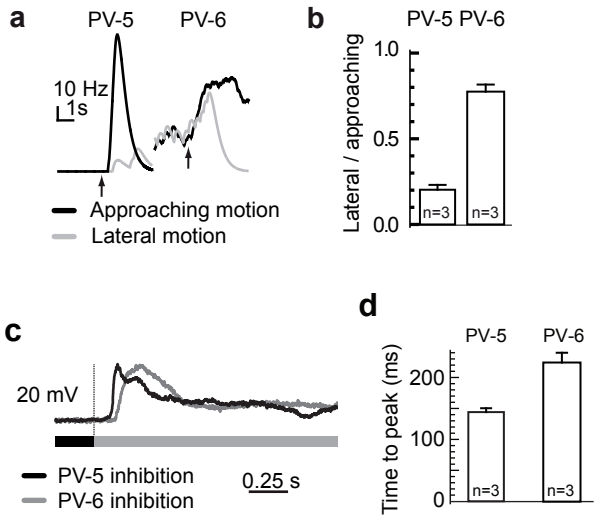

Figure 3.3. PV-6 OFF ganglion cells respond to lateral motion. (a-b) Responses to a black-and-gray grating (100 µm bar width), with edges moving at 500 µm s^{-1}, within a 300 µm diameter mask. (a) Spiking rates in PV-5 and PV-6 cells, in response to approaching motion and to lateral motion. Arrows, motion onset. (b) Ratio of peak spiking rate responses to lateral motion and approaching motion, in PV-5 and in PV-6 cells. Error bars, s.e.m. (c) Inhibitory currents in PV-5 and PV-6 at light ON (after a 2 s 400 µm black spot). Peak amplitudes are normalized to emphasize the relative timing of the responses. (d) Time to peak of the inhibitory inputs to PV-5 and PV-6. 'Time to peak' is the delay, counting from stimulus onset, before the response reaches 67% of its peak.

Figure 3.3

Fast inhibition acts through an electrical synapse

To determine the origin of fast inhibition and the difference between the two cell types, I dissected the inhibitory pathways of both PV-5 and PV-6. Both ON and OFF pathways in the light-adapted (i.e. cone-driven) retina involve sign-conserving ionotropic glutamate receptors at the synapse between cone photoreceptors and OFF cone bipolar cells, and between cone bipolar cells and amacrine cells (see Introduction). Therefore I measured inhibitory currents in the presence of 10 mM (±)-3-(2-Carboxypiperazin-4-yl) propyl-1-phosphonic acid (CPP) and 10 mM 6-nitro-2,3-dioxo-1,4-dihydrobenzo[f]quinoxaline-7-sulfonamide (NBQX), which block NMDA and AMPA/kainate ionotropic glutamate receptors, respectively. If inhibition acted through classical glutamatergic synapses, CPP/NBQX would block ON inhibition (bipolar to amacrine cell synapse). Surprisingly, in PV-5 cells a transient component was resistant to CPP/NBQX (Fig. 3.4a, and Münch et al. 2009), whereas in PV-6 cells inhibition was blocked entirely (Fig. 3.4b. n = 3). Interestingly, the slow component of PV-5 inhibition was blocked, indicating that PV-5 receives at least two forms of inhibition: one through a classical glutamatergic pathway and the other through a CPP/NBQX resistant pathway.

To determine the origin of the CPP/NBQX-resistant fast inhibitory component of PV-5, which is the component responsible for approach sensitivity, I investigated non-glutamatergic synapses. Thus, I turned to electrical synapses. Electrical synapses consist of Connexin proteins, of which Connexin36 (Cx36) is one of the most abundant in the mouse retina (Mills et al. 2001, Feigenspan et al. 2001, Massey et al. 2003). In mice lacking Cx36 (Cx36-/-), CPP/NBQX completely blocked the inhibitory input to PV-5 cells (Fig. 3.4c and Münch et al. 2009). Since Cx36-/- mouse retinas do not contain YFP-expressing cells, large soma OFF-spiking cells were targeted and filled with neurobiotin and the dendritic field diameter and stratification were compared to PV-5 cells of the PV retina (Fig 3.4d). These ‘PV-5’ cells in the Cx36-/- retina had a similar morphology to ‘wild-type’ PV-5 cells (n = 4 recorded cells, Fig. 3.4e). Interestingly, no homotypic coupling was seen for Cx36-/- PV-5 cells (Fig. 3.4d), suggesting that the gap junctions between PV-5-like ganglion cells in wild type also contain Cx36 Connexins (Schubert et al.

2005). Due to the reduced targeting algorithm in these unlabelled Cx36-/- retinas, 'PV-6'-like cells (which have a similarly large soma) were also filled (Fig. 3.4d,f). These data, together with the pharmacological observations described above, indicate that rapid inhibition in light-adapted conditions transits between ON cone bipolar cells and amacrine cells through an electrical synapse that requires functional Cx36.

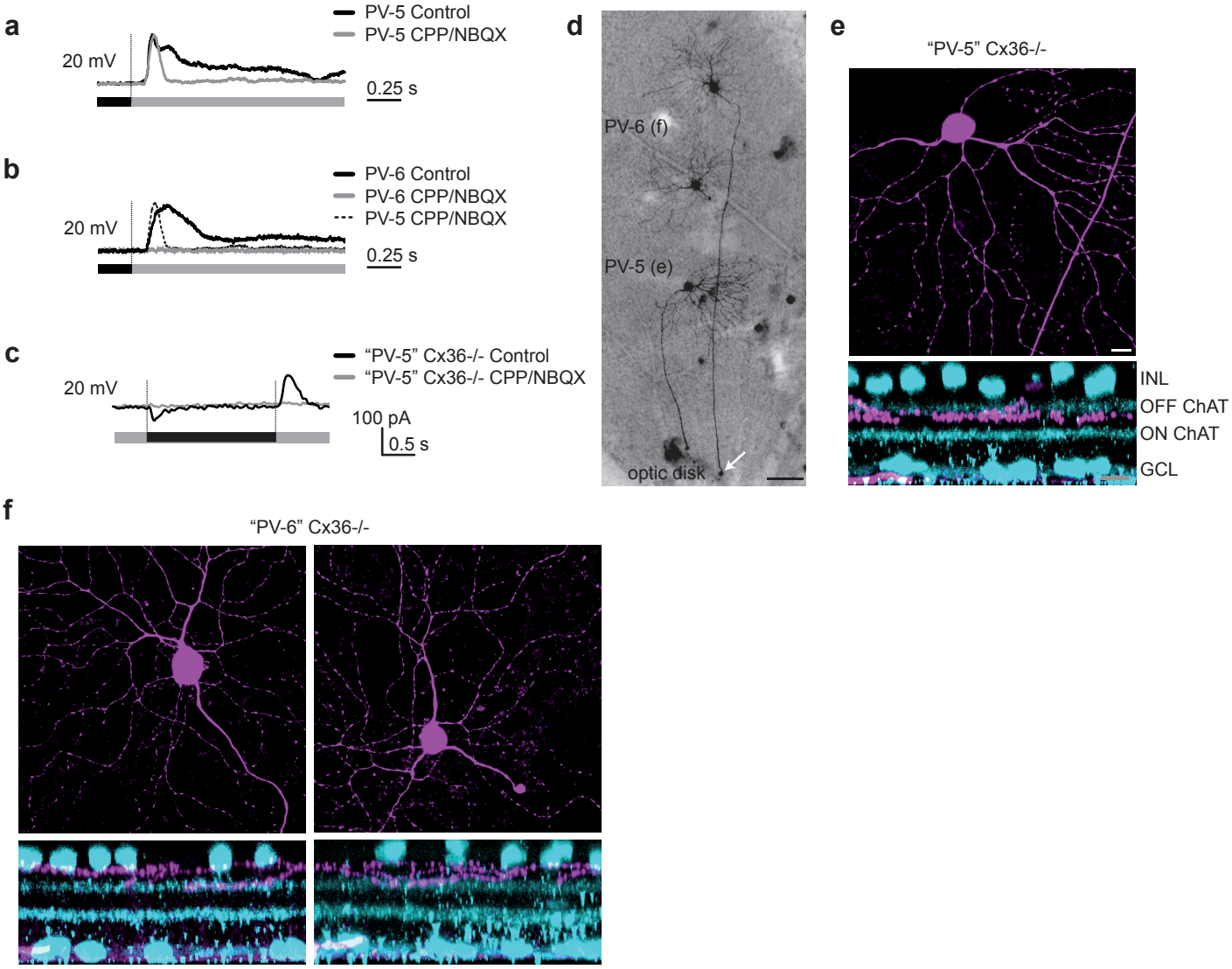

Figure 3.4. 'Fast inhibition' in PV-5 acts though an electrical (non-glutamatergic) synapse. (a,b) Inhibitory currents in PV-5 and PV-6 at light ON (after a 2 s 400 µm black spot) in control conditions and in the presence of CPP/NBQX. PV-5 inhibition in the presence of CPP/NBQX is shown again in (b) for comparison with PV-6. (c) Synaptic currents of PV-5 cells in Cx36-/- mice at 20 mV holding potential in response to a 400 µm black disk presented for 2 s in control conditions and with CPP/NBQX. (d) 'PV-5' and 'PV-6' cells in the Cx36-/- mouse retina, epifluorescence. Note lack of homotypic coupling, compared with PV-5 cells the PV retina (Fig 2.5e). White arrow, axon roll-back. Scale bar: 100 µm. (e) A 'PV-5' cell in the Cx36-/- retina, top view z-projection (neurobiotin, magenta), and side view, xz-projection (ChAT, cyan). Scale bars: 10 µm. Note asymmetric position of soma relative to dendrites, a common property of PV-5 cells (see Chapter 2). Diagonal process across left side of image is a labelled axon from another filled cell. (f) Two 'PV-6' cells in the Cx36-/- retina. Same specifications as in e. Note similar stratification to PV-6 cells of the PV retina (Fig. 2.2e, 2.5g), with dendrites both in the OFF ChAT band and close to the INL.

Figure 3.4

AII amacrine cells are responsible for the mechanism of approach sensitivity

The circuit element responsible for the rapid inhibitory input to PV-5 cells - namely, an ON cone bipolar cell connected by a Cx36-containing electrical synapse to an inhibitory amacrine cell - is reminiscent of the rod pathway circuitry (Mills et al. 2001, Feigenspan et al. 2001, Massey et al. 2003, Bloomfield and Dacheux 2001). During scotopic (night-time) vision, glycinergic AII amacrine cells (Pourcho and Goebel 1985), after activation by rod bipolar cells, transmit signals through Cx36-containing electrical synapses to ON cone bipolar cells (Mills et al. 2001, Feigenspan et al. 2001, Massey et al. 2003, Veruki and Hartveit 2002, also see Introduction). An attractive hypothesis is that the rapid inhibitory pathway afferent to PV-5 cells makes use of the same electrical synapse as the one associated with the rod circuit, but with a reversed information flow (Manookin et al. 2008, Geraghty et al. 1998, Cohen and Miller 1999, Murphy and Rieke 2008, Xin and Bloomfield 1999; also see Introduction and Figure 3.5a). To determine whether AII amacrine cells may be components of the PV-5 neural circuit, I targeted amacrine cells in the most proximal sublayer of the inner nuclear layer (INL), where approximately one-third of the cells are AII amacrine cells. This estimation was based on antibody staining for Dab1, a selective AII amacrine cell marker (Rice and Curran 2000, Münch et al. 2009). I performed the following experiments in wholemount PV retinas, in areas near PV-5 ganglion cells identified by two-photon imaging. AII amacrine cells were identified in the live retina by their morphology (Fig. 3.5b,c, n = 7 cells), and post-hoc by their immunoreactivity with Dab1 and colocalisation with neurobiotin from the patch pipette (Münch et al. 2009). The diameter of the dendrites (Fig. 3.5c, bottom row), was between 20 and 30 µm, consistent with previous observations. PV-5 cells costratified with the OFF-stratifying lobular appendages of the AII cell (Fig. 3.5c). The AII amacrine cells were recorded under voltage clamp conditions (at -60 mV, n = 9). As predicted from the model neural circuit (Fig. 3.5a), light increments evoked excitatory currents in AII amacrine cells, but light decrements did not (Fig. 3.5d). For comparison, a PV-5 cell was simultaneously recorded with this AII cell (see Figure 3.6 for further analysis).

At light OFF (black spot), OFF bipolar cells are activated and ON bipolar cells are deactivated, providing excitation to the PV-5 cell and reduction of excitation for the AII (Fig. 3.5d, consistent with the model in Figure 3.5a). Next I measured the response of AII amacrine cells presented with the same stimulus array used for probing PV-5 cells (Fig. 3.1a). The response map of AII amacrine cells (n = 4) in control conditions and under CPP/NBQX treatment showed a pattern complementary to the response map of PV-5 cells (Fig. 3.5e,f). I also repeated these experiments in the presence of 10 mM ABP, which abolished responses of the AII amacrine cells to both stimulus onset and lateral motion (traces not shown). These data suggest that the AII amacrine cell is responsible for at least the fast-component of ON inhibition to PV-5 cells during non-approach motion.

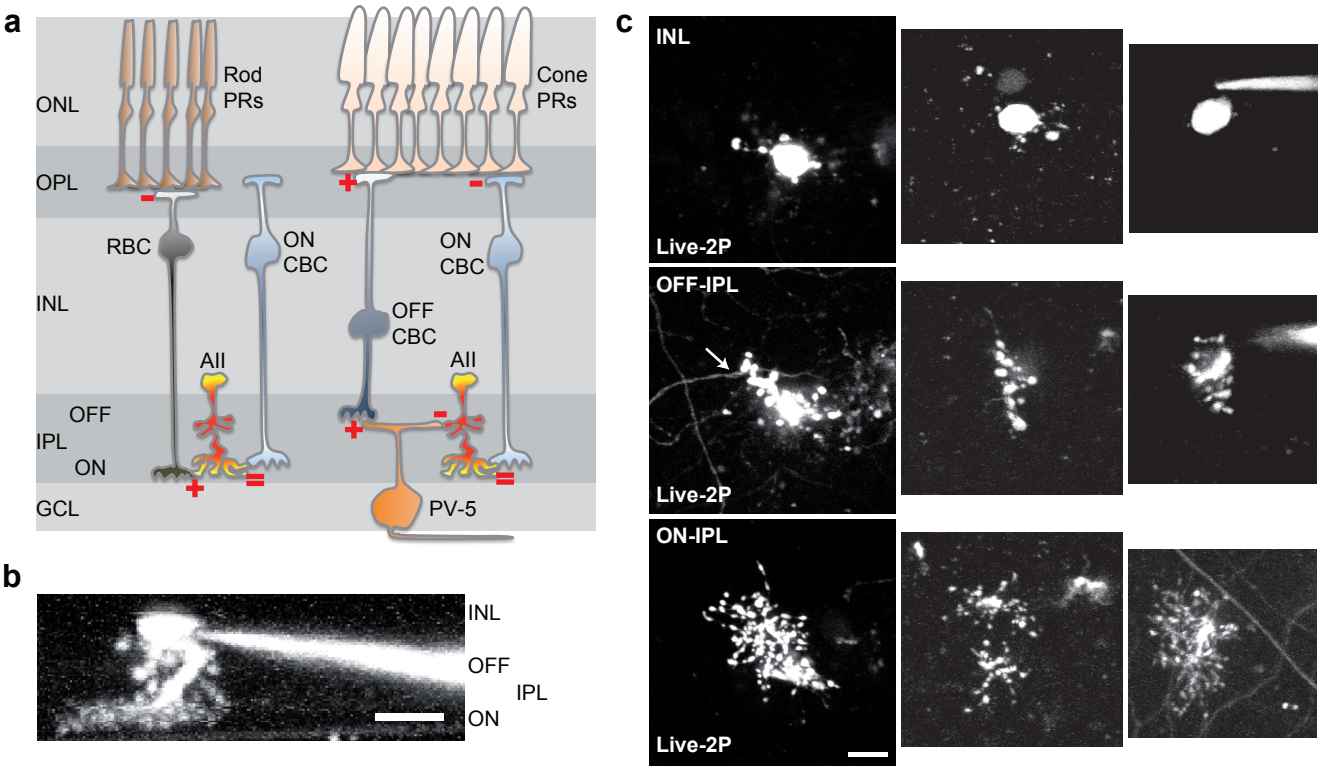
a
ONL
OPL
INL
OFF
IPL
ON
GCL
Rod
PRs
Cone
PRs
RBC
ON
CBC
ON
CBC
OFF
CBC
AII
AII
PV-5
b
INL
OFF
IPL
ON
c
INL
Live-2P
OFF-IPL
Live-2P
ON-IPL
Live-2P

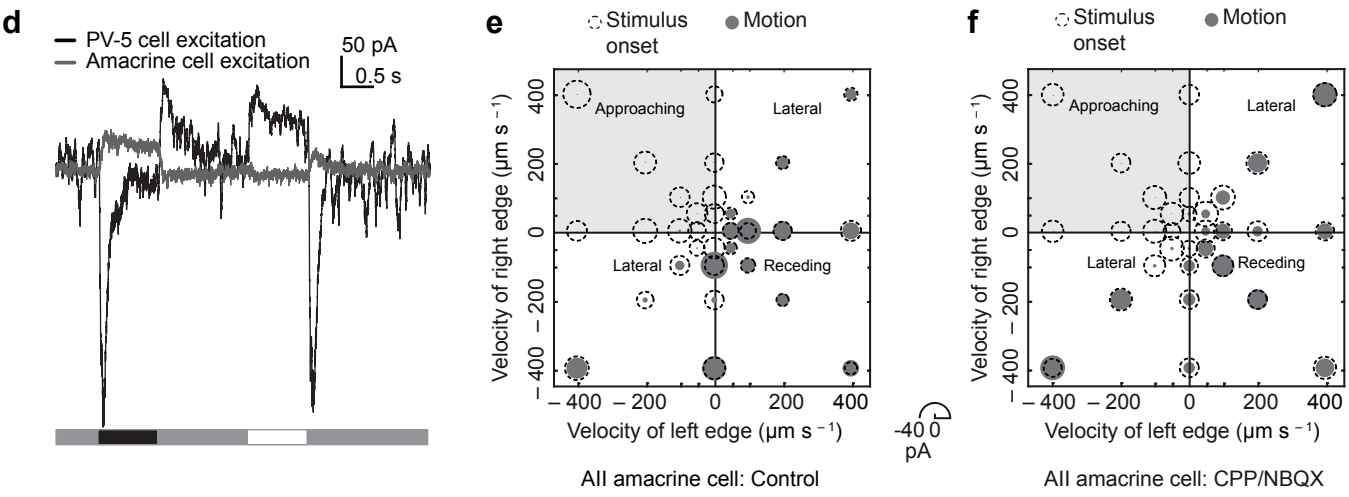
d
PV-5 cell excitation
Amacrine cell excitation
50 pA
0.5 s
e
Stimulus onset
Motion
Approaching
Lateral
Lateral
Receding
Velocity of right edge (µm s⁻¹)
Velocity of left edge (µm s⁻¹)
400
200
0
– 200
– 400
– 400 – 200 0 200 400
-40 0 pA
All amacrine cell: Control
f
Stimulus onset
Motion
Approaching
Lateral
Lateral
Receding
Velocity of right edge (µm s⁻¹)
Velocity of left edge (µm s⁻¹)
All amacrine cell: CPP/NBQX

Figure 3.5

Figure 3.5. The role of AII amacrine cells in photopic (cone dominant) neural circuitry. (a) Putative PV-5 neural circuit that involves AII amacrine cells. Left, scotopic circuit: rod photoreceptors (rod PRs) connect via sign-inverting (ABP sensitive) synapses (-) to rod bipolar cells (RBC), which connect via a sign-conserving (CPP/NBQX sensitive) synapse (+) to AII amacrine cells in the innermost IPL. Signals are conveyed to ON ganglion cells via an electrical synapse (=) between the dendrites of the AII amacrine cells and ON cone bipolar cells, which in turn make sign-conserving synapses with the ON ganglion cells (not shown), as in photopic circuitry. Signals are conveyed to OFF ganglion cells via an inhibitory (sign-inverting glycinergic) synapse between the smaller OFF-stratifying processes of the AII amacrine cells and OFF bipolar cells, which in turn make sign-conserving synapses with the OFF ganglion cells (not shown). Right, photopic circuit for PV-5: Cone photoreceptors connect via a sign-conserving synapse (+) to OFF cone bipolar cells (OFF CBC), which directly contact the dendrites of PV-5 via a sign-conserving synapse (+), providing excitatory input at light OFF. For fast inhibitory input at light ON, cone photoreceptors connect via a sign-inverting synapse (-) to ON cone bipolar cells (ON CBC), which share an electrical synapse (=) with the AII amacrine cells (the same connection used in the scotopic circuit). This electrical synapse mediates fast inhibition to the PV-5 ganglion cell via a sign-inverting synapse (-) between the OFF-stratifying lobular appendages of the AII and PV-5 cells. The slow component of ON inhibition may be mediated by AII amacrine cells or by other types of amacrine cells. (b) Live two-photon image of an AII amacrine cell in the wholemount retina (yz projection). Cell filled with Alexa Fluor 488 by patch pipette (right). Scale bar: 10 µm. (c) Left column: three live two-photon xy-sections of another AII amacrine cell patched in the wholemount PV retina. Top, AII soma in INL. Middle, OFF-stratifying lobular appendages of the AII in the same stratum as a PV-5 dendrite (arrow). Bottom, dendrites in the innermost IPL. Centre and right columns: two more examples of AII amacrine cells. Scale bar: 10 µm. (d) Light responses of simultaneously recorded PV-5 (black) and AII (grey) cells during presentation of a 400 µm black then white spot on a grey background. Both cells were held in voltage clamp mode at -60 mV. (e,f) Motion-response map of an AII amacrine cell in control conditions (e) and in the presence of 10 mM CPP and 10 mM NBQX (f). Map is analogous to that in Figure 3.1a. The recorded cell was clamped to -60 mV. The radii of the disks are proportional to the peak magnitudes of inward currents evoked by stimulus motion. The radii of the dotted circles are proportional to the reduction of the excitatory currents after the initial presentations of the black bar. The quadrant that corresponds to approaching motion is shaded in light grey.

To directly test the hypothesis that AII amacrine cells are components of the PV-5 neural circuit and are responsible for maintaining approach-sensitivity, I performed paired patch clamp recordings of AII amacrine cells and PV-5 ganglion cells in wholemount PV retinas (Fig. 3.6, also see Materials and Methods). In 28 double patch experiments in which I simultaneously recorded

in whole cell voltage clamp mode (with the amacrine cell held as close as possible to ECl (-60 mV) and the PV-5 cell at +20 mV), only two showed a direct connection. In these two cases, depolarizing voltage steps applied to the amacrine cell elicited inhibitory currents in the PV-5 ganglion cell (Fig. 3.6a). Importantly, strychnine abolished the inhibitory currents in PV-5 cells that were otherwise elicited by amacrine cell stimulation in control conditions (Fig. 3.6a). This observation suggests that the inhibitory transmission used glycine receptors, a further indication of AII amacrine cells, which are glycinergic (Pourcho and Goebel 1985). Evoked inhibitory currents were restored after wash (traces not shown). The inhibition evoked in PV-5 in Figure 3.6a was only measurable by first minimising synaptic noise before depolarizing the amacrine cell. During two-photon targeted patching, the retina is illuminated only with infrared light. This slowly 'dark-adapts' the retina, causing fluctuations in the baseline synaptic currents, especially from the tonic inhibitory conductance in PV-5. These fluctuations, or 'synaptic noise', were greater than 20 pA. Therefore, to reduce this noise, I first allowed the retina to light-adapt after double patching, by illuminating the retina with visible light. After 1-2 min, when the retina was sufficiently adapted, I switched back to infrared light, and the synaptic noise was significantly reduced, i.e. holding the PV-5 cell at +20 mV provided a stable, non-fluctuating baseline current. Immediate electrical depolarization of the amacrine cell evoked inhibition in PV-5 with a maximum amplitude of 150 pA above baseline (Fig. 3.6a). In the other connected pair, this time without reducing synaptic noise (note the fluctuating baseline), depolarization of the amacrine cell evoked quanta of glycine release, shown as transient outward currents in the PV-5 cell (Fig. 3.6b). These quanta were blocked by application of 10 mM strychnine. Furthermore, during the paired recording, it was possible to use visual stimulation to simultaneously measure the inhibitory and excitatory responses to lateral motion in the PV-5 cell and the AII cell respectively. As predicted, the two components were complementary (Fig. 3.6c). AII excitation was slightly phase-shifted relative to PV-5 inhibition due to the spatial offset of the moving bars in the receptive field rather than temporal offset since inhibition to PV-5 via the AII is fast (Fig. 3.3c,d). To confirm the identity of the two amacrine cells that evoked inhibitory currents in PV-5 cells when

electrically stimulated, I visualized their morphology under the two-photon microscope after the recordings (Fig. 3.5d). The connected cells were also visualized by confocal microscopy with antibodies against Dab1 as before (Münch et al. 2009). AII amacrine cells were found to be homotypically coupled. Interestingly, during live two-photon imaging, Alexa Fluor dye was observed in cells in the distal INL beyond the soma of the AII cell (Fig. 3.6e). These cells stained positive for Gg13, a marker for ON cone bipolar cells (Huang et al. 2003, Münch et al. 2009), but were negative for PKC, a marker for rod bipolar cells (Greferath et al. 1990). These data provide further evidence that AII amacrine cells are electrically coupled to ON cone bipolar cells (Fig. 3.5a) and that this synapse may be permeable to fluorescent dyes. Since the AII amacrine cells were homotypically coupled (Münch et al. 2009), it is likely that the inhibition evoked in PV-5 was from the integration of several connected AII amacrine cells.

Figure 3.6. PV-5 ganglion cells receive an inhibitory input from AII amacrine cells. (a) Inhibitory currents in a PV-5 cell (black, control; gray, 10 mM strychnine) evoked by stimulating the double-patched amacrine cell by depolarizing from -60 mV to 0 mV (light grey). Note stable baseline holding current. (b) Quanta of inhibition measured in a PV-5 cell (+20 mV holding, black traces) during amacrine stimulation (grey boxes). Top four traces, 0.5 s stimulation. Bottom two traces, 1 s stimulation. Note noisy baseline holding current. (c) Complementary light responses of PV-5 inhibition (black) and amacrine cell excitation (grey) during lateral motion (top, grey box, 250 μm s^{-1} moving bars). (d) Two-photon maximum intensity z-projection of the PV-5 cell from a and c (left, filled with lucifer yellow) and connected amacrine cell (right, with pipette still attached, filled with Alexa Fluor 488). Other somata are YFP-positive PV cells of the PV retina. Scale bar: 20 µm. (e) Zoomed images of the amacrine cell from d, at three positions: top, strongly-coupled cells in the INL; middle, PV-5 dendrite with costratifying amacrine cell lobular appendages; bottom, dendrites in the innermost ON layer of the IPL.

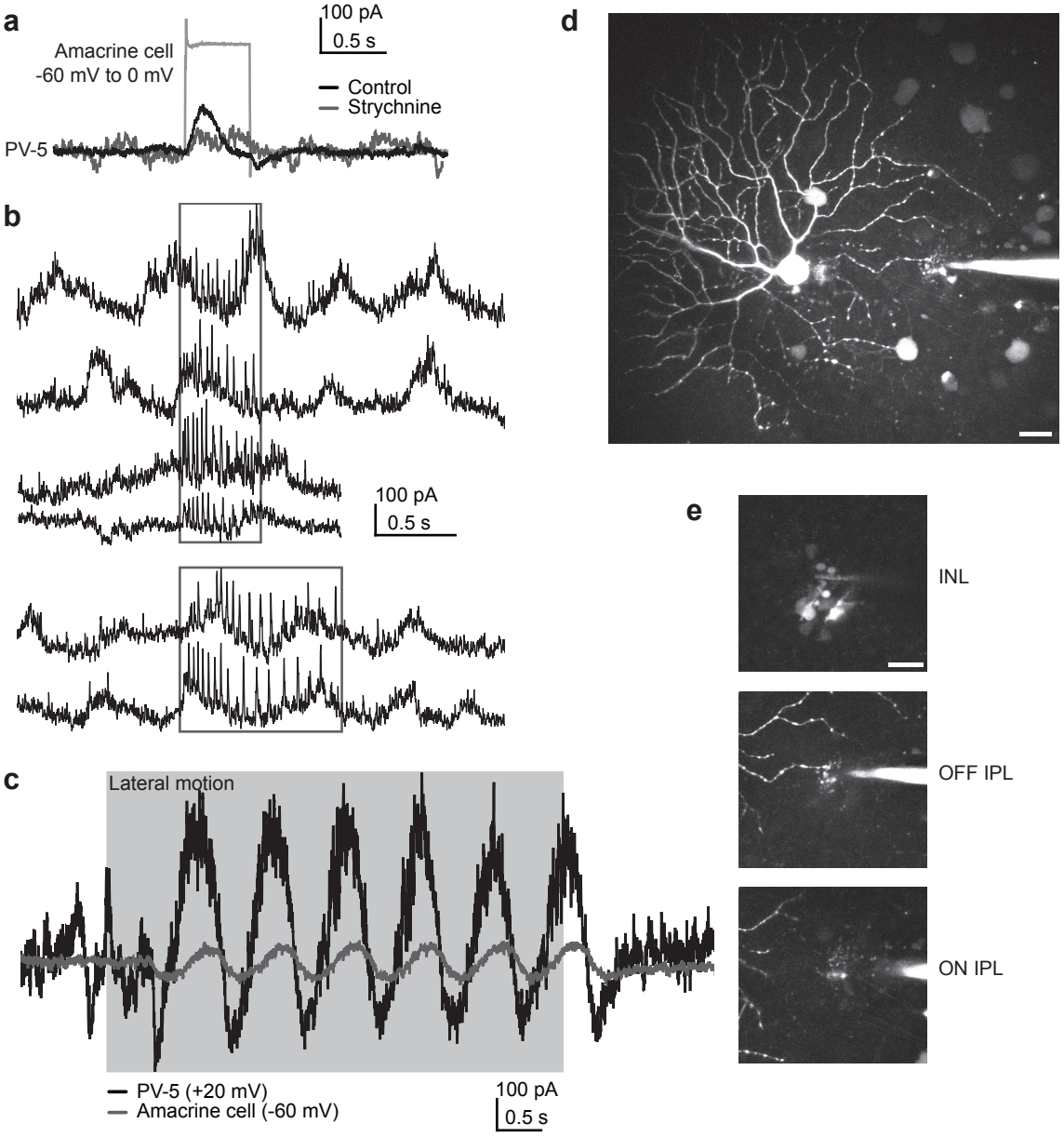
a
100 pA
0.5 s
Amacrine cell
-60 mV to 0 mV
Control
Strychnine
PV-5
b
100 pA
0.5 s
c
Lateral motion
PV-5 (+20 mV)
Amacrine cell (-60 mV)
100 pA
0.5 s
d
e
INL
OFF IPL
ON IPL

Figure 3.6

AII amacrine cells are components of day and night vision

A key property of the approach-sensitive circuit is the rapid inhibition mediated by the AII amacrine cell: it arrives in time to cancel excitation. In this scenario, the AII amacrine cell fulfills a function very different from the one it is well known for - namely, amplifying rod signals by conveying them to ON and OFF cone pathways (Wässle 2004). The experiments described in this chapter suggest that the AII amacrine cell is also relevant to photopic (daytime) vision (Oesch and Diamond, 2009), a conclusion that supports recent results in guinea pig (Manookin et al. 2008) and mouse (Pang et al. 2007). The direct demonstration of AII amacrine cell to PV-5 cell connectivity with double-patch experiments and, hence, of the involvement of the AII amacrine cell in the approach-sensitive circuit (Münch et al. 2009) establishes a functional role of AII amacrine cells in photopic conditions. Notably, neural signals flow along the same circuit module - an ON cone bipolar cell through an electrical synapse to an AII amacrine cell - under photopic and scotopic conditions, but the direction of the flow is reversed in photopic conditions as compared to scotopic conditions (Fig. 3.5a). It thus seems that the nervous system can use the same circuit for entirely different functional purposes under different physiological conditions - an illustration of the efficiency with which biological function can be packed into neural circuits.

The finding that inhibition in PV-6 does not contain the fast component (Fig. 3.3), suggests that the AII pathway in photopic conditions is a specific feature of the PV-5 neural circuit that infers approach sensitivity. The question remains as to the origin of the slower CPP/NBQX-sensitive forms of inhibition observed in both PV-5 and PV-6. It was fortunate that the subunit responsible for fast inhibition - the AII amacrine cell - was already well described in the context of scotopic circuitry, thereby providing a basis for targeting the cell in the wholemount retina. Identification of the other inhibitory components of the PV-5 (and all of the PV-6) neural circuits requires alternative strategies, since the INL contains at least 60 amacrine cell types (MacNeil and Masland 1998). This could be achieved through transsynaptic tracing (as with the identification of dopaminergic amacrine cells in Chapter 1 and Viney et al. 2007) or using

BAC transgenic libraries where single cell types are labelled with GFP in a large number of mouse lines (Siegert et al. 2009 and see Discussion).

The essence of circuit computation in the retina

The most intriguing property of the PV-5 neural circuit in the mechanism of fast inhibition 'borrowed' from the rod pathway circuitry. Regardless of the direction of information flow through the AII cell, PV-5 but not PV-6 receives an inhibitory input that is fast enough to cancel excitation during non-approach motion. This is the essence of circuit computation in the retina: in PV-5, motion sensitivity arises due to the suppression of responses to so-called *null stimuli*, i.e. those cases in which the approach-sensitive cell does not respond. Thus it is only when inhibition overlaps with excitation that the firing rate of the cell is significantly affected to fulfil a functional role. This reasoning has been applied to all PV cells (Chapter 2) and therefore all ganglion cells. Indeed, an appreciable fraction of retinal circuitry is devoted to the analysis of different categories of motion alone. In addition to the approach-sensitive PV-5 ganglion cell type (Münch et al. 2009), eight types of direction-selective ganglion cell have been found: four ON-OFF types (PV-8 from Chapter 2 and Oyster 1968), three ON types (Oyster 1968, Yonehara et al. 2008, Yonehara et al. 2009), and one OFF type (PV-7 from Chapter 2 and Kim et al. 2008). These cell types report either the direction of lateral object motion or the direction of global image drift. Still other ganglion cell types respond to ‘differential’ object motion relative to global background motion (Olveczky et al. 2003). In all three cases of motion sensitivity - lateral-direction selectivity, differential-motion sensitivity and approach sensitivity - the ganglion cells respond most vigorously to the 'preferred stimulus', whereas their responses to the null stimuli are suppressed (or ‘irrelevant’ information, see Chapter 2). The preferred stimuli are object motion in a given direction, differential object-background motion and approaching motion, respectively, whereas null stimuli are motion in the opposite direction, overlapping object-background motion and receding or lateral motion, respectively. However, ganglion cells are broadly tuned, and ‘sensitivity’ does not mean ‘exclusivity’: motion-sensitive cells do not respond to their preferred stimulus alone. For example,

an OFF direction-selective, differential motion-sensitive, or approach-sensitive cell will respond to a dark flash, like any other OFF ganglion cell.

It is worth highlighting that the first step in finding the function of a neural circuit (and the resulting mechanism for the function) is to present the spot stimuli. As seen in Chapter 2, the retina responds to changes in contrast, therefore, presenting black and white spots is the simplest method of revealing the input pathways to the ganglion cell. Here, I have shown that by using black and white spots, the 'out of phase' motif of a quantified and defined ganglion cell type, PV-5 (Fig. 2.5e), is due to direct excitatory input from OFF bipolar cells and inhibitory input from amacrine cells in the ON pathway. The next step was finding the preferred and null stimuli in the parameter space (Fig. 3.1) and discovering the function (Münch et al. 2009). This lead to the comparison of another ganglion cell type with a similar motif (PV-6, Fig. 3.3) and the property of the inhibitory conductance unique to PV-5 that is responsible for the nature of the null stimuli (suppressing non-approach motion, i.e. fast inhibition). Fortunately, the fast component was found to be electrical and narrowed down to the candidate AII amacrine cell. Finally, the mechanism for the function was explored using targeted patching of the putative fast inhibitory subunit - the AII amacrine cell (Fig. 3.5) - and double patching of the PV-5 cell and AII cell to demonstrate a direct connection. These steps for uncovering circuit function represent 'building blocks' of the circuit itself. Future studies will require similar approaches, and the first step, i.e. identifying the inhibitory-excitatory motifs of defined cell types, has already been achieved here.

Discussion

This thesis has examined the diverse roles that inhibitory neurons play in identified local neural circuits in the mammalian retina. In Chapter 1 I demonstrated that entire neural circuits can be identified through retrograde transsynaptic tracing and that dopaminergic interneurons are presynaptic to an intrinsically photosensitive ganglion cell type (ipRGC Type 1). The ipRGCs were ideal for these tracing experiments since the output of the pupillary reflex circuit was in a highly accessible region, near the anterior chamber of the eye, making it possible to reliably carry out injections of the retrograde virus. Furthermore, the transsynaptic tracing lead to the discovery of three types of ipRGC, based on the three different stratification patterns observed in the inner plexiform layer (Fig. 1.1f) (Viney et al. 2007). The local circuitry of the Type 3 ipRGCs remains unknown. Unexpectedly, one of the ipRGC types (Type 2) was found to have 'specialised contacts' with Müller glial cells (Fig. 1.3). This suggested that glia can be strongly associated with certain types of ganglion cells, in this case a melanopsin-expressing type. Since Müller cells span the entire retina, and that melanopsin (Opn4) has been found in the retinal pigment epithelium (RPE) (Peirson et al. 2004), it is possible that these glia provide a 'bridge' between the classical photoreceptors, which are nourished by the RPE, and the ganglion cell photoreceptors. Interestingly, Müller cells also act as 'light guides' or 'optical cables' that help propagate the light through the retina to the photoreceptors (Franze et al. 2007). It was fortunate that the marker for dopaminergic amacrine cells, tyrosine hydroxylase, was already known and that its stratification had been previously identified (Gustincich et al. 1997). The inhibitory neurons providing input to the Type 2 ipRGC were not identified since no molecular marker is known. However, it was possible to record from the ipRGC type and isolate the inhibitory input (Fig. 1.6). Following on from this study (Viney et al. 2007), it has been demonstrated physiologically that the dopaminergic neurons themselves receive input from (as well as provide input to) the Type 1 ipRGCs (now called M1 cells in the literature) (Zhang et al. 2008). This input drives the

sustained light responses of the dopaminergic neurons, and it is argued that it is the melanopsin phototransduction that influences the modulatory role of the dopaminergic system in the retina, responsible for light-dark adaptation. The discovery that horizontal cells, known for their role in modulating light levels, are presynaptic to the dopaminergic neurons (Fig. 1.7f) (Viney et al. 2007), gives stronger support for a broad physiological role in light-dark adaptation. Further anatomical and physiological work has shown that certain ON cone bipolar cells have 'ectopic ribbon synapses' in the OFF IPL (outermost IPL), and suggest that these form synaptic contact with the Type 1 ipRGCs (M1 cells) and the dopaminergic amacrine cells (Dumitrescu et al. 2009). These recent findings, combined with the transsynaptic tracing, provide deeper insight into the structure and function of local neural circuitry, and particularly the organisation of the inner synaptic layer of the retina. This raises questions about the 'fundamental plan of the retina' (Masland 2001), and challenges concepts that are often taken for granted, such as the direction of information flow, the role of dual-neurotransmitter releasing neurons (such as the dopaminergic neurons which release GABA and dopamine), and the division between the ON and OFF pathways.

In Chapter 2, the role of inhibition was studied in eight 'classical' (non-intrinsically photoreceptive) ganglion cell types. Unlike Chapter 1, this approach did not involve transsynaptic tracing to label cell types, instead it involved a transgenic mouse line with a subpopulation of neurons genetically labelled. Before starting this project I screened many different mouse lines, generated through the same conditional system used for the PV mouse, where a Cre-line was crossed with a Reporter-line (see Materials and Methods) to produce a mouse with a subset of fluorescently-labelled neurons. The PV retina was the brightest, had the optimal density of labelled cells, and consequently was the preferred line (see Chapter 2 first section). Using a two-photon microscope, I targeted and recorded from 600 PV cells and characterised them using physiology and morphology. In order to study the differences between the cell types, I argued that each cell type had to be properly quantified and defined. This multi-dimensional approach lead to the conclusion that timing is very precise, and the interactions between excitation

and inhibition lead to the specific spike-timing observed in the natural scenes (Fig. 2.8). The motifs provide a 'signature' of cell type that may be useful for future studies (Fig. 2.6). And displaying the interactions as parametric plots provide further insight into how inhibition modulates the activity of ganglion cells during visual stimulation (Fig. 2.7). However, the presynaptic bipolar and amacrine cells were only revealed through their isolation with whole cell voltage clamp and not morphologically. If the PV cell types could be labelled using a retrograde tracing technique such as that used in Chapter 1, perhaps some of the cell types that provide excitation and inhibition could be identified (given the correct markers or previous characterisation). For the bipolar cell types providing input, it is more straightforward to predict, since bipolar cells have been characterised based on their axonal terminal stratification in the IPL, and may be matched with the stratification of the PV cell types. Inhibitory neurons - amacrine cells - are more difficult to characterise owing to their diversity and their multiple levels of stratification. Also given that there are two 'major groups' of amacrine cells - widefield amacrine cells (GABAergic) and narrowfield amacrine cells (glycinergic), it is difficult to predict based on physiology alone the relative contributions of the two groups. For instance, the surround effects of inhibition could be directly due to widefield amacrine cells, but also presynaptic inhibition to the bipolar cells, or some form of feedback to other amacrine cells. Narrowfield amacrine cells can also be coupled, which greatly amplifies their contribution to include the surround. And for the centre-surround antagonism, it is difficult to prove whether the horizontal cells or widefield amacrine cells have the most influence. Unfortunately inhibitory pharmacological blockers can often have unwanted secondary effects, especially when the type of inhibition being studied is unknown. An alternative method to identifying the components of the ganglion cell local circuits is to use BAC transgenics (Siegert et al. 2009). Here, a very large number of transgenic mouse lines exist from the GENSAT project whereby specific cell types have been labelled with GFP driven by selected molecular markers. If the stratification depth is known (as it is for all eight PV cell types), this depth can be correlated with those BAC lines which have subsets of cells that stratify at the same depth. For example, the PV-3 cell type, which stratifies in the middle of the IPL (colocalising with the middle Calretinin band), has the

same stratification as a BAC line known as 'Doc2b', which has GFP positive somata in the INL. If the PV mouse line was crossed with this line, it may be possible to target these cells in the INL and the PV-3 cell in the GCL and test for a connection. However, these types of experiments are physiologically demanding (see Chapter 3), so an alternative approach would be to use conditional tracing, where a transsynaptic virus containing a LoxP-STOP-LoxP cassette driving a reporter such as RFP is used to infect only Cre-expressing cells, such as the PV cells in the PV retina (DeFalco et al. 2001). Indeed viruses already exist that can spread monosynaptically (Wickersham et al. 2007), which would be useful for restricting the population of presynaptically labelled cells. The virus (in this case a rabies virus, which could be made conditional) could be injected into the Superior colliculus and be titred down so that it only infects a few PV-Cre-positive ganglion cells. Even if presynaptic cells were identified, it still requires more work to determine their functional role in the neural circuit of that ganglion cell type. In Chapter 1, the transsynaptically-labelled dopaminergic amacrine cells had already been linked to a physiological function, that of light-dark adaptation. So far, the only PV cell circuit to be investigated further is that of PV-5.

Chapter 3 described the mechanism of fast inhibition in the PV-5 local circuit, and the specific functional role of the AII amacrine cell, another well-characterised inhibitory interneuron from the rod pathway (Pourcho and Goebel 1985, Bloomfield and Dacheux 2001). In this case, a function had already been assigned to PV-5, that of approach sensitivity (Münch et al. 2009). For this study I used double patch experiments to show that the AII amacrine cells provide input to the PV-5 ganglion cell via a cone pathway (Fig. 3.6). Therefore this was a physiological strategy, rather than an anatomical one (Chapter 1), and it revealed that during photopic (day-time) vision, the information flow through the electrical synapses between ON cone bipolar cells and AII amacrine cells is reversed, compared with the classically-described scotopic (night-time) vision pathway where the AII cells relays rod signals to ganglion cells via the cone bipolar cells. AII amacrine cells are glycinergic, and fortunately the pharmacology used here was beneficial in showing that the connection between the AII and PV-5 was indeed mediated

by glycine receptors (Fig. 3.6). The experiments therefore suggested that a three-synapse pathway carries the rapid inhibitory component: cones to ON bipolar cells via metabotropic glutamate synapses, ON bipolar cells to amacrine cells through a conduit unimpaired by CPP/NBQX, and amacrine cells to PV-5 ganglion cells through glycine receptors. The slow inhibitory pathway occurred though CPP/NBQX-sensitive glutamate synapses. In contrast, the excitatory pathway is conventional: cones to OFF bipolar cells, and OFF bipolar cells to the PV-5 cell through ionotropic glutamate receptors. Furthermore, without the PV retina, the PV-5 cell type would have been very difficult to target for the double patch experiments, where the identity was required before attempting the AII targeting. It would also have been challenging to reliably find another OFF-firing OFF-stratifying cell to compare the circuitry (Fig. 3.3, 3.4). The origin of inhibition in PV-6, and the slower component of inhibition in PV-5, remains to be determined. It would also be interesting to determine the role of the other electrically coupled amacrine cells found within the dendritic tree of PV-5 after neurobiotin filling. For this study, a fluorescent dye would be required that passes through gap junctions in the living retina.

So far I have discussed the presynaptic circuitry. It would also be interesting to investigate the projection patterns of the PV ganglion cell types (Chapter 2). The main ipRGC projections are already known (Chapter 1). For the approach-sensitive neuron PV-5 in Chapter 3, where are the 'approach motion spikes' sent? Some studies have already addressed projections of retinal ganglion cells, using specific single-labelled cell types (Yonehara et al. 2009, Huberman et al. 2008, Kim et al. 2008). However the PV retina contains at least eight cell types, so the YFP-positive axonal terminals in the Superior colliculus and Dorsal lateral geniculate nucleus of the PV mouse form a mesh and cannot be traced back and assigned to specific PV cell types. Clearly the site of ganglion cell axon terminals is another parameter that defines cell type, and would perhaps provide further insight into how the output of the retina is organised. For example, given a direction selective cell type of one preferred direction (such as PV-0), does every cell of that type terminate with corresponding cells of the other three types (forming a functional group)? How

are the four different directions integrated in the brain? To determine projection patterns of the PV cells, I used a viral-mediated approach. I injected a conditional adeno-associated virus (AAV) that only expresses RFP in cells that contain Cre (Kuhlman and Huang 2008) into the vitreous chamber of the PV mouse eye. I found that after three weeks (and also for times greater than a year), 90% of PV cells (YFP positive cells) were very brightly labelled with RFP. Since most of the PV cells were labelled, it was not possible to trace individual axons. Consequently, the entire optic tract appeared to be labelled. I titred down the virus, by diluting the stock, but there were either too many cells labelled for tracing studies, or no cells labelled at all. These experiments suggest that a fine balance is required in order to label single PV cells, and hence a significant amount of time and animals. An alternative approach involved single-cell targeting, where I used two-photon targeted patching to fill single PV cells with neurobiotin, *ex vivo*, but with the whole brain still attached via the optic nerve. The idea (from K. Balint) was to patch a ganglion cell for long enough that the neurobiotin would diffuse through the entire axon and reach the terminal. This technique required the whole brain to be only partially nourished with Ringers solution, at the side of the microscope objective, and a filling time of at least one hour at physiological temperature for any significant diffusion. In all experiments, it was not possible to find the labelled axon in brain slices after staining with an streptavidin-Alex Fluor dye that binds neurobiotin, or even with the DAB staining method. These experiments suggest that higher concentrations of neurobiotin and/or longer incubation times are necessary, or a longer recovery time (the time after filling before fixation) is used so that neurobiotin reaches the terminal, but this would involve keeping the brain alive for a significantly longer period. Currently, retrograde transsynaptic tracing has been the most successful for tracing in central brain regions (Chapter 1), but only due to the specific projection patterns of the target ganglion cell types (Fig. 1.1a,e). Before the studies described in Chapter 2, I looked for another ganglion cell type that had specific projection patterns. The so-called 'ON direction selective' ganglion cells consist of three types that are responsible for a feedback system that stabilises head movements in the accessory optic system (Buhl and Peichl 1986, Giolli et al. 2006). Each type projects to a different brain region, and the

preferred direction is thought to be related to the corresponding terminal nucleus (Dorsal terminal nucleus (DTN), Lateral terminal nucleus (LTN), Medial terminal nucleus (MTN)) for the three dimensions of head movement. I performed stereotaxic injections in the mouse MTN, the most accessible, isolated nucleus of the three, using either fluorescent microbeads that are transported retrogradely, or with a transsynaptic virus that became known as TimerPRV (Boldogkoi et al. 2009). The idea was to first label the MTN-projecting ON direction selective cells in the retina and determine whether they were direction selective using electrophysiology (targeted patching), and second to study the role of inhibition in these cells. The ON direction selective ganglion cells are known to colocalise with the ON ChAT (starburst amacrine cell) band, similar to that of the ON stratum of the ON OFF direction selective cells (PV-0-like cell types). In other words, this was a method for targeted recordings and circuit tracing of an functionally-defined ganglion cell type, similar to the strategy for Chapter 1 with the ipRGCs. The TimerPRV was used for the transsynaptic tracing component of the project. I discovered that this virus, unlike PRV152 (Chapter 1), first labelled neurons green, and later red (since it encodes two fluorescent proteins, GFP and RFP, localised to different regions of the cell). Therefore it happened to work as a 'timer' for circuit tracing (Boldogkoi et al. 2009). The GFP was expressed first, soon after the virus infected the first neuron in the local circuit. Then later, as more neurons in the circuit became labelled with GFP, the earlier ones started expressing RFP. Therefore, I used TimerPRV to track the temporal sequence of neurons labelled in local circuits. For low-titre injections to the MTN, I observed GFP and RFP positive ganglion cells in the retina, surrounded by only GFP positive amacrine cells. Furthermore, using different incubation times at the resolution of half a day, I was able to inject the virus into the Flocculus and Medial vestibular nuclei, which are components of the accessory optic system, and confirm that they were presynaptic to the MTN and that ganglion cells in the retina could become infected. This technique is feasible for studying local neural circuits and their inhibitory neurons, but again can be very time consuming, since every electrophysiological experiment requires a stereotaxic surgery, and there is no guarantee that the correct cell types would be labelled. Clearly the optimal strategy is to use

transgenic mice. The generation of a mouse line that had MTN-projecting ON direction selective cells labelled was clearly an advantage (Yonehara et al. 2008). Therefore, I turned to the PV retina, which requires no prior surgeries or significant preparation in order to reliably record from identified ganglion cell types. Given the wide range of resources available today, from immunohistochemical markers, to BAC transgenic mouse lines and transsynaptic viruses, it is highly possible that in the future, the combined anatomical, molecular, morphological and physiological components of local neural circuits will be understood.

Summary

This thesis has described the diverse roles of inhibition in identified neural circuits in the mouse retina. Identification, in the first chapter, referred to fluorescently labelling the local circuits of specific ganglion cell types with a retrograde transsynaptic virus. Here, the identity of these labelled cell types was known by their expression of melanopsin, revealed using the melanopsin antibody. This protein identified the cells as intrinsically-photosensitive retinal ganglion cells (ipRGCs). The virus also revealed that there are three types of ipRGC, and that the nuclei retrogradely labelled in the brain matched the previously characterised pathways that involved ipRGCs, including the entire pupillary reflex circuit. Furthermore, the inhibitory neuron presynaptic to one type of ipRGC had also been previously characterised, again using a marker, tyrosine hydroxylase, that identified the cell type as the dopaminergic interplexiform cell, which is involved in light-dark adaptation. Moreover, horizontal cells were found to be presynaptic to the dopaminergic neurons. Therefore, the first chapter used a reverse approach to study the role of inhibition: it linked two physiological functions - that of a GABAergic dopaminergic neuron and an intrinsically photosensitive ganglion cell - both involved in relatively slow biological processes in the brain. In the second chapter, the identification of neural circuits was carried out using a forward approach: from an unknown subpopulation of genetically-labelled neurons, eight ganglion cell types were gradually characterised quantitatively, and the local circuits were studied through physiology. By voltage clamping the cell, it was possible to isolate excitation and inhibition, and explore how they interacted during visual stimulation. The role of inhibition was found to be important for detecting 'irrelevance' in the visual scene, so when inhibition changed faster than excitation, the cell did not fire. Inhibition was shown to be circuit-specific, and in combination with excitation provided a 'motif' for each cell type that was useful in predicting the behaviour of the cell during more natural visual stimulation. Finally, in the third chapter, the role of a specific inhibitory subunit - the AII amacrine cell - was investigated in the context of

one of the eight identified ganglion cell types from the previous chapter. This interneuron was previously identified as a key cell type involved in night vision circuitry - providing a link between the highly sensitive rod pathway (rod photoreceptors to rod bipolar cells) and the ganglion cells via an electrical connection with cone bipolar cells. In day vision circuits - the conditions used throughout this thesis work - the AII amacrine cell was found to relay information in the reverse direction, from cone bipolar cells to ganglion cells via the same electrical synapse. This 'fast' version of inhibition - through electrical coupling - is an example of the 'irrelevance detection'. Here, the mechanism of fast inhibition is to prevent the ganglion cell from firing during non-approach motion, meaning that the function of the ganglion cell is precisely the opposite - to detect approaching objects. Therefore all three chapters have analysed different aspects of inhibition, from the identified circuits that fulfil broad physiological roles over relatively slow time scales, to the very fast mechanics of small inhibitory neurons involved in feature detection.

Acknowledgements

First I would like to thank my thesis committee, Botond Roska, Silvia Arber, and Reto Weiler for their time given to my thesis and their excellent advice and support. Botond has been a fantastic group leader throughout my PhD studies, and I have learned a great deal from him, not only in how to do science but also how to think about science. I am delighted to have become a neurophysiologist in his group. I would also like to thank all the members of the Roska group (past and present) for valuable discussions, and their enthusiasm during the lab meetings. During my time here, Brigitte Gross-Scherf has been a highly capable research associate running the lab, and has made the lab a very positive and organised environment to work in. I give special thanks to Thomas Münch and Botond, who introduced me to Mathematica, and David Balya, for teaching me the principles of functional programming, which has been absolutely essential for my research. I am grateful to the support of the FMI facilities and departments, especially for the use of the confocal microscope in the Imaging Facility. The animal facility has been essential to my studies and I thank the caretakers there and also Sabrina Djaffer for providing me with an unlimited supply of PV mice. Finally I would like to acknowledge my family and Stéphanie Dujardin for all their support during my PhD studies.

References

Ascoli, G.A., Alonso-Nanclares, L., Anderson, S.A., Barrionuevo, G., Benavides-Piccione, R., Burkhalter, A., Buzsaki, G., Cauli, B., Defelipe, J., Fairen, A.*, et al.* (2008). Petilla terminology: nomenclature of features of GABAergic interneurons of the cerebral cortex. Nat Rev Neurosci *9*, 557-568.

Awatramani, G.B., and Slaughter, M.M. (2000). Origin of transient and sustained responses in ganglion cells of the retina. J Neurosci *20*, 7087-7095.

Badea, T.C., and Nathans, J. (2004). Quantitative analysis of neuronal morphologies in the mouse retina visualized by using a genetically directed reporter. J Comp Neurol *480*, 331-351.

Ball, W., and Tronick, E. (1971). Infant responses to impending collision: optical and real. Science *171*, 818-820.

Banfield, B.W., Kaufman, J.D., Randall, J.A., and Pickard, G.E. (2003). Development of pseudorabies virus strains expressing red fluorescent proteins: new tools for multisynaptic labeling applications. J Virol *77*, 10106-10112.

Barlow, H.B., Hill, R.M., and Levick, W.R. (1964). Retinal Ganglion Cells Responding Selectively to Direction and Speed of Image Motion in the Rabbit. J Physiol *173*, 377-407.

Belenky, M.A., Smeraski, C.A., Provencio, I., Sollars, P.J., and Pickard, G.E. (2003). Melanopsin retinal ganglion cells receive bipolar and amacrine cell synapses. J Comp Neurol *460*, 380-393.

Berry, M.J., Warland, D.K., and Meister, M. (1997). The structure and precision of retinal spike trains. Proc Natl Acad Sci U S A *94*, 5411-5416.

Betsch, B.Y., Einhäuser, W., Körding, K.P., and König, P. (2004). The world from a cat's perspective | statistics of natural videos. Biol. Cybern. *90,* 41-50.

Bloomfield, S.A., and Dacheux, R.F. (2001). Rod vision: pathways and processing in the mammalian retina. Prog Retin Eye Res *20*, 351-384.

Bloomfield, S.A., and Miller, R.F. (1986). A functional organization of ON and OFF pathways in the rabbit retina. J Neurosci *6*, 1-13.

Boldogkoi, Z., Balint, K., Awatramani, G.B., Balya, D., Busskamp, V., Viney, T.J., Lagali, P.S., Duebel, J., Pasti, E., Tombacz, D.*, et al.* (2009). Genetically timed, activity-sensor and rainbow transsynaptic viral tools. Nat Methods *6*, 127-130.

Boldogkoi, Z., Erdelyi, F., Sik, A., Freund, T.F., and Fodor, I. (1999). Construction of a recombinant herpesvirus expressing the jellyfish green fluorescent protein. Luminescence *14*, 69-74.

Boldogkoi, Z., Reichart, A., Toth, I.E., Sik, A., Erdelyi, F., Medveczky, I., Llorens-Cortes, C., Palkovits, M., and Lenkei, Z. (2002). Construction of recombinant pseudorabies viruses optimized for labeling and neurochemical characterization of neural circuitry. Brain Res Mol Brain Res *109*, 105-118.

Boycott, B.B., and Wassle, H. (1974). The morphological types of ganglion cells of the domestic cat's retina. J Physiol *240*, 397-419.

Buffelli, M., Burgess, R.W., Feng, G., Lobe, C.G., Lichtman, J.W., and Sanes, J.R. (2003). Genetic evidence that relative synaptic efficacy biases the outcome of synaptic competition. Nature *424*, 430-434.

Buhl, E.H., and Peichl, L. (1986). Morphology of rabbit retinal ganglion cells projecting to the medial terminal nucleus of the accessory optic system. J Comp Neurol *253*, 163-174.

Card, J.P. (2000). Pseudorabies virus and the functional architecture of the circadian timing system. J Biol Rhythms *15*, 453-461.

Card, J.P., Whealy, M.E., Robbins, A.K., Moore, R.Y., and Enquist, L.W. (1991). Two alpha-herpesvirus strains are transported differentially in the rodent visual system. Neuron *6*, 957-969.

Cardin, J.A., Carlen, M., Meletis, K., Knoblich, U., Zhang, F., Deisseroth, K., Tsai, L.H., and Moore, C.I. (2009). Driving fast-spiking cells induces gamma rhythm and controls sensory responses. Nature *459*, 663-667.

Cohen, E.D., and Miller, R.F. (1999). The network-selective actions of quinoxalines on the neurocircuitry operations of the rabbit retina. Brain Res *831*, 206-228.

Connaughton, V.P., Graham, D., and Nelson, R. (2004). Identification and morphological classification of horizontal, bipolar, and amacrine cells within the zebrafish retina. J Comp Neurol *477*, 371-385.

Contini, M., and Raviola, E. (2003). GABAergic synapses made by a retinal dopaminergic neuron. Proc Natl Acad Sci U S A *100*, 1358-1363.

Coombs, J., van der List, D., Wang, G.Y., and Chalupa, L.M. (2006). Morphological properties of mouse retinal ganglion cells. Neuroscience *140*, 123-136.

Crowley, J.J., Fioravante, D., and Regehr, W.G. (2009). Dynamics of fast and slow inhibition from cerebellar golgi cells allow flexible control of synaptic integration. Neuron *63*, 843-853.

Dacey, D.M., Liao, H.W., Peterson, B.B., Robinson, F.R., Smith, V.C., Pokorny, J., Yau, K.W., and Gamlin, P.D. (2005). Melanopsin-expressing ganglion cells in primate retina signal colour and irradiance and project to the LGN. Nature *433*, 749-754.

Deans, M.R., Gibson, J.R., Sellitto, C., Connors, B.W., and Paul, D.L. (2001). Synchronous activity of inhibitory networks in neocortex requires electrical synapses containing connexin36. Neuron *31*, 477-485.

DeFalco, J., Tomishima, M., Liu, H., Zhao, C., Cai, X., Marth, J.D., Enquist, L., and Friedman, J.M. (2001). Virus-assisted mapping of neural inputs to a feeding center in the hypothalamus. Science *291*, 2608-2613.

Devries, S.H., and Baylor, D.A. (1997). Mosaic arrangement of ganglion cell receptive fields in rabbit retina. J Neurophysiol *78*, 2048-2060.

Doi, M., Yujnovsky, I., Hirayama, J., Malerba, M., Tirotta, E., Sassone-Corsi, P., and Borrelli, E. (2006). Impaired light masking in dopamine D2 receptor-null mice. Nat Neurosci *9*, 732-734.

Dowling, J.E., and Ehinger, B. (1975). Synaptic organization of the amine-containing interplexiform cells of the goldfish and Cebus monkey retinas. Science *188*, 270-273.

Dumitrescu, O.N., Pucci, F.G., Wong, K.Y., and Berson, D.M. (2009). Ectopic retinal ON bipolar cell synapses in the OFF inner plexiform layer: contacts with dopaminergic amacrine cells and melanopsin ganglion cells. J Comp Neurol *517*, 226-244.

Eggers, E.D., and Lukasiewicz, P.D. Interneuron circuits tune inhibition in retinal bipolar cells. J Neurophysiol *103*, 25-37.

Euler, T., and Masland, R.H. (2000). Light-evoked responses of bipolar cells in a mammalian retina. J Neurophysiol *83*, 1817-1829.

Famiglietti, E.V., Jr. (1983). 'Starburst' amacrine cells and cholinergic neurons: mirror-symmetric on and off amacrine cells of rabbit retina. Brain Res *261*, 138-144.

Famiglietti, E.V. (2005). Synaptic organization of complex ganglion cells in rabbit retina: type and arrangement of inputs to directionally selective and local-edge-detector cells. J Comp Neurol *484*, 357-391.

Famiglietti, E.V., Jr., and Kolb, H. (1976). Structural basis for ON-and OFF-center responses in retinal ganglion cells. Science *194*, 193-195.

Feigenspan, A., Teubner, B., Willecke, K., and Weiler, R. (2001). Expression of neuronal connexin36 in AII amacrine cells of the mammalian retina. J Neurosci *21*, 230-239.

Flores-Herr, N., Protti, D.A., and Wässle, H. (2001). Synaptic currents generating the inhibitory surround of ganglion cells in the mammalian retina. J Neurosci *21*, 4852-4863.

Franze, K., Grosche, J., Skatchkov, S.N., Schinkinger, S., Foja, C., Schild, D., Uckermann, O., Travis, K., Reichenbach, A., and Guck, J. (2007). Müller cells are living optical fibers in the vertebrate retina. Proc Natl Acad Sci U S A *104*, 8287-8292.

Fried, S.I., Münch, T.A., and Werblin, F.S. (2002). Mechanisms and circuitry underlying directional selectivity in the retina. Nature *420*, 411-414.

Fu, Y., Liao, H.W., Do, M.T., and Yau, K.W. (2005). Non-image-forming ocular photoreception in vertebrates. Curr Opin Neurobiol *15*, 415-422.

Gabbiani, F., Cohen, I., and Laurent, G. (2005). Time-dependent activation of feed-forward inhibition in a looming-sensitive neuron. J Neurophysiol *94*, 2150-2161.

Gabbiani, F., Krapp, H.G., and Laurent, G. (1999). Computation of object approach by a wide-field, motion-sensitive neuron. J Neurosci *19*, 1122-1141.

Gentet, L.J., Avermann, M., Matyas, F., Staiger, J.F., and Petersen, C.C. Membrane potential dynamics of GABAergic neurons in the barrel cortex of behaving mice. Neuron *65*, 422-435.

Geraghty, R.J., Krummenacher, C., Cohen, G.H., Eisenberg, R.J., and Spear, P.G. (1998). Entry of alphaherpesviruses mediated by poliovirus receptor-related protein 1 and poliovirus receptor. Science *280*, 1618-1620.

Ghosh, K.K., Bujan, S., Haverkamp, S., Feigenspan, A., and Wassle, H. (2004). Types of bipolar cells in the mouse retina. J Comp Neurol *469*, 70-82.

Giolli, R.A., Blanks, R.H., and Lui, F. (2006). The accessory optic system: basic organization with an update on connectivity, neurochemistry, and function. Prog Brain Res *151*, 407-440.

Gollisch, T., and Meister, M. Eye smarter than scientists believed: neural computations in circuits of the retina. Neuron *65*, 150-164.

Gollisch, T., and Meister, M. (2008). Rapid neural coding in the retina with relative spike latencies. Science *319*, 1108-1111.

Greferath, U., Grünert, U., and Wässle, H. (1990). Rod bipolar cells in the mammalian retina show protein kinase C-like immunoreactivity. J Comp Neurol *301*, 433-442.

Gustincich, S., Feigenspan, A., Wu, D.K., Koopman, L.J., and Raviola, E. (1997). Control of dopamine release in the retina: a transgenic approach to neural networks. Neuron *18*, 723-736.

Hannibal, J., and Fahrenkrug, J. (2004). Target areas innervated by PACAP-immunoreactive retinal ganglion cells. Cell Tissue Res *316*, 99-113.

Hannibal, J., Hindersson, P., Knudsen, S.M., Georg, B., and Fahrenkrug, J. (2002). The photopigment melanopsin is exclusively present in pituitary adenylate cyclase-activating polypeptide-containing retinal ganglion cells of the retinohypothalamic tract. J Neurosci *22*, RC191.

Harvey, C.D., Collman, F., Dombeck, D.A., and Tank, D.W. (2009). Intracellular dynamics of hippocampal place cells during virtual navigation. Nature *461*, 941-946.

Hatsopoulos, N., Gabbiani, F., and Laurent, G. (1995). Elementary computation of object approach by wide-field visual neuron. Science *270*, 1000-1003.

Hattar, S., Kumar, M., Park, A., Tong, P., Tung, J., Yau, K.W., and Berson, D.M. (2006). Central projections of melanopsin-expressing retinal ganglion cells in the mouse. J Comp Neurol *497*, 326-349.

Hattar, S., Liao, H.W., Takao, M., Berson, D.M., and Yau, K.W. (2002). Melanopsin-containing retinal ganglion cells: architecture, projections, and intrinsic photosensitivity. Science *295*, 1065-1070.

Haverkamp, S., and Wässle, H. (2000). Immunocytochemical analysis of the mouse retina. J Comp Neurol *424*, 1-23.

Hippenmeyer, S., Vrieseling, E., Sigrist, M., Portmann, T., Laengle, C., Ladle, D.R., and Arber, S. (2005). A developmental switch in the response of DRG neurons to ETS transcription factor signaling. PLoS Biol *3*, e159.

Hombach, S., Janssen-Bienhold, U., Sohl, G., Schubert, T., Bussow, H., Ott, T., Weiler, R., and Willecke, K. (2004). Functional expression of connexin57 in horizontal cells of the mouse retina. Eur J Neurosci *19*, 2633-2640.

Huang, L., Max, M., Margolskee, R.F., Su, H., Masland, R.H., and Euler, T. (2003). G protein subunit G gamma 13 is coexpressed with G alpha o, G beta 3, and G beta 4 in retinal ON bipolar cells. J Comp Neurol *455*, 1-10.

Hughes, A. (1979). A rose by any other name... on 'naming of neurones' by Rowe and Stone. Brain Behav Evol *16*, 52-64.

Isayama, T., Berson, D.M., and Pu, M. (2000). Theta ganglion cell type of cat retina. J Comp Neurol *417*, 32-48.

Ishikane, H., Gangi, M., Honda, S., and Tachibana, M. (2005). Synchronized retinal oscillations encode essential information for escape behavior in frogs. Nat Neurosci *8*, 1087-1095.

Jacoby, R., Stafford, D., Kouyama, N., and Marshak, D. (1996). Synaptic inputs to ON parasol ganglion cells in the primate retina. J Neurosci *16*, 8041-8056.

Jeon, C.J., Strettoi, E., and Masland, R.H. (1998). The major cell populations of the mouse retina. J Neurosci *18*, 8936-8946.

Jons, A., and Mettenleiter, T.C. (1997). Green fluorescent protein expressed by recombinant pseudorabies virus as an in vivo marker for viral replication. J Virol Methods *66*, 283-292.

Kayser, C., Einhäuser, W., and König, P. (2003). Temporal correlations of orientations in natural scenes. Neurocomputing. *52-54,* 117-123.

Kim, I.J., Zhang, Y., Yamagata, M., Meister, M., and Sanes, J.R. (2008). Molecular identification of a retinal cell type that responds to upward motion. Nature *452*, 478-482.

King, J.G., Jr., Lettvin, J.Y., and Gruberg, E.D. (1999). Selective, unilateral, reversible loss of behavioral responses to looming stimuli after injection of

tetrodotoxin of cadmium chloride into the frog optic nerve. Brain Res *841*, 20-26.

King, S.M., and Cowey, A. (1992). Defensive responses to looming visual stimuli in monkeys with unilateral striate cortex ablation. Neuropsychologia *30*, 1017-1024.

King, S.M., Dykeman, C., Redgrave, P., and Dean, P. (1992). Use of a distracting task to obtain defensive head movements to looming visual stimuli by human adults in a laboratory setting. Perception *21*, 245-259.

Klausberger, T., Magill, P.J., Marton, L.F., Roberts, J.D., Cobden, P.M., Buzsaki, G., and Somogyi, P. (2003). Brain-state- and cell-type-specific firing of hippocampal interneurons in vivo. Nature *421*, 844-848.

Klausberger, T., Marton, L.F., Baude, A., Roberts, J.D., Magill, P.J., and Somogyi, P. (2004). Spike timing of dendrite-targeting bistratified cells during hippocampal network oscillations in vivo. Nat Neurosci *7*, 41-47.

Klausberger, T., Marton, L.F., O'Neill, J., Huck, J.H., Dalezios, Y., Fuentealba, P., Suen, W.Y., Papp, E., Kaneko, T., Watanabe, M.*, et al.* (2005). Complementary roles of cholecystokinin- and parvalbumin-expressing GABAergic neurons in hippocampal network oscillations. J Neurosci *25*, 9782-9793.

Kolb, H. (1974). The connections between horizontal cells and photoreceptors in the retina of the cat: electron microscopy of Golgi preparations. J Comp Neurol *155*, 1-14.

Kong, J.H., Fish, D.R., Rockhill, R.L., and Masland, R.H. (2005). Diversity of ganglion cells in the mouse retina: unsupervised morphological classification and its limits. J Comp Neurol *489*, 293-310.

Kuffler, S.W. (1953). Discharge patterns and functional organization of mammalian retina. J Neurophysiol *16*, 37-68.

Kuhlman, S.J., and Huang, Z.J. (2008). High-resolution labeling and functional manipulation of specific neuron types in mouse brain by Cre-activated viral gene expression. PLoS One *3*, e2005.

Lasater, E.M., and Dowling, J.E. (1985). Dopamine decreases conductance of the electrical junctions between cultured retinal horizontal cells. Proc Natl Acad Sci U S A *82*, 3025-3029.

Levick, W.R. (1967). Receptive fields and trigger features of ganglion cells in the visual streak of the rabbits retina. J Physiol *188*, 285-307.

MacNeil, M.A., and Masland, R.H. (1998). Extreme diversity among amacrine cells: implications for function. Neuron *20*, 971-982.

Mangel, S.C., and Dowling, J.E. (1985). Responsiveness and receptive field size of carp horizontal cells are reduced by prolonged darkness and dopamine. Science *229*, 1107-1109.

Manookin, M.B., Beaudoin, D.L., Ernst, Z.R., Flagel, L.J., and Demb, J.B. (2008). Disinhibition combines with excitation to extend the operating range of the OFF visual pathway in daylight. J Neurosci *28*, 4136-4150.

Marc, R.E., and Liu, W.L. (1984). Horizontal cell synapses onto glycine-accumulating interplexiform cells. Nature *312*, 266-269.

Masland, R.H. (2001). The fundamental plan of the retina. Nat Neurosci *4*, 877-886.

Massey, S.C., O'Brien, J.J., Trexler, E.B., Li, W., Keung, J.W., Mills, S.L., and O'Brien, J. (2003). Multiple neuronal connexins in the mammalian retina. Cell Commun Adhes *10*, 425-430.

Meister, M., and Berry, M.J., 2nd (1999). The neural code of the retina. Neuron *22*, 435-450.

Metzger, D., and Feil, R. (1999). Engineering the mouse genome by site-specific recombination. Curr Opin Biotechnol *10*, 470-476.

Mills, S.L., O'Brien, J.J., Li, W., O'Brien, J., and Massey, S.C. (2001). Rod pathways in the mammalian retina use connexin 36. J Comp Neurol *436*, 336-350.

Münch, T.A., da Silveira, R.A., Siegert, S., Viney, T.J., Awatramani, G.B., and Roska, B. (2009). Approach sensitivity in the retina processed by a multifunctional neural circuit. Nat Neurosci *12*, 1308-1316.

Murphy, G.J., and Rieke, F. (2008). Signals and noise in an inhibitory interneuron diverge to control activity in nearby retinal ganglion cells. Nat Neurosci *11*, 318-326.

Nawy, S., and Jahr, C.E. (1990). Suppression by glutamate of cGMP-activated conductance in retinal bipolar cells. Nature *346*, 269-271.

Nawy, S., and Jahr, C.E. (1991). cGMP-gated conductance in retinal bipolar cells is suppressed by the photoreceptor transmitter. Neuron *7*, 677-683.

O'Brien, B.J., Isayama, T., Richardson, R., and Berson, D.M. (2002). Intrinsic physiological properties of cat retinal ganglion cells. J Physiol *538*, 787-802.

O'Malley, D.M., Sandell, J.H., and Masland, R.H. (1992). Co-release of acetylcholine and GABA by the starburst amacrine cells. J Neurosci *12*, 1394-1408.

Oesch, N., and Diamond, J. (2009). A night vision neuron gets a day job. Nat Neurosci *12*, 1209-1211.

Olveczky, B.P., Baccus, S.A., and Meister, M. (2003). Segregation of object and background motion in the retina. Nature *423*, 401-408.

Oyster, C.W. (1968). The analysis of image motion by the rabbit retina. J Physiol *199*, 613-635.

Pang, J.J., Abd-El-Barr, M.M., Gao, F., Bramblett, D.E., Paul, D.L., and Wu, S.M. (2007). Relative contributions of rod and cone bipolar cell inputs to AII amacrine cell light responses in the mouse retina. J Physiol *580*, 397-410.

Pang, J.J., Gao, F., and Wu, S.M. (2003). Light-evoked excitatory and inhibitory synaptic inputs to ON and OFF alpha ganglion cells in the mouse retina. J Neurosci *23*, 6063-6073.

Peirson, S.N., Bovee-Geurts, P.H., Lupi, D., Jeffery, G., DeGrip, W.J., and Foster, R.G. (2004). Expression of the candidate circadian photopigment melanopsin (Opn4) in the mouse retinal pigment epithelium. Brain Res Mol Brain Res *123*, 132-135.

Pickard, G.E., Smeraski, C.A., Tomlinson, C.C., Banfield, B.W., Kaufman, J., Wilcox, C.L., Enquist, L.W., and Sollars, P.J. (2002). Intravitreal injection of the attenuated pseudorabies virus PRV Bartha results in infection of the hamster suprachiasmatic nucleus only by retrograde transsynaptic transport via autonomic circuits. J Neurosci *22*, 2701-2710.

Pomeranz, L.E., Reynolds, A.E., and Hengartner, C.J. (2005). Molecular biology of pseudorabies virus: impact on neurovirology and veterinary medicine. Microbiol Mol Biol Rev *69*, 462-500.

Pourcho, R.G., and Goebel, D.J. (1985). A combined Golgi and autoradiographic study of (3H)glycine-accumulating amacrine cells in the cat retina. J Comp Neurol *233*, 473-480.

Puopolo, M., Hochstetler, S.E., Gustincich, S., Wightman, R.M., and Raviola, E. (2001). Extrasynaptic release of dopamine in a retinal neuron: activity dependence and transmitter modulation. Neuron *30*, 211-225.

Rabut, G., and Ellenberg, J. (2004). Automatic real-time three-dimensional cell tracking by fluorescence microscopy. J Microsc *216*, 131-137.

Remtulla, S., and Hallett, P.E. (1985). A schematic eye for the mouse, and comparisons with the rat. Vision Res *25*, 21-31.

Renteria, R.C., Tian, N., Cang, J., Nakanishi, S., Stryker, M.P., and Copenhagen, D.R. (2006). Intrinsic ON responses of the retinal OFF pathway are suppressed by the ON pathway. J Neurosci *26*, 11857-11869.

Rice, D.S., and Curran, T. (2000). Disabled-1 is expressed in type AII amacrine cells in the mouse retina. J Comp Neurol *424*, 327-338.

Rockhill, R.L., Daly, F.J., MacNeil, M.A., Brown, S.P., and Masland, R.H. (2002). The diversity of ganglion cells in a mammalian retina. J Neurosci *22*, 3831-3843.

Rodieck, R.W., and Brening, R.K. (1983). Retinal ganglion cells: properties, types, genera, pathways and trans-species comparisons. Brain Behav Evol *23*, 121-164.

Roska, B., Molnar, A., and Werblin, F.S. (2006). Parallel processing in retinal ganglion cells: how integration of space-time patterns of excitation and inhibition form the spiking output. J Neurophysiol *95*, 3810-3822.

Roska, B., and Werblin, F. (2001). Vertical interactions across ten parallel, stacked representations in the mammalian retina. Nature *410*, 583-587.

Roska, B., and Werblin, F. (2003). Rapid global shifts in natural scenes block spiking in specific ganglion cell types. Nat Neurosci *6*, 600-608.

Rowe, M.H., and Stone, J. (1977). Naming of neurones. Classification and naming of cat retinal ganglion cells. Brain Behav Evol *14*, 185-216.

Sakamoto, K., Liu, C., Kasamatsu, M., Pozdeyev, N.V., Iuvone, P.M., and Tosini, G. (2005). Dopamine regulates melanopsin mRNA expression in intrinsically photosensitive retinal ganglion cells. Eur J Neurosci *22*, 3129-3136.

Sakamoto, K., Liu, C., and Tosini, G. (2004). Classical photoreceptors regulate melanopsin mRNA levels in the rat retina. J Neurosci *24*, 9693-9697.

Schiff, W., Caviness, J.A., and Gibson, J.J. (1962). Persistent fear responses in rhesus monkeys to the optical stimulus of "looming". Science *136*, 982-983.

Schmucker, C., and Schaeffel, F. (2004). A paraxial schematic eye model for the growing C57BL/6 mouse. Vision Res *44*, 1857-1867.

Schubert, T., Degen, J., Willecke, K., Hormuzdi, S.G., Monyer, H., and Weiler, R. (2005). Connexin36 mediates gap junctional coupling of alpha-ganglion cells in mouse retina. J Comp Neurol *485*, 191-201.

Sekaran, S., Foster, R.G., Lucas, R.J., and Hankins, M.W. (2003). Calcium imaging reveals a network of intrinsically light-sensitive inner-retinal neurons. Curr Biol *13*, 1290-1298.

Siegert, S., Scherf, B.G., Del Punta, K., Didkovsky, N., Heintz, N., and Roska, B. (2009). Genetic address book for retinal cell types. Nat Neurosci *12*, 1197-1204.

Slaughter, M.M., and Miller, R.F. (1981). 2-amino-4-phosphonobutyric acid: a new pharmacological tool for retina research. Science *211*, 182-185.

Smeraski, C.A., Sollars, P.J., Ogilvie, M.D., Enquist, L.W., and Pickard, G.E. (2004). Suprachiasmatic nucleus input to autonomic circuits identified by retrograde transsynaptic transport of pseudorabies virus from the eye. J Comp Neurol *471*, 298-313.

Smith, B.N., Banfield, B.W., Smeraski, C.A., Wilcox, C.L., Dudek, F.E., Enquist, L.W., and Pickard, G.E. (2000). Pseudorabies virus expressing enhanced green fluorescent protein: A tool for in vitro electrophysiological analysis of transsynaptically labeled neurons in identified central nervous system circuits. Proc Natl Acad Sci U S A *97*, 9264-9269.

Sollars, P.J., Smeraski, C.A., Kaufman, J.D., Ogilvie, M.D., Provencio, I., and Pickard, G.E. (2003). Melanopsin and non-melanopsin expressing retinal ganglion cells innervate the hypothalamic suprachiasmatic nucleus. Vis Neurosci *20*, 601-610.

Stanford, L.R. (1987). W-cells in the cat retina: correlated morphological and physiological evidence for two distinct classes. J Neurophysiol *57*, 218-244.

Steenhard, B.M., and Besharse, J.C. (2000). Phase shifting the retinal circadian clock: xPer2 mRNA induction by light and dopamine. J Neurosci *20*, 8572-8577.

Sun, H., and Frost, B.J. (1998). Computation of different optical variables of looming objects in pigeon nucleus rotundus neurons. Nat Neurosci *1*, 296-303.

Sun, W., Deng, Q., Levick, W.R., and He, S. (2006). ON direction-selective ganglion cells in the mouse retina. J Physiol *576*, 197-202.

Sun, W., Li, N., and He, S. (2002). Large-scale morphological survey of mouse retinal ganglion cells. J Comp Neurol *451*, 115-126.

Taylor, W.R., and Vaney, D.I. (2002). Diverse synaptic mechanisms generate direction selectivity in the rabbit retina. J Neurosci *22*, 7712-7720.

Thomson, A.M., and Lamy, C. (2007). Functional maps of neocortical local circuitry. Front Neurosci *1*, 19-42.

Tomishima, M.J., and Enquist, L.W. (2002). In vivo egress of an alphaherpesvirus from axons. J Virol *76*, 8310-8317.

Trong, P.K., and Rieke, F. (2008). Origin of correlated activity between parasol retinal ganglion cells. Nat Neurosci *11*, 1343-1351.

Trümpler, J., Dedek, K., Schubert, T., de Sevilla Muller, L.P., Seeliger, M., Humphries, P., Biel, M., and Weiler, R. (2008). Rod and cone contributions to horizontal cell light responses in the mouse retina. J Neurosci *28*, 6818-6825.

van Wyk, M., Taylor, W.R., and Vaney, D.I. (2006). Local edge detectors: a substrate for fine spatial vision at low temporal frequencies in rabbit retina. J Neurosci *26*, 13250-13263.

van Wyk, M., Wässle, H., and Taylor, W.R. (2009). Receptive field properties of ON- and OFF-ganglion cells in the mouse retina. Vis Neurosci *26*, 297-308.

Veruki, M.L., and Hartveit, E. (2002). Electrical synapses mediate signal transmission in the rod pathway of the mammalian retina. J Neurosci *22*, 10558-10566.

Viney, T.J., Balint, K., Hillier, D., Siegert, S., Boldogkoi, Z., Enquist, L.W., Meister, M., Cepko, C.L., and Roska, B. (2007). Local retinal circuits of melanopsin-containing ganglion cells identified by transsynaptic viral tracing. Curr Biol *17*, 981-988.

Völgyi, B., Abrams, J., Paul, D.L., and Bloomfield, S.A. (2005). Morphology and tracer coupling pattern of alpha ganglion cells in the mouse retina. J Comp Neurol *492*, 66-77.

Völgyi, B., Chheda, S., and Bloomfield, S.A. (2009). Tracer coupling patterns of the ganglion cell subtypes in the mouse retina. J Comp Neurol *512*, 664-687.

Waldeck, R.F., and Gruberg, E.R. (1995). Studies on the optic chiasm of the leopard frog. I. Selective loss of visually elicited avoidance behavior after optic chiasm hemisection. Brain Behav Evol *46*, 84-94.

Wässle, H. (2004). Parallel processing in the mammalian retina. Nat Rev Neurosci *5*, 747-757.

Wässle, H., and Boycott, B.B. (1991). Functional architecture of the mammalian retina. Physiol Rev *71*, 447-480.

Wässle, H., and Riemann, H.J. (1978). The mosaic of nerve cells in the mammalian retina. Proc R Soc Lond B Biol Sci *200*, 441-461.

Weng, S., Sun, W., and He, S. (2005). Identification of ON-OFF direction-selective ganglion cells in the mouse retina. J Physiol *562*, 915-923.

Werblin, F.S., and Dowling, J.E. (1969). Organization of the retina of the mudpuppy, Necturus maculosus. II. Intracellular recording. J Neurophysiol *32*, 339-355.

Wickersham, I.R., Lyon, D.C., Barnard, R.J., Mori, T., Finke, S., Conzelmann, K.K., Young, J.A., and Callaway, E.M. (2007). Monosynaptic restriction of transsynaptic tracing from single, genetically targeted neurons. Neuron *53*, 639-647.

Williams, R.W., Strom, R.C., Rice, D.S., and Goldowitz, D. (1996). Genetic and environmental control of variation in retinal ganglion cell number in mice. J Neurosci *16*, 7193-7205.

Witkovsky, P. (2004). Dopamine and retinal function. Doc Ophthalmol *108*, 17-40.

Xin, D., and Bloomfield, S.A. (1999). Comparison of the responses of AII amacrine cells in the dark- and light-adapted rabbit retina. Vis Neurosci *16*, 653-665.

Yonehara, K., Ishikane, H., Sakuta, H., Shintani, T., Nakamura-Yonehara, K., Kamiji, N.L., Usui, S., and Noda, M. (2009). Identification of retinal ganglion cells and their projections involved in central transmission of information about upward and downward image motion. PLoS One *4*, e4320.

Yonehara, K., Shintani, T., Suzuki, R., Sakuta, H., Takeuchi, Y., Nakamura-Yonehara, K., and Noda, M. (2008). Expression of SPIG1 reveals development of a retinal ganglion cell subtype projecting to the medial terminal nucleus in the mouse. PLoS One *3*, e1533.

Yoon, H., Enquist, L.W., and Dulac, C. (2005). Olfactory inputs to hypothalamic neurons controlling reproduction and fertility. Cell *123*, 669-682.

Zeck, G.M., and Masland, R.H. (2007). Spike train signatures of retinal ganglion cell types. Eur J Neurosci *26*, 367-380.

Zhang, D.Q., Wong, K.Y., Sollars, P.J., Berson, D.M., Pickard, G.E., and McMahon, D.G. (2008). Intraretinal signaling by ganglion cell photoreceptors to dopaminergic amacrine neurons. Proc Natl Acad Sci U S A *105*, 14181-14186.